THE UNIVERSITY OF CHICAGO

PHOSPHORUS BIOGEOCHEMISTRY IN MICROBIAL AQUATIC ECOSYSTEMS: INSIGHTS INTO P REMINERALIZATION

A DISSERTATION SUBMITTED TO

THE FACULTY OF THE DIVISION OF THE PHYSICAL SCIENCES

IN CANDIDACY FOR THE DEGREE OF

DOCTOR OF PHILOSOPHY

DEPARTMENT OF THE GEOPHYSICAL SCIENCES

BY

ARIC HOWARD MINE

CHICAGO, ILLINOIS

DECEMBER 2015

Table of Contents

List of Figures

List of Tables

Acknowledgements

This work could not have been completed without the generous financial support of the Department of Geophysical Sciences and the EPA STAR Fellowship.

I must also thank Albert for his endless curiosity and support. Your feedback and suggestions along the way have been crucial to the success of this work and instrumental to its completion. Thanks also for benevolently supporting your students and myself; altruism is an underappreciated quality in science.

My family has been essential to helping me navigate the difficulties of this degree and life in general. Without your never-ending support this would most definitely not have been possible. Thank you for providing me with the foundations that have allowed me to succeed thus far.

Finally, a simple thank you to my wife, Mara, does not encompass the shear amount of gratitude I owe her. Finding such a remarkably intelligent, caring, and thoughtful companion during graduate school has made the journey an unforgettably exciting one. You inspire me to be a better person and challenge me to be a better scientist. Your excitement about life is infectious and provides me with nothing but a smile when I think of our future together. Without your input during the writing of this thesis, it would surely be illegible.

Abstract

The availability of phosphate plays a critical role in limiting primary production in large regions of the oceans, including major ocean gyres. Phosphorus is a primary limiting nutrient in the surface ocean, where phosphate availability controls the extent of primary production and carbon export fluxes. In phosphate-limited regions of the ocean, organisms rely on efficient recycling of nutrients to meet metabolic demand when nutrient concentrations are low. However, the process of recycling and transformation of reduced organic matter to dissolved nutrient forms is poorly understood. This thesis investigates the mechanisms responsible for nutrient availability and nutrient cycling of phosphorus in the surface ocean at the microbial level. The microbial loop of phosphate is primarily comprised of uptake, release, and regeneration fluxes, although release and recycling of phosphate remains to be quantified. To resolve the release of phosphate and enzyme-mediated reactions involved in nutrient regeneration, detailed laboratory experiments with model bacteria were completed alongside field investigations with natural surface ocean microbial populations. In this study, the role of cell lysis as a mechanism for nutrient release is assessed and quantified along with nutrient regeneration, or remineralization, catalyzed by enzymes to better understand how organic matter is transformed to dissolved nutrient forms in the surface ocean.

First, this work presents a refined procedure for tracking phosphorus cycling in the ocean and identifying the important modes of nutrient cycling. An improved technique for the isolation and subsequent measurement of the stable isotopic composition of phosphate provides insight towards the significant enzyme-mediated reactions carried out by microbes.

Second, the importance of cell lysis as a mode of phosphate release and nutrient stress relief was assessed both in the laboratory and the surface ocean. A primary finding of this study is the role of cell lysis in relieving nutrient stress in nutrient starved regions of the ocean. Following lysis, cells release a pulse of phosphate in organic and inorganic dissolved forms. This flux is supplemented by a continued release of phosphate from organic and particulate reservoirs of phosphorus that are degraded in the pool of cellular debris. Continued enzymatic activity in the lysate is responsible for the breakdown of particulate and organic phosphate well after cell death. This mode of enzymatic regeneration is significant, resulting in the generation of more inorganic phosphate than the immediate release after lysis.

Moreover, the flux of phosphate subsequent to lysis is on par with phosphate demand by microbes in oligotrophic regions of the ocean. The transformation of organic forms of phosphate after cell death has potential to produce a larger, additional flux of phosphate available for uptake. In addition, the continued enzymatic breakdown of phosphorus after cell death serves to explain the observed decoupling of carbon and phosphorus in the ocean. Characterization of release and transformation fluxes of phosphate is essential in determining the role of phosphate in controlling primary production, carbon export, and ocean biogeochemistry. This work highlights the importance of nutrient regeneration pathways on biogeochemical dynamics in marine ecosystems and ultimately the amount of carbon exported to the deep ocean.

Dissertation Introduction

Primary production in the ocean exhibits important controls on the magnitude of carbon fluxes in the ocean. The availability of nutrients and the efficiency of nutrient cycling act to limit and/or enhance primary production and the biological carbon pump. In particular, the production of organic matter requires a supply of essential elements, including carbon, nitrogen, and phosphorus, as well as minor essential elements such as iron and other trace metals.

In the ocean, phosphorous exists as dissolved inorganic orthophosphate (P_i) and in dissolved organic phosphorus compounds (DOP). The relative concentration of P_i and DOP varies in the surface ocean. However, orthophosphate concentrations are often low in gyre regions. As a result, phosphorus is invoked as a primary limiting nutrient in large gyre regions of the ocean, including the North Pacific Subtropical Gyre (NPSG) and the Sargasso Sea. Gyre regions of the ocean receive limited allochthonous nutrient supply and rely on efficient recycling of organic matter to sustain primary production. Concentrations of DOP in the surface ocean in the NPSG can exceed orthophosphate by more than five times. Therefore, to overcome nutrient limitation microbes use a range of strategies, including expression of enzymes such as alkaline phosphatase (APase), to access organic reservoirs of phosphate to meet metabolic demand and overcome nutrient limitation.

In gyre ecosystems of the ocean, primary productivity is sustained by efficient recycling of organic matter. Approximately 90% of gross primary production in open-ocean ecosystems is supported through recycling of phosphorus (Karl, 2014). Although primary productivity relies on efficient recycling, the magnitude of recycling fluxes, major components of the microbial loop, remains to be quantified. Recycling involves the breakdown of organic matter to organic,

inorganic, and particulate forms. Orthophosphate can be directly taken up, but organic and particulate pools of phosphate must be enzymatically transformed prior to uptake. The primary modes of dissolved and particulate organic matter release include sloppy feeding by larger heterotrophs and cell death or lysis, both of which release contents in the cell. Efficient recycling requires the release of reduced nutrient forms is balanced by rapid uptake of nutrients by ambient microbes.

The release of nutrients from cells after cell death is essential to understanding controls on primary productivity and carbon export from the surface ocean. In addition to nutrients, enzymes are also released from cells following lysis and may play an important role in facilitating the transformation of organic and particulate forms of carbon, nitrogen and phosphorus in the surface ocean to drive more primary production and export. Particulate export of carbon, nitrogen, and phosphorus from the surface ocean is a function of the relative timescales of remineralization for these elements. Although increasing particulate C:N, and C:P is observed with depth, the mechanism and reactions involved in this carbon and phosphorus decoupling remain elusive (Knauer, 1979). In this work, we explore the significance of enzymes from lysed cells in determining the remineralization of organic matter. This work quantifies the rate of nutrient remineralization and mechanisms and reactions responsible for the processing of organic matter to better understand surface ocean organic matter cycling and export.

Chapter 1 refines a tool to understand the recycling and turnover of phosphate in the surface ocean. Here I provide a new rapid technique for conversion of phosphate to silver phosphate for isotopic analysis. Isolation of orthophosphate from the surface ocean allows for measurement of isotopic composition of phosphate oxygen. Exchange of oxygen molecules in phosphate is facilitated by enzyme-mediated reactions. During oxygen exchange, isotopic

fractionations take place in a temperature-dependent or kinetic fashion. The type of fractionation imprinted by specific phosphatases has been previously characterized (Liang and Blake, 2006). This allows one to isolate phosphate from the ocean and assess the relative significance of certain enzymatic pathways in phosphate cycling and turnover in the ocean.

In chapter 2, I characterize the release and recycling of phosphate from cells subsequent to cell death, or lysis. The flux of dissolved organic and inorganic forms of phosphate is characterized with model strains grown in the laboratory and also with mixed communities of surface ocean microbes to determine cell-level contributions to the release. Following the initial nutrient release, assaying of enzymes in the pool of cellular debris provides constraints on rates of transformation of organic to inorganic phosphate. The transformation, or remineralization, of organic and particulate forms of phosphate is monitored to determine rates of release of preferred orthophosphate from organic and particulate reservoirs. Viewed alongside previously published rates of uptake, the quantification of phosphate released from cells provides understanding of recycling of nutrients in gyre-regions of the ocean.

Chapter 3 quantifies the regeneration and release of phosphate from cyanobacterium *Synechococcus* WH7803 during infection with phage, Syn9. Virally infected *Synechcococcus* is lysed after approximately five hours of infection. Phosphosphatase activity in the lysate and release and regeneration flux is monitored to provide rate estimates for nutrient cycling by virally infected cells. When compared with measured rates of phosphate uptake in the surface ocean lysozyme and virally lysed cell experiments underscore the significance of cell lysis as a means to relieve nutrient stress and fuel productivity.

This work highlights the significance of microbe-scale nutrient cycling and its controls global carbon fluxes. Targeted experiments quantify regeneration and release of phosphate from

ubiquitous cyanobacteria in the ocean and provide flux estimates for pathways governing nutrient limitation and thus rates of primary production. Laboratory and surface ocean experiments underscore the importance of physiochemical measurements in characterizing rates and fluxes relevant to ocean biogeochemistry. Quantifying and understanding the cycling of nutrients by abundant photosynthetically active microbes in the surface ocean constitutes a significant contribution to determining and predicting the fate of carbon in the ocean.

Chapter 1 – Microprecipitation and $\delta^{18}O$ Analysis of Phosphate for Paleoclimate and Biogeochemistry Research

Abstract

Phosphate oxygen isotope ratios provide a powerful tool for paleoclimate reconstruction and the study of phosphorus biogeochemistry in aquatic systems. The temperature dependent offset between the oxygen isotope composition of phosphate and water in biogenic minerals and in solutions has been used extensively in paleoclimate research and the study of phosphorus cycling in aquatic and soil environments. Sample sizes are small in many applications, e.g., serial sampling of mammalian tooth enamel for paleoseasonality studies, the use of conodont elements for climate and ocean $\delta^{18}O$ reconstruction, or the isolation and analysis of phosphate from marine and freshwater environments in biogeochemistry studies. This has pushed the development of techniques that allow for processing and analysis of a few micromoles of phosphate.

Current approaches to phosphate oxygen isotopic composition ($\delta^{18}O_p$) determination require purification of phosphate as silver phosphate (Ag_3PO_4). The techniques for the final precipitation of Ag_3PO_4 fall into two categories: slow vs. rapid microprecipitations. We have tested both and identify artifacts that impact measured $\delta^{18}O_p$ values resulting from commonly used methods for rapid Ag_3PO_4 precipitation. In particular, commonly used methods are prone to (a) incomplete precipitation of phosphate, with associated isotopic fractionation, and (b) the production of silver oxide contaminants whose oxygen isotope composition is sensitive to the $\delta^{18}O$ of water used to prepare the precipitation reagent solution. These artifacts are commonly

on the order of 0.5 to 2 ‰, which is subtle enough to go undetected in many studies but large enough to cause errors in temperature estimates on the order of 2-8°C.

Slow microprecipitations lead to complete precipitation of phosphate without contaminating O-bearing phases. We develop a rapid precipitation technique that avoids the problems noted above. Both the slow microprecipitation and the rapid microprecipitation developed herein lead to $\delta^{18}O_p$ measurements that are indistinguishable from those made on conventional large-batch precipitations of Ag_3PO_4.

1. Introduction

Paleoclimate reconstruction is central to assessing the range of climate variability over geologic time, the controls on climate feedbacks, and paleoecological relationships. Oxygen isotope compositions of biogenic carbonate and phosphate minerals, clumped isotope measurements on carbonate minerals, Mg/Ca ratios in marine calcite, TEX86, and paleobotanical leaf margin and leaf area analyses are among the most commonly used techniques (Epstein, 1953; Tudge, 1960; Chave, 1954; Schouten *et al.*, 2002; Bailey and Sinnot, 1915). Because biogenic minerals are well preserved from many marine and terrestrial environments, their oxygen isotope compositions provide one of the most broadly applicable records of paleotemperature. Early applications of oxygen isotope thermometry targeted marine shell carbonate and tested the proxy with modern shells (Epstein *et al.*, 1953). However, carbonate minerals are prone to diagenetic alteration that can reset their oxygen isotope composition and therefore overprint the primary temperature signals. Phosphate oxygen is much more resistant to diagenetic alteration than carbonate (Tudge, 1960), and thus phosphatic minerals are prime targets for paleothermometry.

Phosphate oxygen isotope compositions in biogenic minerals record the solution temperature from which the minerals precipitated. Several phosphate oxygen isotope thermometers have been put forth to describe the temperature dependence of the equilibrium offset between phosphate and water oxygen isotope compositions (e.g., Longinelli and Nuti, 1973, Shemesh *et al*., 1983, Kolodny, 1983, O'Neil et al., 2003, Puceat *et al.,* 2010, Lecuyer *et al.*, 2013, Chang and Blake, 2014). Regardless of the exact formulation, a 1‰ shift in measured $\delta^{18}O_p$ corresponds to roughly a 4 to 4.5°C shift in paleotemperature estimate.

Phosphate oxygen isotopic compositions also have utility for studying modern phosphorus cycling in aquatic ecosystems and in soils (Colman, 2002, Paytan *et al.,* 2002, Colman *et al*., 2005, McLaughlin *et al*., 2006, Jaisi and Blake, 2010). Microbial cycling of phosphate causes exchange of oxygen atoms in phosphate during biological cycling. This provides unique insight to tracking of biological reactions and turnover of phosphate in modern environments to understand controls on biogeochemistry. Moreover, these studies require processing of small amounts of phosphate through microprecipitation techniques where dissolved phosphate is isolated from water and porewater fluids (McLaughlin *et al,* 2004; Colman, 2002; Goldhammer *et al.,* 2010).

Accurate and precise $\delta^{18}O_p$ measurements are a prerequisite for quantitative paleoclimate reconstruction. In recent years, methods for purification of phosphate have focused on handling smaller samples and increasing the speed of sample processing. The work reveals shortcomings in some of the micro-scale techniques commonly used to isolate phosphate for isotopic analysis.

The analysis of $\delta^{18}O_p$ has undergone significant methodological shifts over the last five decades owing to the linked challenges of (a) producing phosphate analytes that are devoid of exogenous oxygen and (b) reacting these analytes cleanly to produce an oxygen bearing gas on

which highly reproducible oxygen isotope measurements can be made. $\delta^{18}O_p$ was first measured by fluorination of $BiPO_4$ with BrF_3 (Tudge, 1960; Longinelli and Nuti, 1973) or BrF_5 (Kolodny *et al.,* 1983) to liberate phosphate oxygen as O_2. In this approach, samples were first carried through a series of precipitations to remove cations and anions that could interfere with fluorination. Samples were sequentially precipitated as ammonium phosphomolybdate (APM), redissolved, precipitated as magnesium-ammonium-phosphate (MAP), and finally as the analyte phase, bismuth phosphate ($BiPO_4$) (Tudge, 1960).

The fluorination method presented many challenges in that it was cumbersome and involved the use of dangerous chemicals and required intricate extraction lines (Kolodny *et al*., 1983). In addition, contaminating oxygen phases were a primary concern given the hygroscopic nature of $BiPO_4$ and the efficient liberation of oxygen from all sources by fluorination. In response to these problems with the conventional fluorination method, a series of studies (Wright and Hoering, 1989, Crowson *et al*., 1991) proposed Ag_3PO_4 as an analyte phase for $\delta^{18}O_p$ measurements. Silver phosphate was fluorinated and the liberated oxygen was reacted with graphite to produce CO_2 for isotopic analysis. The anhygroscopic nature of silver phosphate reduced the potential for direct contamination with water oxygen.

O'Neil et al. (1994) suggested an alternative to fluorination in the form of high temperature decomposition of silver phosphate. Thermal decomposition resolves issues with fluorination methods to cleanly liberate oxygen from phosphate precipitates, and achieved similar precision measurements. This method improved sample throughput and reduced measurement costs. Silver phosphate decomposition at 1200°C in the presence of graphite was the first method to eliminate the need for fluorination and allow for precise analysis of sample oxygen as CO_2 (O'Neil et al., 1994).

Because thermal decomposition methods increased efficiency without significantly sacrificing analytical precision, automated online procedures for high temperature pyrolytic decomposition of silver phosphate became the primary method for analysis of phosphate $\delta^{18}O$ values. Instrumentation, such as high temperature conversion analyzers (TCEA), are used for decomposition of silver phosphate in a glassy carbon tube at 1400°C or above. At such high temperatures, the oxygen released in a carbon rich reactor converts entirely to CO instead of CO_2 with approximately 100% oxygen yield (Kornexl et al., 1999, Vennemann et al., 2002). The isotopic composition of CO is then followed to determine $\delta^{18}O$. This method allowed smaller samples sizes, higher throughput, and is the most widespread analytical approach for $\delta^{18}Op$ analysis today.

The first silver phosphate precipitations used approximately 10-20mg of starting bioapatite material (O'Neil et al., 1994). Owing to their relatively large size, we refer to them here as macroprecipitations. However, these material requirements are problematic for many paleoclimate applications, including use of conodont elements, which target small sample sizes. These applications require methods for preparing small (<1 mg bioapatite) samples via microprecipitations of silver phosphate. Nevertheless, the established robustness of the Ag_3PO_4 macroprecipitations commends them for use as a reference against which to compare the isotopic fidelity of microprecipitation techniques.

Two primary methods currently exist for the microprecipitation of Ag_3PO_4 for $\delta^{18}O$ analysis via TCEA. The first is a slow precipitation (Wenzel et al., 2000; Colman, 2002, Wiedemann-Bidlack et al., 2008) in which phosphate is precipitated in a buffered solution over a period of 12-16hrs. The second is a rapid precipitation in an unbuffered solution that goes to completion nearly instantaneously (Dettman, 2001). Heretofore, neither the slow nor rapid

microprecipitations have been subject to rigorous examination of phosphate precipitation efficiency, isotopic fractionation during incomplete precipitations, nor formation of secondary oxygen-bearing phases that could cause reproducible but inaccurate $\delta^{18}O$ determinations for the starting phosphate. This study assesses both methods in this manner.

Slow microprecipitation of silver phosphate results in large crystals that are relatively easy to manipulate physically when weighing prior to analysis (i.e., minimizing static charge problems that complicate working with small powdered samples). This method has been tested and implemented for use with small sample sizes (<1mg-2mg bioapatite or equivalently small amounts of phosphate derived from aqueous sources) (Wenzel et al., 2000, Colman, 2002, Wiedemann-Bidlack et al., 2008). However, slow precipitations are labor intensive and precipitation time is variable. This increases the risk of human error in determining when the precipitation is complete.

Alternatively, the conversion of phosphate in solution to silver phosphate can be performed with a rapid and relatively easy "crash" microprecipitation. The resultant very fine crystals are more difficult to work with due to static charging issues, but this is a surmountable problem that is offset by the overall ease with which this technique can be executed. We began this study with the hope of verifying that these widely employed rapid precipitation techniques could be used without compromising $\delta^{18}O_p$ measurements. Unfortunately, we discovered small, systematic, and quantitatively important artifacts associated with the most widely used rapid precipitation techniques. We then developed a modified-rapid precipitation technique that avoids the problems attendant to previously published rapid precipitation methods while retaining the advantages.

2. Materials and Methods

2.1. Reagents and bioapatite

Silver phosphate microprecipitation techniques were tested using reagent grade (KH_2PO_4), hydroxyapatite, and modern (Goat tooth enamel, Cocinetas Basin, Colombia) and fossil (Miocene South American Toxodont, Subhyracodon, Shark Tooth) biogenic apatite as sources of phosphate. All of the chemical reagents used in this study were of ACS grade or higher from Sigma Aldrich and Fisher, and solutions were made using deionized (DI; 18.2 MΩ, Nanopure, Thermo) water. A series of tracer experiments was conducted in solutions containing ^{18}O-labelled water from Stuart Oxygen Company (formerly of San Francisco, CA, and provided by R.N. Clayton).

2.2. Ag_3PO_4 precipitation and bioapatite processing techniques

Phosphate was isolated as Ag_3PO_4 via slow and rapid precipitations, and the component solution compositions for each of these precipitations are listed in Tables 1.1 and 1.2. All Ag_3PO_4 microprecipitations using KH_2PO_4 were conducted from a single stock solution for a given series of experiments, while those employing fossil and modern biogenic apatite were from homogenized fossil and modern tooth enamel. Homogenized bioapatite was dissolved in nitric acid and treated with NaF for Ca^{2+} removal as CaF_2 precipitate for each individualized treatment with solution compositions and volumes indicated in Table 1.1 and 1.2. However, Rapid UC Conc and Rapid UC Dil bioapatite samples were processed in batch, where a uniform starting material was dissolved and treated to remove Ca^{2+}. Splits of this homogenized bioapatite solution were then processed through Rapid UC Dil and Rapid UC Conc methods. The details of the

Method	Vol 10mM KH_2PO_4 (ml)	Mass Bioapatite Sample (mg)	Vol 2.0M HF (ml)	Vol 2.0M HNO_3 (ml)	Vol Ag-Ammine (ml)	Vol 7.25M NH_4OH (ml)	Vol 1.25M NH_4NO_3 (ml)	Vol 0.5M KOH (ml)	Vol DI H_2O (ml)
Macroprecipitation	4.5	-	-	-	[1]2.28	1.8	-	-	40.5
Slow Microprecipitation	0.5	-	-	-	[1]2.28	0.1	1.25	-	-
Slow (Bioapatite) Microprecipitation	-	1.0	0.1	0.1	[2]0.75	0.1	1.25	0.075	0.1

Table 1.1 Slow Microprecipitation Solution Composition

[1]Ag-Ammine for Macroprecipitations is composed of 0.2M $AgNO_3$, 0.74M NH_4OH, and 0.35M NH_4NO_3

[2]Ag-ammine solution was composed of 0.067M $AgNO_3$, 0.12M NH_4NO_3, and 0.43M NH_4OH.

Method	Vol 10mM KH_2PO_4 (ml)	Mass Bioapatite (mg)	Vol 2.0M HNO_3 (ml)	Vol 2.0M HF (ml)	Vol 0.5M NaF (ml)	Vol 1.0M HNO3/ 0.25M NaF (ml)	Vol 2.0M $AgNO_3$ (ml)	Vol Ag-Ammine (ml)	Vol 7.25M NH_4OH (ml)	Vol 20%v:v NH_4OH (2.9M)(ml)	Vol 2.0M NaOH (ml)	Vol 2.0M KOH (ml)	Vol DI H_2O (ml)	Vol 4% HF (ml)	Vol 0.1M NaF (ml)
[1]ABF_---	0.5	-	-	-	-		0.1	-	-	-			-		-
ABF_--+	0.5	-	-	-	0.19		0.1	-	-	-			-		-
ABF_-+-	0.5	-	-	-	-		0.1	-	0.03	-			-		-
ABF_-++	0.5	-	-	-	0.19		0.1	-	0.03	-			-		-
ABF_+++	0.5	-	0.1	-	0.19		0.1	-	0.03	-			-		-
ABF_++-	0.5	-	0.1	-	-		0.1	-	0.03	-			-		-
[2]Rapid A	-	1.0	0.1	0.1	-		0.1	-	-	0.12		0.1	1.48		-
[2]Rapid B	-	1.0	-	0.2	-		0.2	-	-	0.16			-		-
Rapid UC Conc	[3]0.05	-	*	-	-	0.05	-	[4]0.06	-	-			*		-
Rapid UC Dil	-	1.0	0.05	-	-		-	[5]0.18	-	-	0.05		-	0.03	0.05
[6]Standard Immersion	-	**0.5	-	-	-		0.2	-	0.03	-			0.5		0.5

Table 1.2 Rapid Microprecipitation Solution Composition

[1]The ABF naming scheme is used to identify microprecipitations that include acid (A), base (B), and fluoride (F) in the microprecipitation solution. A minus and/or plus symbol following the underscore indicates the presence of absence of A, B, and/or F in the solution for Ag_3PO_4. [2]Modeled after microprecipitation methodologies in Dettman et al., 2001, but scaled for microprecipitation of 1mg of bioapatite and 5 µmoles KH_2PO_4. [3]PO_4 Stock Solution is composed of 250 µl of 2M HNO_3 added to 22.7mg KH_2PO_4, 600 µl of 2M HF added, 600 µl of 0.5M NaF added. [4]Ag-Ammine is a mixture of 200 µl of 4.4M $AgNO_3$, 300 µl of 7.25M NH_4OH, 300 µl DI H2O. [5]Rapid UC Dil uses an Ag-ammine solution that is a 4-fold dilution of Rapid UC Conc Ag-ammine solution (Rapid UC Dil Ag-ammine = 0.37M $AgNO_3$, 1.09M NH_4OH). [6]Indicates an experiment where isotopic standard Strem was immersed in precipitation solution resembling ABF_-+-. *Volumes of DI H_2O, 2.0M HNO_3 and 1.87M NH_4OH were adjusted to finely tune pH for RapidUC Conc pH precipitations in Figure 5A. **Represents the mass of silver phosphate standard (Strem Chemicals) used in the experiment.

precipitation methods are outlined in Table 1.2. Modern and fossil biogenic apatite and potassium phosphate were precipitated in triplicate for all of the methods listed.

2.2.1. Reference Ag_3PO_4 macroprecipitations

Silver phosphate macroprecipitations (target mass: 20-30mg Ag_3PO_4 corresponding to 8-10mg bioapatite sample material) followed the approach of O'Neil *et al.* (1994). This technique was also used in Vennemann et al. (2002) to precipitate Ag_3PO_4, which has been widely used in subsequent years as isotopic reference material. Our macroprecipitations were used to produce Ag_3PO_4 whose isotopic composition served as a reference against which to compare the microprecipitation experiments.

The starting solution for the slow precipitations (both macroprecipitation and the microprecipitation described below) has a pH around 10 and high concentrations of ammonia. Silver phosphate is soluble in ammonium hydroxide, with the ammonia complexing the silver cation (Firshing, 1961). Precipitation begins after ammonia outgases with a concomitant drop in pH, shift in speciation of NH_3 to NH_4^+, and decomplexation of Ag^+. In the case of microprecipitations, the concentrations of Ag^+ and ΣPO_4 (sum of phosphate species, irrespective of degree of protonation and ion pairing) increase due to significant evaporative reduction of solution volume. This further promotes supersaturation of Ag_3PO_4 and drives the precipitation reaction to complete removal of phosphate at circumneutral pH provided a modest excess of silver over that required for precipitation of all of the phosphate.

2.2.2 Slow Ag3PO4 microprecipitations

Microprecipitations were modeled after the procedures and reagents used in Wenzel et al. (2000), Colman (2002), Wiedemann-Bidlack et al., (2008). An initial solution contained ~5 μmoles of phosphate derived from the KH_2PO_4 reagent or the phosphate derived from the acid

dissolution of 1 mg of bioapatite. Slow microprecipitations were conducted in polypropylene transfer pipet bulbs with stems removed (Colman, 2002; Wiedemann-Bidlack et al., 2008). Component solutions (Table 1.1 and 1.2) were added to the bulb in the order of phosphate bearing solution, silver ammine solution, ammonium nitrate, and then ammonium hydroxide. The order of addition is not particularly important in the case of these slow precipitations. Ammonium hydroxide solutions were made fresh daily and silver nitrate and silver ammine solutions were stored in the dark. The precipitations were conducted at 50°C for approximately 12-15hrs or until solution volume reached 200-300 ml. This final volume ensured complete precipitation of phosphate as Ag_3PO_4 (Figure 1.1). This approach uses a buffered solution with high initial ammonia concentration to promote slow growth of large (usually mm scale) gemmy, yellow Ag_3PO_4 crystals with equant or dendritic habit.

In some cases, a very fine Ag_3PO_4 precipitate can form upon addition of the silver ammine solution to the phosphate bearing solution. It re-dissolves upon continued addition of silver ammine or NH_4OH solution. The precipitation continues over several hours (Figure 1.1). We have extensive observations outside the scope of the present paper that show that one can vary the temperature of precipitation, air flow over the reaction vessels, and NH_4NO_3 content of solution to change the duration of the precipitation. While this may influence crystal size (in general, slower precipitations lead to larger crystals), it has no effect on the resultant measured $\delta^{18}O$ of phosphate ($\delta^{18}O_p$).

At the completion of a microprecipitation, the supernatant was removed by pipet. In many cases a 5-50 µl aliquot of supernatant was sampled for phosphate concentration analysis, described section 2.4 to verify the quantitative removal of phosphate during the precipitation reaction. Silver phosphate crystals were rinsed five times with approximately 3 ml of DI water to

remove thoroughly any residual nitrate and silver from the precipitation solution. The number of DI water rinses reflects a balance between reducing NO_3^- concentrations in the residual solution (to avoid contamination of the Ag_3PO_4 by nitrate oxygen) and minimizing the loss of Ag_3PO_4 crystals during rinsing. Resultant crystals were dried overnight at 60°C, and the crystals were removed from the precipitation vessel using a fine camel hair brush or stainless steel microspatula. Recovery of crystals was aided by cutting the vessel in half and using an antistatic gun (Milty Zerostat 3, Armour, Hertfordshire, UK).

2.2.3. Conventional rapid Ag3PO4 microprecipitations (Rapid A & B)

Rapid microprecipitations were modeled after the procedures and reagents used in Dettman et al. (2001). Rapid microprecipitations were conducted in 2.0 ml microcentrifuge tubes. We based these tests on two protocols from Dettman et al. (2001) which have been widely adapted for processing mg to sub mg samples of bioapatite, and which are outlined in Table 1.2. The original protocols called for 5 to 10mg of bioapatite starting materials. The first method employs nitric acid to dissolve bioapatite, HF treatment to remove Ca^{2+} as CaF_2 precipitate, and the pH is adjusted to circumneutral values prior to rapid precipitation of Ag_3PO_4 by the addition of $AgNO_3$ solution. The second method employs HF to simultaneously dissolve bioapatite and remove Ca^{2+} from solution followed by pH adjustment and $AgNO_3$ addition to rapidly precipitate Ag_3PO_4. Most studies that have used this technique for mg or sub mg samples of bioapatite do not specify which Dettman et al. (2001) protocol is employed nor how the protocol is adapted to smaller scale precipitations.

We have mainly tested variants on the first Dettman et al. (2001) protocol, which we refer to as Rapid A. Reagent concentrations are the same as those originally proposed, and the volumes are scaled down proportionately to match the smaller amounts of phosphate precipitated

here. We use an initial solution (2ml) containing ~5 μmoles of phosphate derived from the KH_2PO_4 reagent or phosphate derived from the nitric acid dissolution of 1 mg of bioapatite (see Table 2). The pH of this phosphate bearing solution was adjusted with nitric acid, ammonium hydroxide and/or potassium hydroxide as noted. The rapid precipitation of Ag_3PO_4 was initiated by addition of 200 μl of 2.0M $AgNO_3$.

We also tested the second Dettman et al. (2001) protocol, again scaled to smaller (~5 μmole) quantities of phosphate. We refer to this second approach as Rapid B, and we tested it on 1 mg bioapatite samples. In Rapid B, HF was used to dissolve the bioapatite and remove Ca^{2+} from solution, and the pH adjustment prior to $AgNO_3$ addition was carried out with a combination of KOH and NH_4OH (details in Table 1.2)

In both Rapid A and Rapid B, following addition of $AgNO_3$, the microcentrifuge tubes were capped, gently mixed by repeated inversion, and allowed to stand for 10 minutes to ensure completion of the precipitation reaction. The tubes were then centrifuged at 5000G for 3 min to pellet the Ag_3PO_4 precipitate. As with the slow precipitations, the supernatant was removed by pipette, and the crystals were rinsed with DI water. Crystals were again pelleted via centrifugation and supernatant removed via pipette. Pellets were cohesive, preventing loss of Ag_3PO_4 crystals during the rinse step. A total of 5 × 2.0ml DI water rinses was sufficient to remove all residual dissolved silver nitrate.

The final DI-rinsed rapid microprecipitate was resuspended in 100-200 μl of DI water and transferred to a 0.6 ml microcentrifuge tube for final recovery of crystals as a single pellet by centrifugation (5000G for five minutes). After removing the rinse supernatant, the pelleted silver phosphate crystals were dried overnight at 60°C. This step of pelleting in a 0.6 ml microcentrifuge tube led to more effective recovery of the entire Ag_3PO_4 pellet for subsequent

weighing than using a 2.0 ml microcentrifuge tube. The recovered pellet was gently crushed to yield a combination of pellet fragments and fine crystalline powder for weighing.

2.2.4. Testing new Rapid UC Ag_3PO_4 microprecipitations

In addition, a modified rapid microprecipitation (Rapid UC Conc) was developed in a buffered microprecipitation solution that was designed to surmount problems that were encountered with the Rapid A and B microprecipitations. The initial solution was composed of potassium phosphate monobasic dissolved in 2.0M HNO_3 to which 50 µl of 1.0M HNO_3 and 0.25M NaF are added to simulate a dissolved apatite solution that has been processed to remove Ca^{2+} and to control pH, followed by the addition of 60 µl of a modified Ag-ammine solution to initiate Ag_3PO_4 precipitation (Table 1.2). Rapid UC Conc microprecipitations were also carried out in 2ml microcentrifuge tubes and allowed 10 minutes for completion of the precipitation following the Ag-ammine addition. Samples were centrifuged at 5000G for 3 min to recover Ag_3PO_4 crystals as a pellet for subsequent DI rinsing and transfer to a 0.6 ml microcentrifuge tube as described for Rapid A and B.

Rapid UC Dil was developed as a safer alternative to Rapid UC Conc. Solutions from Rapid UC Conc require appropriate disposal and storage to prevent contact explosive formation. Rapid UC Dil solution is composed of 1mg of bioapatite dissolved in 50 µl of 2.0M HNO_3. To remove calcium, 2.0M NaOH and 4% HF are used to adjust pH and precipitate CaF_2. Rapid UC Dil uses a modified silver ammine solution that is a 4-fold less concentrated than the silver ammine solution used in Rapid UC Conc. Microprecipitations were completed in 2.0ml microcentrifuge tubes and centrifuged and rinsed as detailed above.

2.3. Stable Isotope Analyses

Phosphate $\delta^{18}O$ values were determined through high temperature reduction of silver phosphate to CO using a TCEA (Thermo, Bremen, Germany) at 1450°C (Vennemann et al., 2002; Kornexl et. al, 1999). Sample CO was entrained in the He carrier gas and passed through a Conflo IV open split to a Delta V Plus isotope ratio mass spectrometer (IRMS; Thermo). The isotopic composition of samples ($\delta^{18}O_p$) was determined by comparing sample isotopic compositions to standard silver phosphate material using house standards. We used commercially available Ag_3PO_4 (>99% purity) from Strem, Sigma-Aldrich, Alfa-Aesar, and Elemental, with $\delta^{18}O_p$ values of 8.20, 10.82, 15.30, and 21.87 ‰ respectively. These isotopic compositions represent the mean values from multiple calibrations in our lab against the fluorination values reported for YR-1, YR-2, YR-3 and TU standards (Vennemann et al., 2002). All reported oxygen isotopic compositions in this study are on the V-SMOW scale.

Samples were loaded in a 50 or 100 position Zeroblank Autosampler (Costech, Valencia, CA, USA). A suite of Ag_3PO_4 standards was run at the beginning and end of each day, with each standard run in triplicate or quadruplicate. Triplicate standards were inserted after every 8 to 12 samples and spanned the full range of sample masses and sample isotopic compositions to monitor for linearity effects and drift. Benzoic acid was analyzed at the beginning of each run and used as an oxygen yield standard.

2.4. Additional Experimental and Analytical Techniques

Dissolved phosphate concentrations were analyzed in the supernatant from slow and rapid Ag_3PO_4 precipitations in order to test for incomplete precipitation of dissolved phosphate. We adapted the soluble reactive phosphorus (SRP) spectrophotometric technique from Murphy

and Riley (1978) for use with our reagent solutions. In particular, residual silver must be removed from solution prior to spectrophotometric assay for [SRP] to prevent interference in color development. Supernatant samples were diluted in DI water to reduce phosphate concentrations to the linear absorbance response range of KH_2PO_4-based standard curves. The silver was removed by adding 1.0 M NaCl to the subsample of supernatant used for SRP analysis, achieving approximately an 8:1 Cl:Ag ratio in solution and precipitating out the Ag^+ as AgCl. After 10 min of reaction, the solution was centrifuged at 5000G for 5 min to pellet AgCl, and the supernatant was removed and analyzed for [SRP]. Phosphate standard curves conducted in an analog matrix showed no evidence for silver interference. The fraction of phosphate remaining in solution following precipitation was calculated relative to the initial quantity of phosphate, assuming bioapatite stoichiometry $Ca_5(PO_4)_3OH$ for the modern and fossil enamel runs.

Ag_3PO_4 crystal size, color, and morphology were observed under an optical microscope (Olympus SZX16 wide zoom stereomicroscope with SDF PLAPO1XPF objective, Olympus, Waltham, MA, USA). Microscopy images were captured using a Canon EOS T2i DSLR camera (Canon, Melville, NY, USA) mounted on a MDSLR-BX 1.38x Widefield T-mount adapter (Martin Microscope Co., Easley, SC, USA).

Scanning electron microscopy (SEM) and Energy Dispersive X-Ray Spectroscopy (EDS) were used to examine Ag_3PO_4 from slow and rapid microprecipitations using a Hitachi S-3400N SEM. Precipitate morphology and compositional determinations were used to test for the presence of spurious oxygen-bearing phases as primary precipitates or overcoatings on Ag_3PO_4 crystals. Precipitates were mounted on glass microscope slides using double sided conductive tape and were carbon coated. EDS spectra were collected on spot sizes ranging down to 1μm

diameter and were used to calculate molar ratios of Ag:P as a test of the purity of crystalline silver phosphate generated by different precipitation methods. The spectra are influenced mainly by the outermost 1-3 μm thick layer of precipitate. Identification of elemental peaks was completed by calibrating spectral peaks to known mineral standards with well-characterized stoichiometry and elemental abundances. Deviations from the Ag_3PO_4 stoichiometry (i.e., Ag:P = 3) indicated impurities in the precipitate.

As described in the Results and Discussion section, both isotopic measurements and SEM EDS spectra indicated the presence of contaminating phases in Rapid A and B precipitates. We tested for presence of residual ammonium nitrate or silver nitrate, occluded water, or silver carbonate precipitate. Nitrogen in samples (e.g., from NH_4^+ or NO_3^- that may persist if Ag_3PO_4 crystals are inadequately rinsed or if the crystals host fluid inclusions) is easily detected during phosphate $\delta^{18}O$ analysis. These ions produce N_2 in the TCEA reactor, which appears as an N_2 peak chromatographically separated from the main CO peak on the IRMS m/z 28 trace.

Occluded water in the Ag_3PO_4 crystals can be detected by processing the Ag_3PO_4 on the TCEA-Conflo IV-Delta V Plus system in the same manner as for the determination of $\delta^{18}O$ on CO produced in the reactor. Oxygen in occluded H_2O will be liberated in the TCEA as CO, which is difficult to quantitate separately from the much larger release of CO from phosphate oxygen. However, hydrogen is liberated as H_2 in the TCEA reactor, and H_2 can be detected sensitively on the IRMS. Thus, H_2 yield can prove a useful monitor for presence of water or other H-bearing species, e.g., NH_4^+ or AgOH, in Ag_3PO_4. Previous tests (Colman, 2002) had shown that even finely powdered Ag_3PO_4 does not adsorb appreciable amounts of water vapor from water saturated air. Therefore, any detected H_2 would derive from the sample precipitates, not adsorbed water.

Ag_3PO_4 precipitates were analyzed for the presence of carbonates by following standard protocols for carbonate mineral analysis using 103% phosphoric acid digestions. Samples were weighed out into Exetainer tubes (12mL, Labco), capped, and flushed with He (Airgas). Carbonate standards were also prepared (10's to 100's of μg) in order to calibrate CO_2 yields. Then the tubes were placed in the GasBench II thermostated sample holder (26°C, Thermo). Phosphoric acid digestions of carbonates for mass spectrometric analysis would employ "anhydrous" phosphoric acid to permit $\delta^{18}O$ analysis. The digestions ran overnight, then the headspace gas was analyzed via the GasBench II interfaced to the Delta V Plus IRMS for quantitation of CO_2 release and calculation of initial carbonate content of the precipitate.

2.5. Experiments

Initial testing revealed a dependence of measured Ag_3PO_4 $\delta^{18}O$ values on the method by which the Ag_3PO_4 was precipitated. This dependence could arise from (a) incomplete precipitation of phosphate accompanied by fractionation between the phosphate in solution and that in the precipitate, (b) the formation or occlusion of O-bearing contaminant phases during Ag_3PO_4 precipitation, or (c) incomplete recovery of Ag_3PO_4 crystals from a precipitation paired with an isotopic offset between recoverable and unrecoverable crystals. We designed experiments to test the potential causes behind such a dependence for Ag_3PO_4 precipitation protocols that were susceptible to these problems.

2.5.1. Influence of rapid microprecipitation solution composition, including pH, on Ag_3PO_4 yield and $\delta^{18}Op$

Modified versions of Rapid A microprecipitations were performed on phosphate from a KH_2PO_4 stock solution. The overall precipitation solution composition was designed to mimic

the composition that would result from dissolving bioapatite in acid and removing the resultant Ca^{2+} with a CaF_2 precipitation. This included adding combinations of HNO_3, NaF, and/or NH_4OH, producing a solution with a pH of 8 to 9 prior to the initiation of Ag_3PO_4 precipitation through addition of $AgNO_3$. The targeted pH range was optimal for complete phosphate recovery as Ag_3PO_4 (Figure 1.2A). Several variations on this precipitation were completed by omitting one or more of the solution components (summarized in Table 1.2) to determine how each component impacted measured $\delta\,^{18}O_p$.

Incomplete precipitation of phosphate results mainly from variation in Ag_3PO_4 solubility as a function of pH and ammonia concentration. This was tested systematically on the rapid microprecipitations by varying the starting pH from 3-11 prior to the addition of the $AgNO_3$ to initiate the precipitation. An initial 500 μl solution with 5 μmoles of KH_2PO_4 was adjusted to different pH levels by addition of 5 ml increments of 2.0M HNO_3 and/or 3.75M NH_4OH. Potassium hydroxide was used to adjust pH for a subset of high pH solutions in order to test how ammonia complexation of Ag^+ influences the amount of phosphate remaining in solution. Measurements of pH were made by spotting 1-5 μL of solution onto pH paper from EMD Millipore (scaled with 0.2 or 0.5 pH unit gradations). In order to achieve pH readings that were consistent with pH electrode measurements, it was necessary to take pH paper readings quickly before NH_3 outgassing or reaction with the pH paper could shift the pH reading. The Ag_3PO_4 precipitations were then initiated by the addition of 100 μl of 2.0M $AgNO_3$, and the precipitate was rinsed in DI water, as described earlier. The [SRP] was measured on the supernatant of the precipitation solutions, and Ag_3PO_4 was analyzed for $\delta\,^{18}O$.

2.5.2. Detection of O-bearing contaminants in Ag_3PO_4 precipitate

We tested for the production of O-bearing contaminants that would be sensitive to the $\delta^{18}O$ of the aqueous component of the precipitation solution. Initial phosphate solutions (10 mM KH_2PO_4 or bioapatite dissolved in nitric acid) were spiked with an $H_2{}^{18}O$ label to shift $\delta^{18}O_{H2O}$ to ~ +100 ‰ for the total precipitation volume. Additional experiments were run using 10 mM KH_2PO_4 solution prepared in ^{18}O-depleted water ($\delta^{18}O_{H2O}$ of -50‰ and -24‰). Silver phosphate was then precipitated using the Slow, Rapid A, and Rapid B microprecipitation methods, and $\delta^{18}O$ was measured on Ag_3PO_4 precipitated from labeled vs. unlabeled solutions. Aliquots of the Ag_3PO_4 from unlabeled precipitations were examined for Ag:P stoichiometry using SEM EDS spectra. Measurements of occluded water, AgOH, residual NO_3^-, and Ag_2CO_3, were completed as described in section 2.4.

2.5.3. The effect of vacuum roasting on removing contaminant O from Ag_3PO_4 precipitates

Vacuum roasting of Ag_3PO_4 prior to isotopic analysis has entered the lore on sample preparation, especially for precipitates that are initially dark yellow trending towards dark green or black (Dettman et al, 2001). The vacuum roasting generally shifts the color of Ag_3PO_4 crystals in the direction of the bright yellow typical of pure crystals. We tested whether roasting can successfully remove contaminant oxygen-bearing phases (e.g., water or Ag_2O) by roasting precipitates that were produced in $H_2{}^{18}O$-labeled solutions and that exhibited a resultant shift in measured $\delta^{18}O_p$ as compared to when they were prepared in unlabeled solutions. Vacuum roasting of silver phosphate was conducted at 400°C for 30 min on a glass vacuum line at a pressure of 20-30 mtorr. We compared $\delta^{18}O$ values measured on roasted and unroasted Ag_3PO_4. An assessment of the potential for elemental silver and Ag_2O coatings was made using EDS spectra and oxygen yields from TC/EA analysis.

2.5.4. Formation of O-bearing coatings on Ag_3PO_4 powder exposed to silver ammine solution

Early results suggested that oxygen-bearing coatings could form on the fine-grained Ag_3PO_4 produced by the rapid microprecipitations and contribute sufficient O to shift the measured isotopic compositions. The formation of a coating on preexisting crystals, as opposed to the simultaneous precipitation of Ag_3PO_4 and contaminant phases, was tested by immersing a Ag_3PO_4 isotopic standard (Strem) in a solution that was identical to the rapid precipitation solution except free of phosphate (100 μl of 2.0M $AgNO_3$ and 30 μl of 7.25M NH_4OH, and 500 μl of DI water). The Strem standard was a finer powder than our typical rapid precipitates, thus it had a higher specific surface area. If this were strictly a surface phenomenon, the Strem standard would have been more sensitive than our typical precipitates.

The formation of oxygen-bearing contaminants during the Strem immersion experiments was monitored by comparison of measured $\delta^{18}O_p$ after treatment in either silver ammine solutions spiked with ^{18}O-labeled H_2O ($\delta^{18}O_{H2O} \approx 100‰$) or unlabeled solutions ($\delta^{18}O_{H2O} \approx -5‰$). The label was added either prior to addition of the Strem silver phosphate or 10 min after the incubation had started. The comparison between solutions that were labeled from the start with those receiving the label after 10 minutes was meant to test whether significant coatings could develop over the same interval of time that we use to allow the Rapid precipitations to go to completion.

We also tested whether the elapsed time between Ag_3PO_4 rapid precipitation and removal of crystals from the residual supernatant influences resultant measured $\delta^{18}O$ (10min and 4 days, see Table 1.2). We reasoned that the extent of formation of O-bearing mineral surface coatings and secondary precipitates could scale with contact time between rapid precipitate and the precipitation solution. These tests were completed in triplicate, and the Strem Ag_3PO_4 was

weighed before and after immersion in precipitation solution to determine whether surface coatings contributed appreciably to sample mass. Portions of the samples were also vacuum roasted, as above, to determine whether oxygen from secondary phases could be removed.

2.5.5. Effect of bioapatite pretreatment with NaOCl on Ag_3PO_4 $\delta^{18}O$

Bioapatite samples rich in organic matrix (e.g., dentine, cancellous bone) can give rise to the production of discolored Ag_3PO_4 crystals, which has been interpreted as containing impurities that could impact measured $\delta^{18}O$ values. Sodium hypochlorite (i.e., "bleach") treatments are frequently used on such samples and on modern enamel to oxidize the organic matrix. We tested pretreatment of 1 mg of homogenized modern tooth enamel by immersion for 24hrs in 0.055 ml 2.5% NaOCl on a shaker table. This NaOCl soak was followed by five DI water rinses and overnight drying. The enamel was then dissolved in 2.0M nitric acid and carried through both slow and rapid microprecipitation methods (Tables 1.1 and 1.2, Slow, Rapid A and B). Splits of the solutions derived from modern enamel were spiked with isotopically enriched water to raise the precipitation solution $\delta^{18}O_w$ to roughly +100‰. These were precipitated via Rapid and Slow methods and compared against control precipitations from solutions with $\delta^{18}O_w \approx$ -5‰. Parallel experiments were carried out with Slow microprecipitations of unbleached modern bioapatite.

2.5.6. Development of a rapid Ag_3PO_4 microprecipitation (Rapid UC Conc and Rapid UC Dil) for successful determination of $\delta^{18}O_p$ on phosphate derived from bioapatite and aqueous phosphate samples

Rapid UC Conc and Rapid UC Dil were tested over a wide pH range to determine SRP in solution after precipitation and changes in $\delta^{18}O_p$. The primary difference in these precipitation methodologies is the silver ammine solution, which is 4-fold less concentrated in the Rapid UC

Dil methodology. The protocol for both methods is outlined in Table 1.2, with a modified silver ammine solution added last to precipitate out the silver phosphate. For this series of tests, an additional NH_4OH (2.9M), HNO_3 (2M) and/or DI was added to the phosphate solution, total addition brought up to 50 µL with DI if needed, to adjust final pH. An initial test run was done to check the final pH and estimate the amounts needed to cover the desired pH range. If only base was added, we would not see any precipitation. Acid would then be added to crash out the silver phosphate. After the initial precipitation of silver phosphate, aliquots of the supernatant were taken and analyzed for SRP. The pellet was washed and analyzed for $\delta^{18}O_p$ as described previously.

Experiments were also completed with labeled-water to test for incorporation of contaminant phases during precipitation. The protocol is outlined in Table 2, with a series of runs spiked with 1.4% $\delta^{18}O$ labelled water to bring the final concentration (after silver ammine solution is added) to ca. +100 per mil. Precipitation, clean up and analysis were completed as described above.

3. Results and Discussion

3.1. Sensitivity of Ag_3PO_4 microprecipitation $\delta^{18}O$ to solution composition, pH, and precipitation efficiency

The Slow Ag_3PO_4 microprecipitations proceed via outgassing of NH_3 and evaporative reduction of the solution volume. We performed tests to monitor the scaling of phosphate removal to solution volume reduction, essentially determining the volume at which the Ag_3PO_4 precipitation can be considered to have reached completion. During the initial stages of the precipitation incubation, evaporative loss acts to concentrate remaining solutes, and phosphate

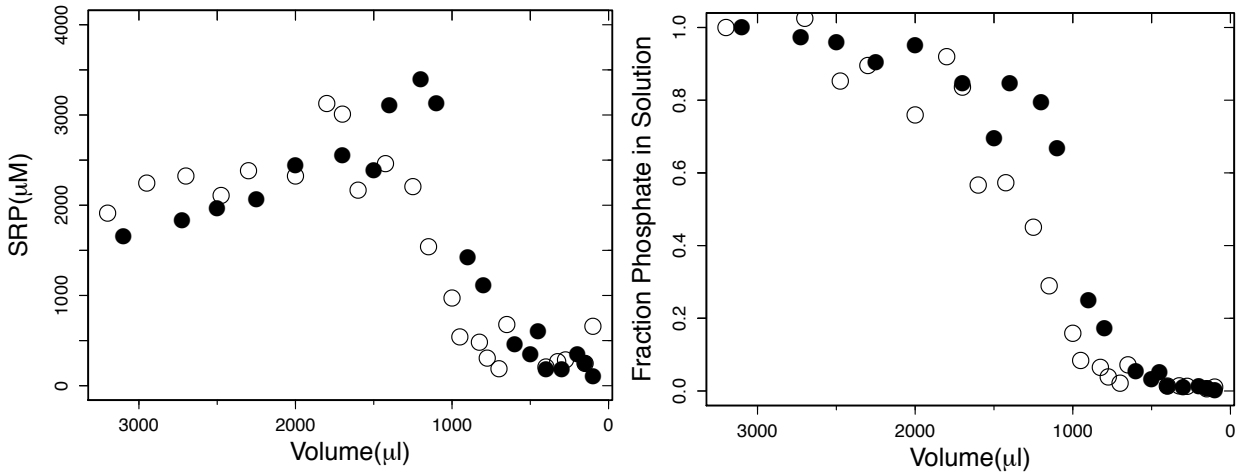

Figure 1.1 Slow Microprecipitation Solution Changes.
The slow microprecipitation proceeds as ammonium in the solution outgases and releases silver it previously complexed to the solution. As the microprecipitation solution declines, soluble reactive phosphorus (SRP) reaches a maximum at which Ag_3PO_4 precipitation begins. Ag_3PO_4 precipitation results in rapid declines in [SRP] and the fraction of phosphate remaining in solution. The fraction of phosphate remaining in solution when the volume is <300μl is zero and the precipitation is complete.

concentrations rise slightly with only minor removal to Ag_3PO_4 precipitate (Figure 1.1). The onset of rapid precipitation begins between 2000 and 1000 µl volume as a result of NH_3 outgassing and volume reduction supersaturating the solution with respect to silver phosphate. The pattern in phosphate removal related to solution volume is highly repeatable, with both replicates in Figure 1.1 exhibiting completion of Ag_3PO_4 precipitation by the time the solution had reduced to 500 µl. In subsequent testing of the Slow microprecipitation, we terminated precipitations when the volume reached 250 – 400 µl. Continued volume reduction leads to flash crystallization of the remaining solution, likely as a hydrated NH_4NO_3 salt. When this happens, preliminary testing suggests that removal of the highly soluble NH_4NO_3 by repeat DI water rinses has minimal to no impact on the $\delta^{18}O$ of Ag_3PO_4. We still advise avoiding this condition out of concern that insoluble silver oxides could form and contaminate the Ag_3PO_4 under certain circumstances.

Complete removal of phosphate to Ag_3PO_4 in the Slow microprecipitation results in precipitate with $\delta^{18}O$ indistinguishable from the values measured for the macroprecipitations (Figure 1.2C). We also note that the phosphate removal curves in Figure 1.1 are specific to working with roughly 5-6 micromoles of phosphate and initial precipitation solution volumes and compositions indicated in Table 1.2. These patterns can change when using smaller amounts of phosphate and downscaling the volume of silver ammine solution, discussed in Section 3.6

The Rapid A and B precipitations are initiated by addition of $AgNO_3$ to a phosphate containing solution. We tested the efficiency with which phosphate is removed by these precipitations as a function of the solution pH prior to addition of $AgNO_3$. These solutions were initially acidic, simulating the Rapid A protocol with HNO_3 and NaF. The pH was raised to the

indicated values using NH_4OH for most scenarios, replicated with KOH for the two most basic conditions.

A substantial portion of the starting phosphate remained in solution when these Rapid A precipitations were initiated in solutions starting at pH ≤ 7 and pH > 10 (Figure 1.2A). The increase in silver phosphate solubility at low pH causes approximately 20-30% of initial phosphate to remain in solution at a starting pH of 6 or lower. The solubility of Ag_3PO_4 increases as the degree of phosphate protonation increases under acidic conditions (1^{st}, 2^{nd}, and 3^{rd} acid dissociation constants with pKa of ~2.12, 7.21, 12.67 at 25°C in dilute solution) (Dean, A.J., 1999). Increasing pH to high values with NH_4OH produces a similar trend, leaving roughly 65% of the original phosphate in solution at pH 10.5-11. Silver phosphate is soluble in ammonium hydroxide, and for a fixed amount of ammonia/ammonium, this effect becomes pronounced at pH approaching or exceeding the pKa of ammonium (~ 9.3 at 25°C in dilute solution). When this experiment was repeated with the substitution of KOH for NH_4OH in the pH adjustment step, > 95% of sample phosphate was precipitated at high pH, confirming the role of silver-ammonia complexes in enhancing Ag_3PO_4 solubility in that pH range. Thus, for fixed total concentrations of dissolved silver and phosphate, Ag_3PO_4 solubility in ammonia/ammonium solutions is greatest at high pH (due to reduced free $[Ag^+]$) and low pH (due to reduced free $[PO_4^{3-}]$).

The $\delta^{18}O$ measurements of the Ag_3PO_4 crystals precipitated using Rapid A show substantial offsets towards lighter isotopic compositions than expected for nearly all of the samples precipitated at pH ≤ 7 and for a sample precipitated at pH = 11. The only sample whose isotopic composition was indistinguishable from the macroprecipitation was the pH 10 precipitate (the pH 9 precipitate was lost during weighing, and therefore not analyzed). This was

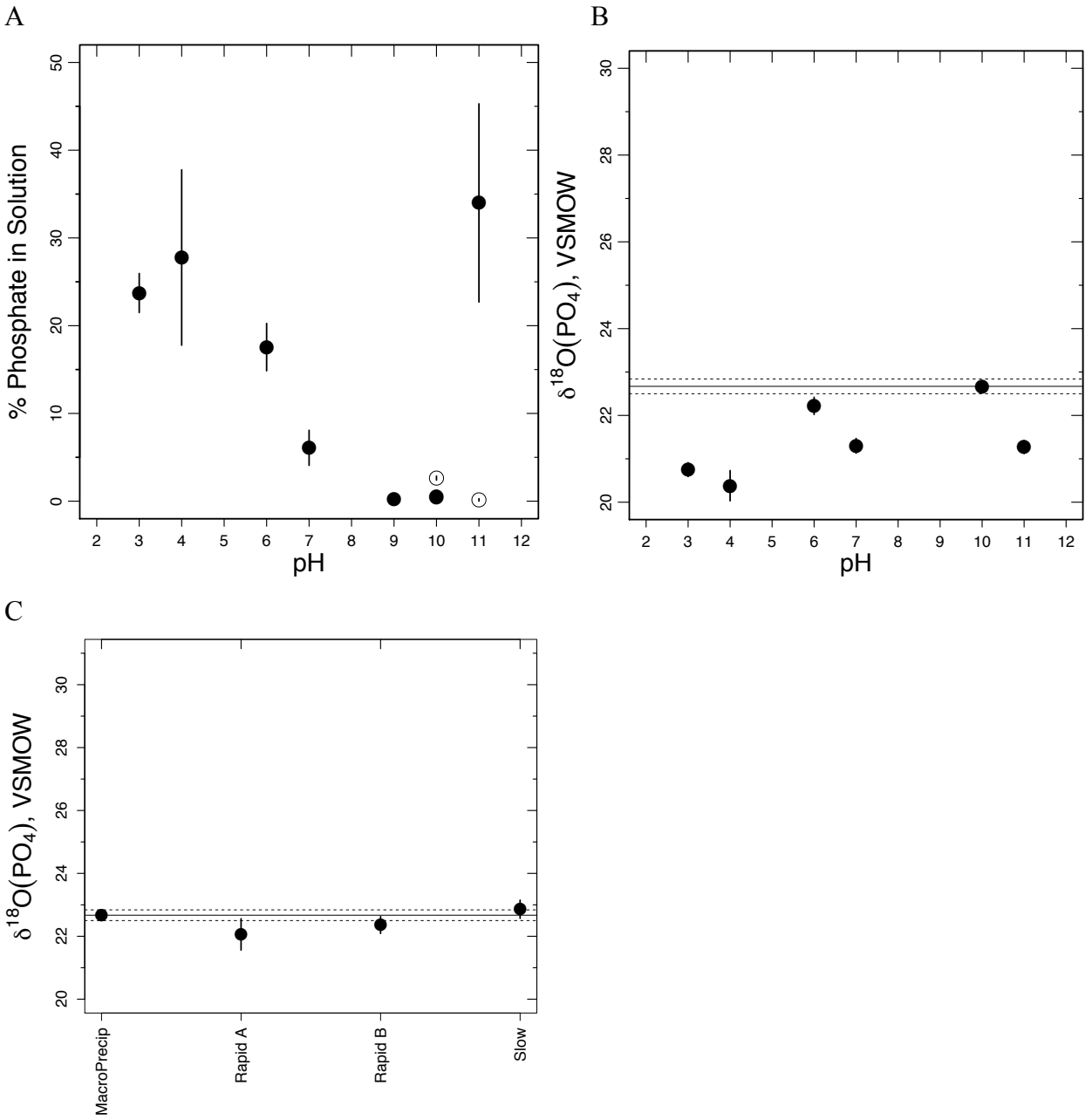

Figure 1.2 Rapid A Microprecipitations

(A) Phosphate in Solution– Percentage of sample phosphate remaining in solution subsequent to silver phosphate precipitation at specified pH. Adjusting pH outside the circumneutral range increases the amount of phosphate in solution by up to 35% of original sample phosphate. Open symbols represent precipitation solutions where pH was adjusted with KOH, while black, filled symbols are solutions pH adjusted with NH_4OH. Error bars represent the standard deviation for a measurement completed at least in triplicate. (B) Phosphate Oxygen Isotopic Composition vs. pH– Samples precipitated in solutions with pH <10 and >10 show marked deviations from the expected $\delta^{18}O_p$. Error bars represent the standard deviation for a measurement completed at least in triplicate. The mean and standard deviation for the expected $\delta^{18}O_p$ are shown by the **Figure**

1.2 continued…horizontal solid and dashed lines respectively. (C) Comparison of Macroprecipitation and Microprecipitation Compositions– Monobasic potassium phosphate was precipitated via three different microprecipitation methodologies and compared against a macroprecipitation of the same phosphate stock solution. The dark line represents the mean and the dashed lines represent standard deviation for macorprecipitation samples measured in triplicate.

also the only sample for which all phosphate was removed from solution during the precipitation, indicating a quantitative recovery of phosphate as Ag_3PO_4. However, the observed $\delta^{18}O_p$ values appear to be a complicated function of phosphate precipitation efficiency and pH (Figure 1.2B). The results could be explained by incomplete phosphate recovery coupled with kinetic isotope effects or the presence of O-bearing contaminants or a shifting combination of the two.

3.2. Testing for contaminants in Ag_3PO_4 precipitates

3.2.1. Precipitation experiments with KH_2PO_4 and ^{18}O-labeled water

The original testing of slow and rapid microprecipitations (Fig. 1.2C employed laboratory DI water ($\delta^{18}O_w$= -5‰) for making all salt solutions and diluting concentrated HNO_3 and NH_4OH. Slow and Rapid A microprecipitations were then run in solutions spiked with $H_2{}^{18}O$ to produce reagent water with $\delta^{18}O_w$= +100‰. The resultant slow microprecipitation using KH_2PO_4 as a phosphate source gave a measured $\delta^{18}O_p$ of 24.1‰ (+/- 0.12‰, 1 s.d.) as compared with 22.7‰ (+/- 0.29‰, 1 s.d.) for the unspiked treatment. Rapid A microprecipitations in the $H_2{}^{18}O$ spiked solutions measured 30.2‰ (+/- 0.5‰, 1 s.d.), as compared with 22.1‰ (+/- 0.5‰, 1 s.d.) for the unspiked treatment. Both microprecipitations shifted in the direction of the $\delta^{18}O_w$ in the spiked solutions (Figure 1.3). Vacuum roasting helped to correct at least some of the shift, and is discussed in detail later. The magnitude of these isotopic shifts points to minor presence of a contaminating oxygen phase in the slowly precipitated Ag_3PO_4 and much more significant contamination in the rapidly precipitated Ag_3PO_4. This could be caused by direct incorporation of water (e.g., as fluid inclusions) in the Ag_3PO_4 crystals, or the incorporation of a solid O-bearing contaminant on or in the Ag_3PO_4 crystals. Given the solution composition, candidates for solid phases contaminants include AgOH, Ag_2O via an AgOH intermediary, and Ag_2CO_3.

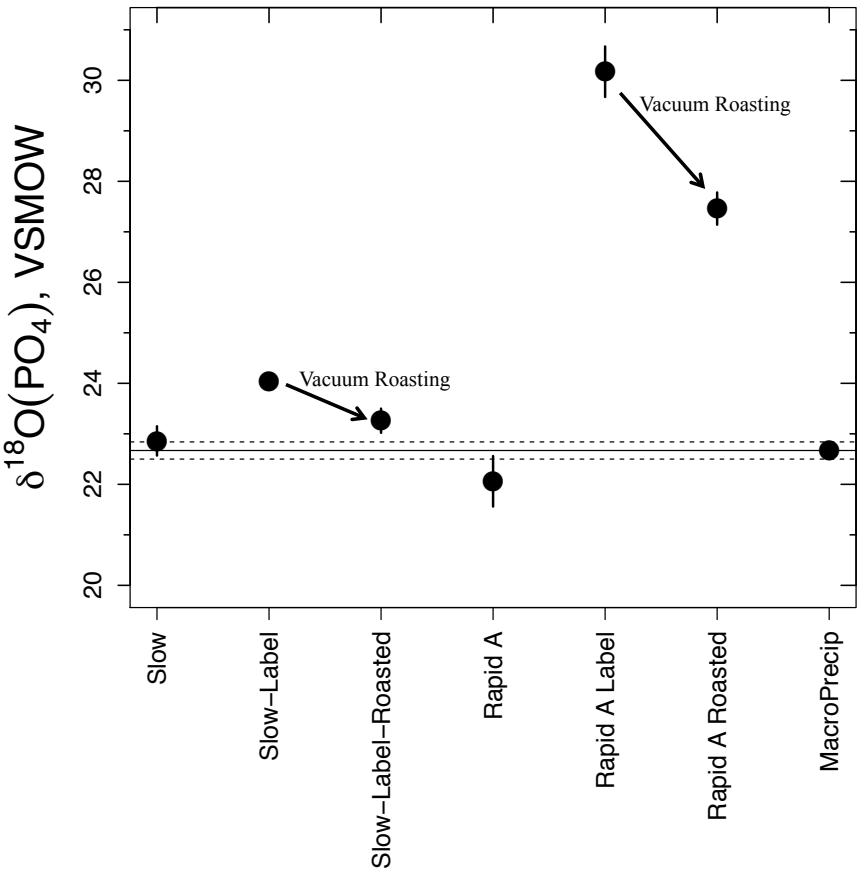

Figure 1.3 The $\delta^{18}O$ measured on Ag_3PO_4 microprecipitation in $H_2{}^{18}O$ solutions. Monobasic potassium phosphate precipitated via slow and Rapid A microprecipitations. Precipitation solutions spiked with ^{18}O-label to bring solution with $\delta^{18}O_w = +100$. Precipitations were then vacuum roasted where observed shifts towards expected isotopic compositions. The mean and standard deviation for the expected $\delta^{18}O_p$ are shown by the horizontal solid and dashed lines respectively. Error bars represent the standard deviation for a measurement completed at least in triplicate.

All three have limited solubility at elevated pH.

Both OH^- and CO_3^{2-} would exchange O with reagent water. Direct reaction of dissolved O_2 with Ag^+ in aqueous solutions has been shown to be slow. However, a two-step reaction in which Ag^+ first forms metastable AgOH that matures to Ag_2O has been observed and would lead to Ag_2O with an oxygen isotope composition that is sensitive to $\delta^{18}O_w$. The $\delta^{18}O$ of OH^- and CO_3^{2-} ions in solution would be offset from $\delta^{18}O_w$, and a combination of equilibrium and kinetic effects could lead to isotopic offsets between these ions in solution and corresponding ions bonded to silver. Nevertheless, the contaminant phase $\delta^{18}O$ would still scale with $\delta^{18}O_w$ for all of the most likely contaminants.

3.2.2. Precipitation experiments with modern bioapatite and ^{18}O-labeled water

We also tested the slow vs. rapid microprecipitation techniques in processing phosphate derived from modern bioapatite using homogenized powdered enamel from a goat in the Cocinetas Basin, Colombia (close to sea level, ~ 12°N, semi-arid climate) was characterized isotopically to be 24.0‰ (+/- 0.26) on Ag_3PO_4 formed via slow microprecipitation. Oxidative pretreatment procedures, e.g. treating the sample with a bleach solution, are commonly used to remove organics from modern bioapatite samples prior to silver phosphate precipitation (Wiedemann-Bidlack et al., 2008). In conventional slow precipitations, the presence of dissolved organic molecules can lead to the production of dark brown or black Ag_3PO_4 crystals that are shifted to smaller sizes and less well defined crystal morphologies. This problem is more pronounced with organic rich starting materials such as dentine or bone. A NaOCl pretreatment is generally effective at preventing this problem.

Though enamel has a very low organic matter content, we decided to pretreat the modern enamel with NaOCl to eliminate the potential for small quantities of matrix organics to

compromise the rapid Ag_3PO_4 precipitations. We tested whether standard NaOCl pretreatments impacted measured $\delta^{18}O_p$ on slow Ag_3PO_4 precipitates. The untreated and pretreated samples were within 0.3 per mil (Figure 1.4A) using the slow precipitation method.

Rapid microprecipitations run on the same homogenized enamel, pretreated with NaOCl, show variability and susceptibility to shifts in measured isotopic composition. Silver phosphate precipitates derived from Rapid A and Rapid B measured on average 0.5 and 1.7‰ less than expected with considerable scatter.

The sensitivity of measured $\delta^{18}O_p$ to reagent water $\delta^{18}O$ was tested, again using an $H_2{}^{18}O$ label to produce solutions with $\delta^{18}O_w \sim +100$‰. Slow microprecipitations shifted 0.9-1.0‰ to higher $\delta^{18}O_p$ values; the $\delta^{18}O_p$ values of Rapid A and Rapid B precipitates shifted higher by 5.2 and 2.6‰ respectively. These results indicate that rapid precipitations of phosphate processed from bioapatite are prone to the same issues that were observed using clean potassium phosphate reagent as the phosphate source.

3.2.3. Precipitation experiments with fossil bioapatite and ^{18}O-labeled water

Fossil enamel apatite has insignificant preservation of organic matrix, so we followed standard practices and did not treat this material with NaOCl. The $\delta^{18}O_p$ of a homogenized enamel powder derived from a Miocene toxodont tooth from northern South America precipitated via slow microprecipitations was 18.3 ± 0.2‰. Slow microprecipitation of this same bioapatite phosphate, using reagent solutions labelled in $\delta^{18}O_w$ to ~ +100‰, increased measured $\delta^{18}O_p$ values only slightly (~1.0‰, Fig. 1.4B, Table 1.1).

The $\delta^{18}O_p$ measured on Rapid A precipitates derived from the unlabeled precipitation solution are in good agreement with the analogous slow precipitates; Rapid B precipitates are measured $\delta^{18}O_p$ for Rapid A and Rapid B were shifted to significantly higher values by ~10‰

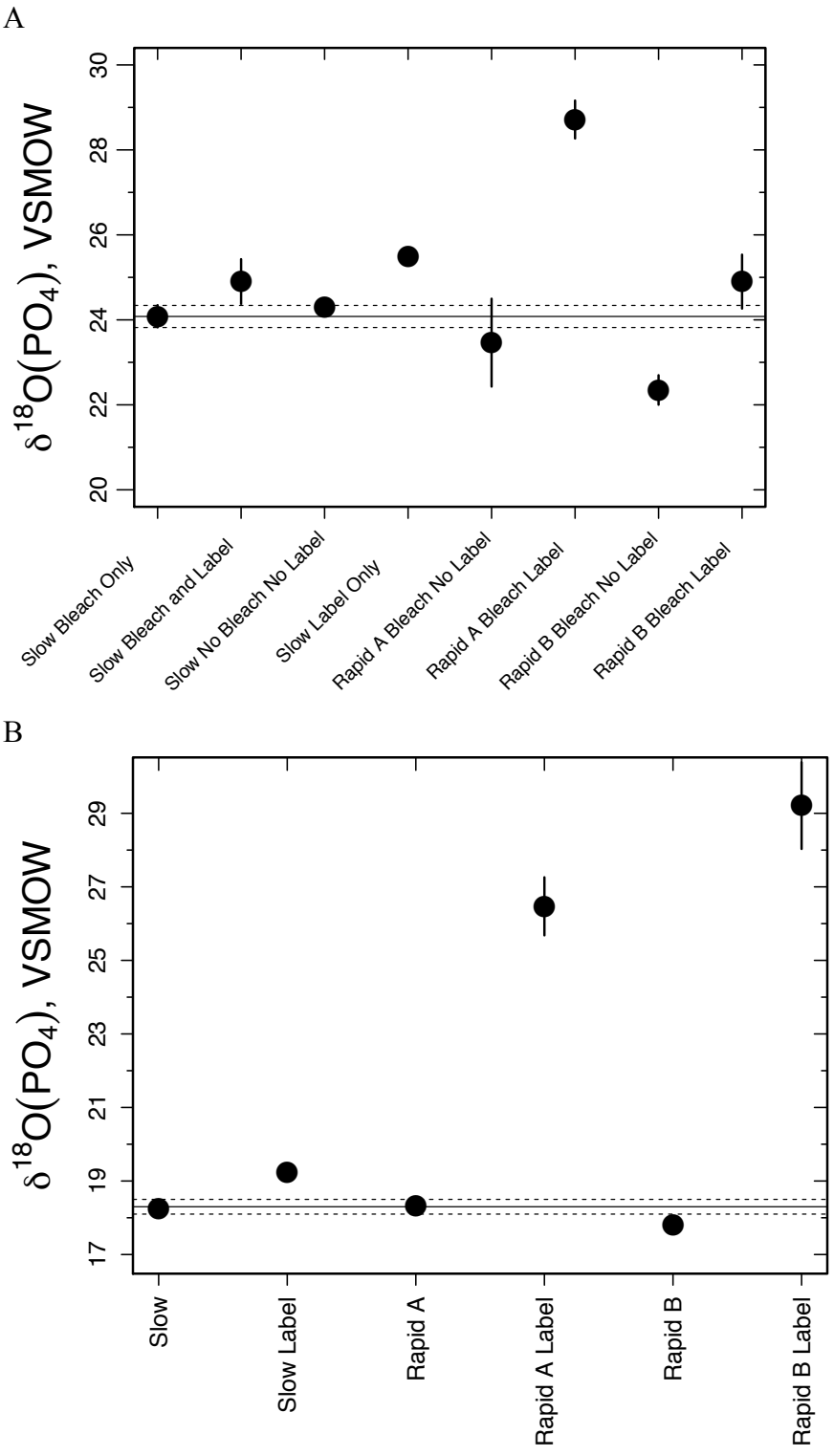

Figure 1.4 Modern and Fossil Bioapatite Microprecipitations
(A) Comparison of Slow and Rapid Microprecipitation on Modern Apatite with ^{18}O-label and bleach - Pretreatment of bioapatite with bleach shows no effect on measured $\delta^{18}O_p$. Silver

Figure 1.4 continued…phosphate slow microprecipitations in ^{18}O-labeled solutions with $\delta^{18}O_w$= +100 ‰ show measured $\delta^{18}O_p$ increases of 0.85-1.0 ‰. Crash microprecipitations via Rapid A and Rapid B methodologies show larger variation from expected value and increased isotopic shifts when precipitated in ^{18}O-labeled solutions. Error bars represent the standard deviation for a measurement completed at least in triplicate. (B) Comparison of Slow and Rapid Microprecipitation on Fossil Apatite with ^{18}O-label- Slow microprecipitations of fossil bioapatite are used as a reference with the mean and standard deviation plotted in solid and dashed lines respectively. Fossil Slow Label is a silver phosphate microprecipation in a solution with $\delta^{18}O_w$ = +100. Similarly Fossil Rapid A Label and Fossil Rapid B Label reflect fossil bioapatite precipitated in a solution with $\delta^{18}O_w$ = +100. Rapid microprecipitations of fossil bioapatite show marked deviation from slow microprecipitations in solutions with $\delta^{18}O_w$ = +100, suggesting exchange oxygen between fossil bioapatite and water. Error bars represent the standard deviation for a measurement completed at least in triplicate.

and ~11‰, respectively. These results are similar to the patterns observed with KH_2PO_4 and modern bioapatite derived phosphate, confirming the susceptibility of rapid microprecipitates to O-bearing contaminants whose isotopic composition is linked to the reagent solution $\delta^{18}O_w$.

Despite the sensitivity of the rapid precipitates to solution $\delta^{18}O_w$, measured $\delta^{18}O_p$ values on rapid precipitates from fossil bioapatite using lab DI water do not deviate significantly from expected $\delta^{18}O_p$ (18.3‰, as determined by the slow precipitations). We speculate that this occurs because the contaminant oxygen is isotopically similar to sample phosphate oxygen. In contrast, the contaminant is isotopically lighter than the phosphate from reagent KH_2PO_4 and modern enamel apatite (22.7‰ and 24.0‰, respectively), causing noticeable shifts to lighter isotopic compositions on the rapid precipitates produced from these samples.

3.2.4. Optical and SEM imaging and EDS compositional analysis

Formation of O-bearing silver coatings or particulate phases is one possible mechanism for shifting measured isotopic composition away from expected $\delta^{18}O_p$ values. We investigated surface contaminant formation initially through optical inspection of Ag_3PO_4 crystals produced via rapid and slow microprecipitations. These observations were extended SEM imaging and EDS compositional analysis to determine the extent of contaminating silver phases.

Optical microscopy of Ag_3PO_4 crystals reveals significant differences in crystal size and morphology between the rapid and slow precipitations. Slow microprecipitations exhibit large (1-2mm), euhedral or dendritic, bright yellow silver phosphate crystals (Figure A2) that occasionally trend towards darker colors. Meanwhile, rapid precpitations are fine (~0.1mm) euhedral crystals with color ranging from bright yellow to dark brown. Color variability is observed in both slow and rapid microprecipitations, but with no observable correlation with the $\delta^{18}O_p$ of slow precipitates.

Rapid microprecipitations frequently darkened from bright yellow to brown during rinsing. This sometimes occurs to a lesser extent with slow microprecipitations. In both cases, this is generally a surficial phenomenon. If the darker layer possesses an oxygen isotope composition that differs from the bulk phosphate, then the effect on measured $\delta^{18}O$ would be much more pronounced for rapid precipitations due to their much higher specific surface area and resultant higher loading with the isotopically anomalous layer.

SEM imaging and EDS reveal textural and compositional differences between slow and rapid microprecipitates. Ag:P ratios are a useful determinant of the extent of contaminant overgrowth. EDS examinations of slow microprecipitations showed Ag:P of 3.0 varying over a total range of ± 0.3. The adherence of slow microprecipitations to the stoichiometric Ag:P ratio demonstrates that the resultant precipitate is very pure Ag_3PO_4, in good agreement with the $H_2{}^{18}O$ label experiments. Rapidly precipitated Ag:P ratios were generally around 4, suggesting that the surface is a mixture of silver phosphate and other silver phases.

3.2.4. Testing for occluded water and AgOH in Ag_3PO_4 precipitates

Occlusion of water or formation AgOH could contribute contaminant H and O to Ag_3PO_4 precipitates. Quantitation of water and AgOH was investigated by monitoring for H_2 release from TCEA processing of Ag_3PO_4 produced via both slow and rapid microprecipitations. If the O derived from either H_2O or hydroxyl ions had an isotopic composition in the realm of bulk solution $\delta^{18}O_w$, then contaminant oxygen would need to represent over 2% of total oxygen in the sample in order to shift the measured isotopic composition beyond instrumental precision. This would have generated H_2 peaks on the order of 500-1000mV. Instead, sample acquisition traces from runs in which H_2 and CO were both monitored show hydrogen peaks that are 2 orders of

magnitude smaller (5-10mV, Figure A1). The absence of large H_2 peaks therefore implicates a solid, anhydrous oxygen-bearing contaminant phase as the cause of the $\delta^{18}O$ shifts.

3.2.5. Testing for presence of $AgNO_3$ or NH_4NO_3 in Ag_3PO_4 precipitates

The amount of residual $AgNO_3$ or NH_4NO_3 on Ag_3PO_4 precipitate that would result from inadequate rinsing can be estimated from the N_2 peak seen eluting prior to the CO peak in a TCEA analysis for $\delta\,^{18}O_p$. Runs on pure AgNO3 gave CO:N_2 area ratios of ca. 6:1. Silver phosphate runs did not have any N_2 peaks above the normal peak detection cutoff. Modification of the peak detection parameters for more sensitive detection of the N_2 peak revealed a very small peak, typically 0.5-1.0 V*s, versus the CO peak of 300-400 V*s. This translates to 0.025% contamination of the oxygen, if the N_2 peak is only from NO_3^-.

3.2.6. Testing for $Ag_2(CO_3)$ as a contaminant phase

Silver carbonate was investigated as a potential contaminant phase on a very fine Ag_3PO_4 powder that developed a significant coating of a silver phase sans phosphate during immersion in silver ammine solution (described more fully in section 3.4). Rapid A, Rapid B, and Slow microprecipitations using standard methodologies were tested for trace amounts of carbonate. Carbonate content analyses were completed a conventional phosphoric acid digestion employed for carbonate $\delta\,^{18}O$ and $\delta\,^{13}C$ measurements. Analysis for CO_2 evolved from carbonate indicated that Ag_2CO_3 was either a trace phase or not present (<0.5 wt% O as carbonate). Silver carbonate was determined to be a minor contaminant phase in all of the microprecipitations tested in this study.

3.3. The Effect of Vacuum Roasting on $\delta^{18}O_p$ of Ag_3PO_4

Vacuum roasting of Ag_3PO_4 crystals has been reported to shift crystal color from brown to yellow (Dettman et al., 2001), and this has been our observation, too. We examined whether vacuum roasting could reverse our observed isotopic shifts in $\delta^{18}O_p$ by removing oxygen contaminants. Rapid A $\delta^{18}O_p$ values from the precipitates that had acquired ^{18}O label decreased upon roasting at 400°C for 30 minutes by 2.7‰ towards the expected isotopic composition for monobasic potassium phosphate (Fig. 1.3). Slow microprecipitations from similarly ^{18}O-labeled solutions show a 0.5‰ decline towards accepted $\delta^{18}O_p$ values after vacuum roasting. Though these shifts were in the direction of restoring measured $\delta^{18}O_p$ to the known Ag_3PO_4 values, the restoration was incomplete. Rapid A microprecipitations maintained compositions 4.7‰ greater than expected even after vacuum roasting. This indicates that either contaminant removal was incomplete or that O from the contaminant exchanged with phosphate O during the heating. The 400°C roasting was above the temperature required for release of occluded water and for thermal decomposition of silver oxide, silver hydroxide, and silver carbonate (L'vov, 1999), which are the most likely contaminants. Therefore O exchange likely occurred between contaminant and phosphate during the vacuum roasting.

3.4. Mass gain and isotopic shift due to exposure of fine grained Ag_3PO_4 to silver ammine solution

We tested whether exposure of fine-grained Ag_3PO_4 to silver ammine solution could result in the same issues with formation of a contaminant phase that we observed during rapid precipitations. We incubated reagent Ag_3PO_4 from Strem Chemicals, one of our lab phosphate oxygen isotope standards ($\delta^{18}O_p$ = 8.2 ‰), in a solution that mimicked the composition of the

rapid A precipitation solution, minus the phosphate. In some of the incubations, an $H_2{}^{18}O$ spike was added to raise the solution $\delta\,{}^{18}O_w$ to ca. 100‰. The tests with ^{18}O label included adding the label prior to the start of the incubation or after 10 minutes of incubation. The incubations lasted either 10 minutes or 4 days for the pre-spike treatment and for 4 days for the delayed spike. The length of 10 minutes for the short incubation was chosen as representative of the interval between initiating a rapid precipitation and rinsing that precipitate.

The Strem Ag_3PO_4 that was only briefly exposed (10 minutes) to the silver ammine solution accumulated brown precipitate and gained up to 30% in mass. The isotopic values in experiments using reagents prepared in unspiked DI water exhibited only a slight (< 2 ‰) shift in measured $\delta\,{}^{18}O$ (Fig. 1.5, Table 2) to isotopically lighter compositions. Analogous experiments conducted in the ^{18}O-labelled solution shifted the measured $\delta\,{}^{18}O$ values higher by 4.5 ‰.

For samples of this same Ag_3PO_4 that was left immersed for 4 days, the brown precipitate accumulated rapidly, but did not increase the mass gain beyond the 30% that was also observed for some of the 10 minute incubations. The measured $\delta\,{}^{18}O$ values of these 4 day incubations were an additional ~3-5‰ higher than the values for the spiked incubations that were incubated only 10 minutes. The 4 day incubations that had the $H_2{}^{18}O$ spike administered to the solution prior to immersion of Ag_3PO_4 had similar isotopic compositions to the delayed spike incubations, within statistical uncertainty (Fig. 1.5). The magnitude of these shifts is similar to those observed in the rapid microprecipitation tests described earlier (Fig. 1.3).

These observations indicate that the contaminant phase can form on Ag_3PO_4 surfaces and need not co-occur with precipitation. The incorporation of additional label with longer exposure, even in the absence of additional mass gain, suggests that the phase may continue to exchange O with reagent water.

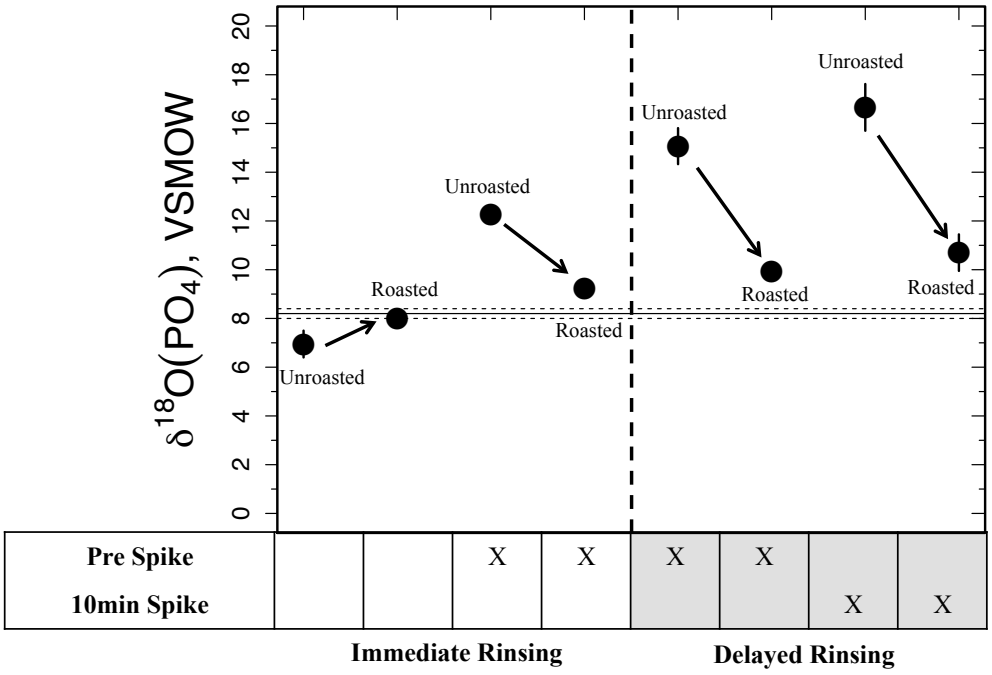

Figure 1.5 Isotopic shifts in Ag_3PO_4 powder immersed in $H_2{}^{18}O$-labeled $AgNO_3$ solution. Silver phosphate standard Strem was immersed in Rapid A microprecipitation solutions free of phosphate. Error bars represent the standard deviation for a measurement completed at least in triplicate. Spike column refers to tests where the ^{18}O-labeled water was added to solution. Pre spike refers to $H_2{}^{18}O$ spike prior to precipitation and 10min spike refers to $H_2{}^{18}O$ spike subsequent to immersion of Strem standard. Other listed rows include details about the timing of crystal rinsing with DI and sample vacuum roasting at 365°C for 30 min. Isotopic measurements showed varying measured $\delta^{18}Op$ values as the solution $\delta^{18}O_w$ was increased to +100 ‰ and as rinsing was delayed. Vacuum roasting of these samples leads to dramatic (~5 ‰) shifts in measured $\delta^{18}O_p$.

In addition, EDS scans revealed widely varying Ag:P ratios in the Ag_3PO_4 powder following the immersion treatments. These Ag:P ratios ranged from 3 to 25, and generally far exceeded the Ag content of Ag_3PO_4, implicating accretion of secondary silver phases in the mass gain and shifts in $\delta\,^{18}O_p$. These data support the hypothesis that fine crystals provide abundant nucleation sites for contaminating oxygen species to form when microprecipitation solutions stray towards basic pH values.

We investigated whether vacuum roasting could remove the contaminant oxygen isotopic signal and mass gain acquired during the powdered reagent Ag_3PO_4 incubations in labeled silver ammine solution. Vacuum roasting shifted $\delta^{18}O_p$ and weight % oxygen toward expected values for the Strem standard (Table 1.2, Fig. 1.5). However, vacuum roasting did not fully restore the Ag_3PO_4 to its original value, with offsets in $\delta\,^{18}O_p$ exceeding 1‰. This indicates that some of the contaminant oxygen is driven off during vacuum roasting, whereas some is either retained or exchanges with phosphate oxygen. The shift in weight % oxygen is consistent with a contaminant that is mainly AgOH, with minor Ag_2O, converting to Ag^0 during roasting. The H_2 yield test on Ag_3PO_4 rapidly precipitated in our lab (Section 3.2.2.) had ruled out AgOH as a significant contaminant phase in that precipitate. However, the mechanism by which Ag_2O forms may require a dehydration reaction approximating $Ag_2(OH)_2 \rightarrow Ag_2O + H_2O$ (Biedermann & Sillén, 1960). We speculate that the very finely powdered Ag_3PO_4 used in the immersion experiments may have a higher density of surface features (steps, screw dislocations, etc.) that could act to stabilize a phase with AgOH stoichiometry against dehydration.

In this study, the roasted samples were weighed and analyzed soon after roasting. Formation of elemental silver during vacuum roasting could prove problematic for longer-term

storage, during which roasted samples may be prone to reoxidation of the elemental silver with an associated shift in measured $\delta^{18}O$.

3.5. General Discussion of Current Protocols

The rapid precipitation approaches tested above frequently produce Ag_3PO_4 with offsets up to 1-2‰ between measured $\delta^{18}O_p$ values and accepted values. This holds true regardless of whether the phosphate source is a reagent KH_2PO_4, modern bioapatite, or fossil bioapatite. The isotopic offsets from accepted values appears to result from two different effects. At moderate to low starting pH (≤ 7), prior to silver nitrate addition, and following the most frequently used protocols from the literature (Rapid A and Rapid B), a significant quantity (5-40%) of phosphate is left in solution following the rapid precipitation. The most likely explanation for these isotopic shifts is fractionation during incomplete precipitation, i.e., kinetic isotope effects result in the precipitate having a different $\delta^{18}O$ from the residual phosphate in solution.

During rapid precipitation under higher pH conditions, the formation of additional O-bearing silver phases occurs and can produce isotopic offsets between phosphate and bulk precipitate. The magnitude and direction of the shifts in measured $\delta^{18}O$ values of rapidly precipitated Ag_3PO_4 (regardless of whether the phosphate derives from reagent KH_2PO_4, modern bioapatite, or fossil bioapatite) vary systematically with precipitation solution $\delta^{18}O_w$. These offsets are typically on the order of 1-2‰ for normal combinations of reagent $\delta^{18}O_w$ and sample $\delta^{18}O_p$. However, sometimes the combination of sample and reagent $\delta^{18}O$ result in a contaminant that is isotopically similar to the phosphate and does not shift measured $\delta^{18}O_p$ beyond the analytical uncertainty.

The most likely candidate phase for the O-bearing contaminant in rapidly precipitated Ag_3PO_4 is Ag_2O, based on the combination of SEM EDS data on Ag:P ratios, the absence of an H_2 peak from TCEA processing of precipitates, and the absence of appreciable CO_2 release following phosphoric acid digestion of the precipitates. The sensitivity of the Ag_2O to solution $\delta^{18}O_w$ likely implicates a reaction mechanism that involves hydroxyl ions with subsequent dehydration of $(AgOH)_n$ clusters either in solution or on Ag_3PO_4 surfaces. This could proceed via a reaction of the type $2\ Ag^+ + 2OH^- \rightarrow Ag_2O + H_2O$, with possible mediation through silver hydroxyl complexes (Biedermann & Sillén, 1960). There may be precipitation conditions under which AgOH (or even Ag_2CO_3) could be produced, as evidenced by the incubation of finely powdered reagent Ag_3PO_4.

We suspect two primary causes for the much greater susceptibility of rapid microprecipitations to acquisition of contaminant oxygen: higher silver concentrations and greater specific surface area of the precipitate. The most commonly used approaches for rapid microprecipitations employ a higher concentration of silver in excess of that needed for stoichiometric removal of all the phosphate as Ag_3PO_4 (Table 1.3). Higher silver concentrations will also lead to greater supersaturation and faster precipitation kinetics for contaminants, AgOH and Ag_2O, all other things being equal. The much smaller crystals produced during rapid precipitations result in a higher specific surface area and may produce more surface defect structures. Both of these effects likely produce a much higher density of nucleation surfaces for Ag_2O or precursor phases in the rapid precipitations. We also speculate that shielding of Ag^+ by complexing it with NH_3, that is starting with a silver amine solution, can also minimize the production of AgOH, and by extension, Ag_2O which can happen when mixing a silver nitrate solution with a basic solution. Using a silver amine solution is the approach taken in the Slow

	Rapid A	Rapid B	Rapid UC Conc	Rapid UC Dil	WLJ	Wiedemann Bidlack	Slow	Macro
$[Ag^+]$	0.0862	0.7143	0.4125	1.40E-01	0.201	0.0853	0.125625	0.0456
$[\Sigma PO_4^{3-}]$	4.31E-04	1.79E-03	3.13E-02	1.39E-02	1.25E-02	1.25E-02	1.25E-02	4.00E-03
Ag:P	200	400	13.2	9.9	16.1	6.8	10.1	11.4
K_{sp}*	2.76E-07	6.51E-04	2.19E-03	3.61E-05	1.02E-04	7.74E-06	2.48E-05	3.79E-07

Table 1.3 Compilation of Solution Compositions.

Concentrations of silver and phosphate vary widely across microprecipitation techniques. Here all values are calculated assuming a starting amount of 5 μmoles of phosphate (~1mg of bioapatite). ΣPO_4^{3-} is used to denote the sum of all dissolved phosphate in solution for a given microprecipitation, regardless of protonation. K_{sp}* is used to highlight that ΣPO_4^{3-} is used in the solubility product calculation. Rapid and Rapid B solution concentrations of silver and phosphate are determined from Dettman et al., 2001 the two methods suggested.

precipitations and the Rapid UC Dil precipitation presented in the next section. The Rapid A and B protocols combine $AgNO_3$ solution with a phosphate bearing solution whose pH has been elevated by addition of NH_4OH. The use of uncomplexed Ag^+ could allow for the reaction of Ag^+ with phosphate and OH^- to compete with one another and with complexation by NH_3 during mixing, potentially favoring production of larger quantities of silver hydroxide and oxide.

Slow microprecipitations result in complete conversion of aqueous phosphate species to precipitated Ag_3PO_4. The quantitative precipitation yields avoid the artifacts produced by kinetic and equilibrium fractionation that occur under standard rapid precipitation approaches in the pH range from circumneutral to acidic. Contaminant phases do not cause problems for $\delta\,^{18}O_p$ measured on slowly precipitated Ag_3PO_4, as evidenced by 3:1 Ag:P stoichiometry on the surfaces of slowly precipitated Ag_3PO_4, the relative insensitivity of measured $\delta\,^{18}O_p$ to precipitation solution $\delta\,^{18}O_w$, and the wt % oxygen results from TCEA analysis that are generally quite close to theoretical values for Ag_3PO_4.

Nevertheless, slow Ag_3PO_4 microprecipitations hinder high sample processing throughput. These precipitations tend to require careful monitoring in their end stages. Evaporation rates, and therefore the duration of precipitations, depend on not only temperature but also relative humidity of lab air, the amount of NH_4NO_3 buffer solution added, and air flow over precipitation vessels. Complete phosphate precipitation requires continuing the precipitation until solution volume diminishes from a starting volume that is usually 2.5 to 3.5 μl down to about 250-400 μl (Figure 1.1). Yet if volumes are reduced substantially further, then the entire solution can flash crystallize as impure, hydrated NH_4NO_3. The NH_4NO_3 is highly soluble; dissolving away the NH_4NO_3 and rinsing the Ag_3PO_4 precipitate that remains does not

shift $\delta^{18}O_p$ values. However we still deem it undesirable out of concern that it could promote the production of insoluble Ag(I) phases that could convert to Ag_2O and contaminate a sample.

We set out to develop a rapid Ag_3PO_4 precipitation technique that would avoid the isotopic artifacts detailed above that can accompany the commonly used rapid precipitation approaches. Samples that have high residual organic, metal (e.g., Fe and Mn staining) and chloride content may pose a challenge to any rapid precipitation protocol, and these samples would include phosphate concentrated from soil, seawater, and fresh water. However, clean samples should be amenable to a well-designed rapid precipitation technique.

3.6. A New Rapid Microprecipitation Technique

The main issues we have seen in the current protocols for the rapid precipitation of silver phosphate, namely incomplete recovery or presence of contaminant silver phases, are briefly mentioned in the classic literature on Ag_3PO_4 precipitations (e.g., Firshing, 1960; O'Neil et al., 1994). However, the rationale and full importance has not been fully discussed. We introduce a revised technique (Rapid UC Dil) that retains the benefits of rapid precipitation and avoids the problems that can arise with previous approaches. The key features of this revised technique are (1) avoiding high pH to prevent the formation of Ag_2O or other O-bearing silver phases and to avoid raising the solubility of Ag_3PO_4 via formation of silver ammine complexes; (2) avoiding low pH due to elevated solubility of Ag_3PO_4 under acidic conditions; (3) achieving high supersaturation with respect to Ag_3PO_4 by using small volumes of solution; (4) using only a moderate excess of Ag^+ to minimize the formation of secondary silver contaminant phases; (5) maintaining Ag^+ solubilization until Ag_3PO_4 precipitation by using silver ammine complex ions.

This shields Ag^+ from reaction with water to form AgOH and Ag_2O during the mixing of the solution with phosphate sample and the solution with Ag^+.

We note that the suite of chemical reactions during mixing of solutions has the potential to be quite complicated, with the competing kinetics of Ag_3PO_4 precipitation, $Ag(NH_3)_2^+$ dissociation, and AgOH formation and conversion to Ag_2O, and phosphate protonation-deprotonation reactions, all occurring in solutions that are changing pH in response to precipitation reactions. In small-volume, circumneutral precipitations, $[HPO_4^{2}]$ and $[H_2PO_4^-]$ are sufficiently high such that precipitation of these ions as Ag_3PO_4 releases enough protons to acidify the solution and produce a 2-3 unit shift in pH. Modest buffering can help prevent these shifts from significantly raising the solubility of Ag_3PO_4.

Rapid UC Dil and Rapid UC Conc microprecipitations were evaluated using both KH_2PO_4 and bioapatite as phosphate sources. The KH_2PO_4-based solutions contained HNO_3 and HF in concentrations used for bioapatite dissolution and subsequent treatment to remove Ca^{2+} as CaF_2. As with Rapid A and B, the Ag_3PO_4 precipitation is carried out by combining a phosphate sample solution with a dissolved silver solution. Unlike Rapid A and Rapid B methods, Rapid UC used a Ag-ammine solution modeled in some respects after Wenzel *et al*. (2001) to pre-complex the silver with ammonia prior to addition to the phosphate bearing solution.

We tested the relationship between final solution pH (following Ag_3PO_4 precipitation), the percentage of phosphate remaining in solution after the precipitation, and measured $\delta\,^{18}O_p$ (Fig. 1.6). The final solution pH was controlled by adjusting the pH of the phosphate solution prior to silver ammine addition. Consistent results require fresh (daily) preparation of ammonium hydroxide and Ag-ammine solutions to avoid significant ammonia outgassing.

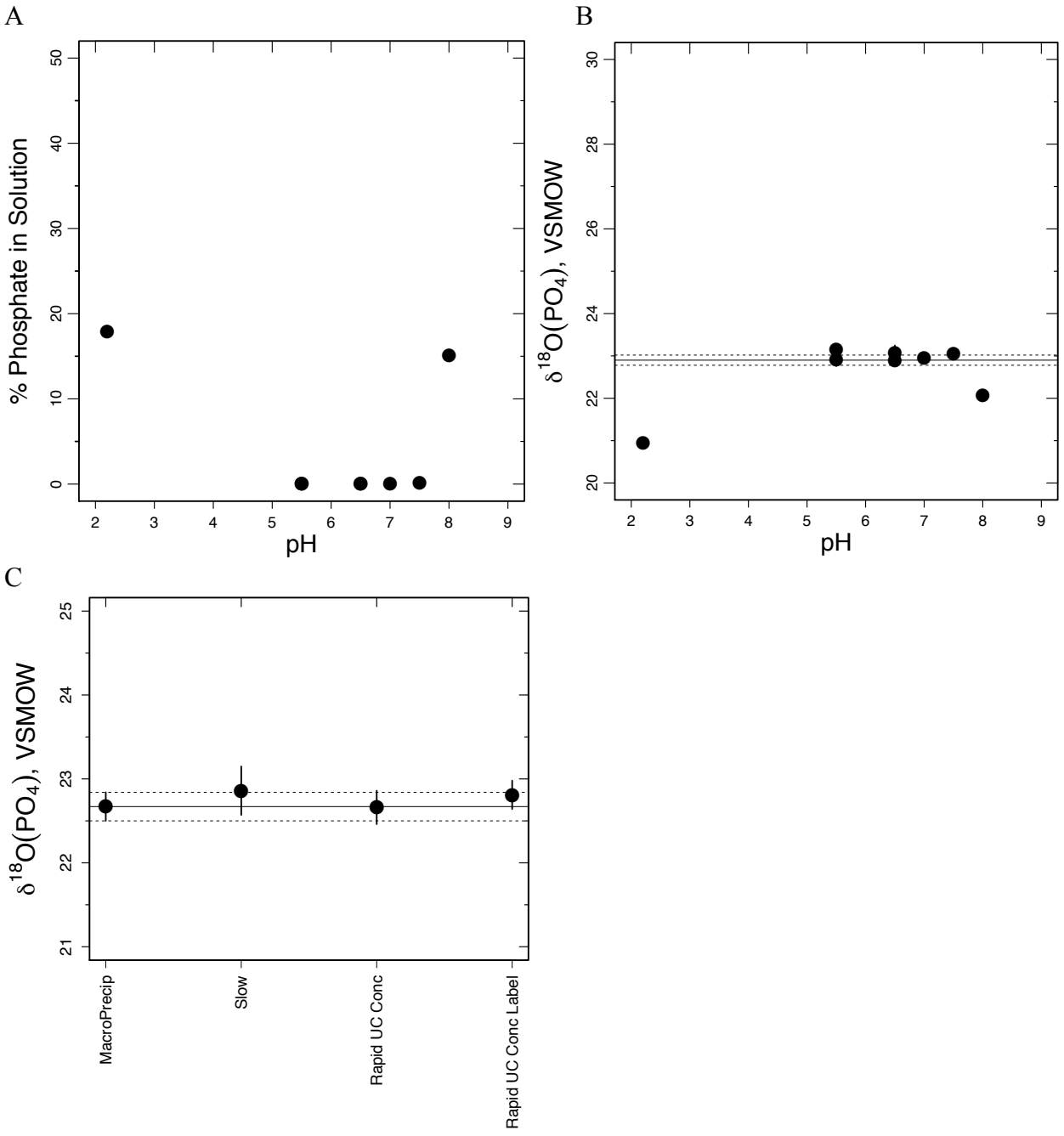

Figure 1.6 Rapid UC Conc and pH:
(A) and (B) The effect of solution pH on phosphate precipitation efficiency $\delta^{18}O_p$ using Rapid UC Conc method: As pH decreases below 5 and above 7 phosphate left in solution leads to a fractionated measured $\delta^{18}O_p$ value. With ca. 20% of phosphate remaining in solution sample $\delta^{18}O_p$ can be shifted by almost 2‰. Each data point represents a duplicate analysis for phosphate remaining in solution and $\delta^{18}O_p$. The solid line represents the expected $\delta^{18}O_p$ for monobasic potassium phosphate and the dashed lines represent the standard deviation. (C) Rapid U Conc comparison of microprecipitations of monobasic potassium phosphate with 18O-label: Rapic UC

Figure 1.6 continued…Conc methodology is in good agreement with macroprecipitation and slow microprecipitation of the same material. The Rapid UC Conc methodology shows a small isotopic shift (0.4 ‰) in precipitation solutions where $\delta^{18}O_w = 100$ ‰. Each data point represents a duplicate analysis for phosphate remaining in solution and $\delta^{18}O_p$. The solid line represents the expected $\delta^{18}O_p$ for monobasic potassium phosphate and the dashed lines represent the standard deviation

The Rapid UC Conc and Rapid UC Dil microprecipitations produces quantitative precipitation of phosphate over a broad range of final pH (ca. 5.5 - 7.5). The resultant $\delta^{18}O$ values agree well with both slow microprecipitations and slow large batch precipitations (Fig. 1.6), with only a small shift produced by precipitation in ^{18}O-labeled water experiments. The pH of the sample solutions requires careful adjustment so that the final pH after mixing with the silver-ammine solutions is in the target range of 6 to 7. In practice, the optimal starting pH is determined empirically on test runs. Precipitates should be rinsed with DI water not long after they are formed. We have found that 10 minutes permits complete precipitation of phosphate and avoids formation of contaminant phases.

If the addition of the silver ammine solution were to bring the pH too high, e.g. > 8, incomplete precipitation will result. The addition of dilute nitric acid can be used to adjust the pH to the target range, which results in the completion of silver phosphate precipitation. The $\delta^{18}O$ of Ag_3PO_4 thus produced agrees within analytical precision with isotopic compositions measured on precipitate that is formed without a pH overshoot and correction.

Rapid UC Dil is a useful methodological approach for processing of modern and fossil enamel samples. This approach provides reliable and isotopically indistinguishable compositions for sample sizes of 2.5 and 5 μmoles (Table 1.4). Our results indicate there is no size effect on measure isotopic compositions such that reproducible data were measured from an array of samples types and with different isotopic compositions: fossil shark enamel, hydroxyapatite, and fossil subhydracodon. Small (2.5μmole) samples precipitated via Rapid UC Dil were within 0.2‰ of 5 μmole counterparts for all samples measured. These precipitations with bioapatite highlight that this safer, dilute method adapted from Rapid UC Conc can be used to ensure complete recovery of samples and with preserved isotopic compositions.

Sample ID	Material	PO_4 (μmoles)	Average $\delta^{18}O_p$	1σ	*n (trials)	**# of capsules
Rapid UC Dil Subhyracodon	fossil subhyracodon enamel	5	16.97	0.08	3	17
Slow Subhyracodon	fossil subhyracodon enamel	5	16.97	0.11	3	12
Rapid UC Dil Subhyracodon	fossil subhyracodon enamel	2.5	16.89	0.06	3	9
Slow Subhyracodon	fossil subhyracodon enamel	2.5	16.52	0.26	3	3
Rapid UC Dil Shark	fossil shark enamel	5	21.06	0.05	3	19
Slow Shark	fossil shark enamel	5	20.96	0.06	3	13
Rapid UC Dil Shark	fossil shark enamel	2.5	21.08	0.07	3	8
Slow Shark	fossil shark enamel	2.5	20.63	0.14	3	6
Hydroxyapatite Slow	hydroxyapatite	5	13.32	0.14	4	11
Hydroxyapatite Rapid UC Dil	hydroxyapatite	5	13.38	0.02	4	9
Hydroxyapatite Rapid UC Dil	hydroxyapatite	2.5	13.45	0.07	3	12
Hydroxyapatite Slow	hydroxyapatite	2.5	12.99	0.14	2	8

Table 1.4 Compilation of Rapid UC Dil Microprecipitations

*n (trials) indicates the number of replicate microprecipitations completed for a given Sample ID and Material.

**# of capsules is the number of capsules weighed and analyzed for $\delta^{18}O_{p.}$

4. Conclusions

The isotopic composition of phosphate oxygen is a central tool for paleoclimate reconstruction and an emerging measure to track phosphorus biogeochemistry in modern aquatic and soil environments. The oxygen isotope analysis of phosphate requires isolation of phosphate as Ag_3PO_4. Initially, Ag_3PO_4 precipitation protocols used large samples and slow precipitations. Many applications require processing of small samples (e.g., 0.3-1 mg bioapatite), and rapid precipitation techniques have gained favor, because they facilitate higher sample throughput. We have tested the most commonly employed approaches for rapid Ag_3PO_4 microprecipitation and discovered a susceptibility to incomplete precipitation of phosphate and to formation of contaminant oxygen-bearing minerals. These effects may result in shifts in measured sample isotopic composition on the order of 1-2‰, representing an uncertainty in calculated paleotemperature of 4.0-8.0°C.

These effects depend on the concentrations and speciation of dissolved silver and phosphate in separate reagent solutions just prior to mixing, and they relate to the saturation state and Ag:P ratio in the mixed solution during and following rapid precipitation of Ag_3PO_4. The most commonly followed rapid microprecipitation protocols depend on moderately elevated pH in order to ensure quantitative removal of sample phosphate from solution into Ag_3PO_4 precipitate. Incomplete recover at slightly acidic to acidic conditions was associated with isotopic fractionation. Yet the same elevated pH conditions that promote quantitative recovery of phosphate also often lead to the formation of silver oxide coatings on Ag_3PO_4 crystals. Labeling experiments with $H_2{}^{18}O$ show that the silver oxide thus produced is sensitive to the $\delta^{18}O$ of H_2O in the aqueous reagents, likely forming via the dehydration of an $(AgOH)_n$ intermediate. The potential for measured $\delta^{18}O_p$ to depend on the $\delta^{18}O_w$ of the precipitation

solution suggests that the same sample processed in labs with different lab water $\delta^{18}O$ (e.g., high latitude, high altitude, inland lab vs. low latitude coastal lab) would appear to have different $\delta^{18}O_p$ if phosphate were isolated using the most prevalent methods for rapid Ag_3PO_4 precipitation. Vacuum roasting of Ag_3PO_4 that has a silver oxide contaminant shifts the sample $\delta^{18}O$ closer to expected values, but $\delta^{18}O$ measurements can still be significantly offset either due to incomplete removal of the contaminant oxygen or exchange of contaminant O with phosphate O under the elevated temperatures that prevail during roasting.

In contrast to the behavior of rapid precipitations, the slow precipitation of Ag_3PO_4 from buffered solutions leads to Ag_3PO_4 microprecipitations that are indistinguishable in $\delta^{18}O$ from classic macroscale precipitations of the same material. We present a modified rapid microprecipitation technique that is suitable for processing bioapatites. This approach employs smaller volumes of solution, careful pH control, slightly buffered conditions, and complexation of Ag^+ with ammonia prior to its addition to a phosphate solution for Ag_3PO_4 precipitation. It results in quantitative recovery of phosphate over a broad pH range that is shifted to mildly acidic conditions, and it avoids the formation of silver oxide contaminants. We recommend both slow and the modified rapid microprecipitation approaches for routine use with bioapatites. The slow microprecipitation is likely more robust for less pure phosphate samples.

Chapter 2 –Nutrient Regeneration in the Wake of Cell Lysis

Abstract

The availability of phosphate plays a critical role in limiting primary production in large regions of the oceans, including major ocean gyres. To meet their metabolic needs, microbes use a variety of strategies to overcome orthophosphate limitation. Up-regulation of enzymes such as alkaline phosphatase (APase) allows hydrolysis of ambient dissolved organic phosphorus (DOP) compounds extracellularly or in the periplasmic space enabling transport of orthophosphate into the cell. Cell lysis releases cell components, including enzymes, into the environment. Enzymatic activity following lysis is an important, unquantified mechanism in nutrient regneration and the microbial loop. Constraining and quantifying the flux of inorganic nutrients produced by lysed cells is essential to our understanding of the microbial loop and controls on ocean biogeochemistry. Using pure cultures of *E.coli* MG1655, *Synechococcus* WH7803, and *Prochlorococcus* MED4, I quantify patterns of nutrient release following cell lysis in relation to continued enzymatic activity. In addition, lysis experiments were carried out with surface ocean microbial communities in the North Atlantic to monitor nutrient release and regneration for a period of days following lysis. Our experiments show that APase activity is sustained for many days after lysis. I observed a significant intial release of orthophosphate that accompanies lysis. This is followed by increasing phosphate concnentrations in lysis solutions over a period of days. Our observations suggest this is due to a combination of direct hydrolysis of DOP released during lysis, solubilization and hydrolysis of particulate organic phosphorus, and possibly polyphosphate decomposition. Incubations with a range of individual DOP compounds spiked into the lysate show rapid release of orthophosphate from phosphomonoesters and

pyrophosphate, modest release rates from phosphonates, and slow release from phosphodiesters. This work highlights the importance of extracellular nutrient regeneration pathways involving cellular debris for biogeochemical dynamics in marine ecosystems and ultimately the amount of carbon exported to the deep ocean.

1. Introduction

Primary production is driven by the availability of nutrients in the surface ocean, where nutrient access enables the production of cellular biomass. Nutrient availability in the ocean is a function of time and scale, where carbon, nitrogen, and phosphorus are the major elements limiting and co-limiting production (e.g. Karl 2002). Orthophosphate (P_i) is the preferred phosphorus substrate and can be readily transported into the cell for use in a variety of cellular processes or materials. However, orthophosphate is low in large regions of the ocean, often limiting or co-limiting production. Phosphorus cycling is inextricably coupled to nitrogen and carbon cycling and the mechanisms of microbes to relieve P-limitation have implications for the export and recycling of phosphorus, nitrogen, and carbon throughout the ocean. Organic nutrient forms, such as dissolved organic phosphorus (DOP), can exist at concentrations up to an order of magnitude above P_i concentrations, but require specialized mechanisms for cellular access (Cavender-Bares et al. 2001). In response to low nutrient availability, cells use selective enzymatic pathways for accessing larger DOP compounds that are broken down prior to transport into the cell (Perry 1972; Perry 1976). In order to sustain productivity, nutrient limitation necessitates efficient nutrient turnover and regeneration.

Nutrient regeneration is a dynamic process controlled by dissolved and particulate nutrient reservoirs. A strong decoupling exists between carbon and phosphorus during

regeneration such that particulate elemental ratios are often phosphorus poor. Phosphorus is preferentially remineralized from sinking particulate matter to relieve local nutrient stress and sustain primary production (Knauer 1979). However, the process of remineralization is poorly understood. The conversion of nutrients from particulate to dissolved forms is facilitated by a number of processes including autolysis, viral infection, or sloppy feeding by zooplankton. Quantification of the phosphorus remineralization flux requires considerations of microbe-scale metabolic reactions and nutrient status and form prior to the remineralization of particulate material.

The lability and form of particulate and dissolved nutrient reservoirs upon lysis is critical to determining the transformations that take place during the process of remineralization. Nutrient stoichiometry within the cell is controlled by cellular metabolism and nutrient status (Loladze & Elser 2011). For instance, increases in nitrogen fixing organisms in the North Pacific Subtropical Gyre has lead to declining particulate organic phosphorus (POP), attributed to shifting metabolic dominance to curb phosphorus demand (Karl, 1999). Therefore the reservoir of POP, DOP, and SRP is partially constrained by the organisms lysing and their respective metabolisms and responses to changes in nutrient availability.

Cellular metabolism is driven by internal phosphorus cycling, largely controlled by transport of phosphorus into the cell via the expression of important phosphorus related genes. Critical components and essential cellular machinery for phosphorus transport has been well characterized. Through the use of model organisms such as *E.coli* MG1655 notable discoveries include the identification of the Pho regulon, which has provided insight into phosphorus uptake in a range of bacterial taxons (Torriani-Gorini *et al.,* 1994). The Pho regulon is a suite of essential genes for transport of P_i across the membrane via activation of high affinity and low

affinity *pst* and *pit* transport systems in *E.coli*. Homologous high affinity (*pst)* transport systems for P_i are in many abundant surface ocean cyanobacteria, such as *Synechococcus* and *Prochlorococcus* strains, with the low-affinity transport system often lacking (Scanlan et al. 1993; Moore et al. 2005; Martiny et al. 2009). Absence of low affinity phosphate transporters in surface ocean phototrophs has been hypothesized as a response to lower orthophosphate availability.

Intracellular cycling of phosphate involves the rapid breakdown and formation of P-rich compounds (DNA, RNA, ATP, ADP *etc.*) essential to continued growth. Cycling of the intracellular P-reservoir is a complex interplay of an array of phosphorylation reactions and associated intermediates. Pyrophosphate (PP_i) is an important intracellular energy source formed during photophosphorylation, oxidative phosphorylation, glycolysis and the breakdown of ATP. Intracellular concentrations of PP_i and its constitutive enzyme pyrophosphatase (PPase) are essential to cellular survival of *E.coli*, where concentrations outside a homestatic mean leads to reduced growth rates and potential cellular death. Inhibition of DNA synthesis leads to build up of PPase intracellularly and in some cases inhibition of organismal growth (Lahti 1983). Considerations of the intracellular cycling of phosphorus and its associated intracellular nutrient forms remain critical to our understanding of the presence of extracellular phosphorus forms (*i.e.* DNA, ATP, PP_i) and their significance.

Nutrient availability plays an important role in the partitioning of phosphorus to different cellular reservoirs (*e.g* nucleotides, lipids etc). Amounts of phosphate in solid and/or cytosolic reservoirs within the cell have important controls on the ultimate regenerated nutrient flux when a cell is lysed. Dissolved intracellular estimates of P_i concentrations range from 2-20mM and derive from studies of *E.coli* (Bennett et al. 2009). Cyanobacterial cell volume is lower, but

estimates of phosphate in major cellular forms in *Synechococcus* and *Prochlorococcus* suggest at least 50% of phosphate is contained in DNA and RNA, while up to 18-28% is present in lipids and other structural materials (Bertilsson et al. 2003; Van Mooy et al. 2006). Moreover, *Synechococcus* and *Prochlorococcus* modulate cellular volume in response to varying nutrient conditions. At a minimum, changes in cellular volume demand changing amounts of phosphate stored in structural lipid components and account for the wide range in P-content of *Synechococcus* WH7803 (2.6 – 7.9 fg/cell). Fluctuatin cell volume increases ability to accommodate storage of surplus polyphosphate (polyP). The cellular form of polyP is often species-specific, but in some cases visible with microscopy as granules (Henry & Crosson 2013). PolyP storage was first thought as an overplus response. However, recent oligotrophic surface ocean populations exhibited polyP storage in seawater with P_i < 40nM in populations thought to be P-stressed. Moreover, the stability of the polyP released from a cell following lysis remains unknown, but preferential remineralization of the particulate polyP in the North Atlantic seems largely controlled by the presence of phosphorus enzymes being expressed and the nutrient status of ambient surface ocean microbes. Thus, an understanding of the impact of microbial metabolism on the rengenerative flux is essential to understanding and quantifying the transformation of phosphorus released in particulate and dissolved forms.

Understanding the significance of expression of P-acquisition strategies requires effective means to quantify expression and is essential to our understanding of nutrient regeneration. Variability in phosphate acquisition is a process of ecotypic and genotypic thrift driven by fluctuating organic and inorganic reservoirs of phosphate accessible for growth. Marine microbes have evolved a variety of enzymatic strategies for meeting their metabolic needs during phosphorus stress (Cembella 1984; Dyhrman & Palenik 2001). A range of P-acquisition genes

(*ppX, ppK, and 5ND*) highlight the variability in mechanisms to access the DOP reservoir notably those for phosphonate, polyphosphate and nucleotide degradation respectively. Enzymatic assays in P-limited regions have shown that phosphohydrolase enzymes and high affinity P_i transporters enable rapid consumption of available P_i and access to P in DOP compounds in the euphotic zone (0-150m) (Bjorkman & Karl 2003).

In addition to targeted enzymatic expression, microbes have evolved a range of other physiological strategies to mitigate nutrient limitation. Sulfur replacement of phosphorus in membrane lipids and streamlining of genomes are both means to overcome nutrient limitation and starvation (Van Mooy & Devol 2008; Kettler et al. 2007; Partensky & Garczarek 2010). Sulfoquinovosyldiacyglcerol (SQDG) formation, or substitution of sulfur lipids for phosphorus cell membrane lipid, reduces cellular P quota while maintaining function and has been observed in a range of phosphorus-limited, gyre ecosystems. Moreover, refining of genome size has reduced phosphorus demand in chromosomal DNA and genomic content to only necessary genes (Coleman & Chisholm 2007). *Prochlorococcus* MED4 contains at least 50% of cellular phosphate in its genome, suggesting that compartmentalization of phosphate in cells is important in nutrient starved regions. Partitioning of cellular phosphorus has important implications for the regeneration of phosphorus rich material with regards to the stability following lysis and the subsequent accessibility for hydrolysis by ambient enzymes.

The presence of dissolved and particulate forms of adenosine triphosphate (ATP) underscores the importance of processes by which phosphorus-rich intracellular material is ultimately released into the dissolved environment (Azam & Hodson 1977). Targeted experiments reveal complexities in the mechanisms by which ATP is ultimately released in dissolved and particulate forms, owing to community bloom conditions and the presence or

absence of larger zooplankton sloppy feeding (Riemann 1979; Berman 1987). In addition to feeding and autolysis, viral lysis is a significant means to release DNA, ATP, and other adenylates to the ambient environment to relieve local nutrient stress (Riemann et al. 2009). Moreover, dissolved nucleotides (*e.g* DNA) appear to be a significant source of phosphate that is released during lysis processes mentioned above. Observations and quantification of extracellular DNA have shown that the dissolved pool of DNA is actively cycled by extracellular DNases on timescales of days to hours in oligotrophic gyres (Brum 2005) with potential to support whole community phosphorus demand. Therefore, quantifying the flux of DOM and trace nutrients from cellular lysis is essential to understanding the fundamentals of remineralization and the microbial loop (Middelboe et al. 1996; Poorvin et al. 2004).

Mechanisms to overcome P-limitation are wide-ranging and taxonomically variable with significant broader implications for biogeochemical nutrient cycling. Following cell lysis, P_i and DOP compounds are released along with an intracellular pool of enzymes and cellular debris. Understanding the transition of DOP to P_i involves characterization of the phosphorus pool and enzymes that can act on larger organic molecules. Cell-scale nutrient cycling is the underpinning of the microbial loop. This study quantifies phosphorus regeneration and release following cell lysis. In addition, enzymatic activity following lysis continues to hydrolyze DOP, increasing ambient P_i concentrations. This report combines field and laboratory approaches to quantify and assesses the significance of phosphorus release from cellular lysis of *Procholorococcus* MED4, *Synechocococcus* WH7803, and *E.coli* K-12 MG1655 during varying degrees of phosphorus nutrient stress. In addition, we quantify the fate of DOM released and ultimately regenerated subsequent to lysis to determine rates of release and timescales of nutrient regeneration.

2. Materials and Methods

2.1 Culturing Techniques

Three model organisms were used in this study: *E.coli* K12 MG1655, *Synechococcus* WH7803, and *Prochlorococccus* MED4. *E.coli* K12 MG1655 provided methodological guidance for lysis studies involving slower growing cyanobacterial strains, *Synechococcus* WH7803 and *Prochlorococccus* MED4. Axenic cultures were completed in batch mode on specified minimal media and harvested during log phase growth (Table A1). *E.coli* log phase was identified by monitoring O.D. 600 and *Synechococcus* WH7803 and *Prochlorococccus* MED4 by recording phycoeritherin and chlorophyll-a and chlorophyll-b fluorescence as a measure of cell density to determine log phase growth.

Cyanobacterial cultures considered phosphorus replete were grown in medium with orthophosphate as the sole phosphorus source (Table A1). P-starved cultures indicate cultures in which cells were grown in P-replete medium, pelleted, and resuspended in phosphorus free medium for 24-48hrs. Previous studies have shown APase expression in *Prochlorococcus* MED4 to increase exponentially following p-starvation (Coleman and Chisholm, 2006). However, *Synechcococcus* WH7803 is able to continue growing for long periods following phosphorus starvation (Moore *et al*, 2005). As a result, this study starved *Synechcococcus* WH7803 cells for ca. 120hrs prior to lysis.

E.coli MG1655 was grown in minimal M9 medium noted P-replete or P-deplete based on the presence or absence of orthophosphate respectively. In P-deplete medium orthophosphate concentrations were reduced and supplemented by sodium glycerophosphate to trigger phosphorus limitation and APase expression.

Phosphorus starvation was confirmed prior to lysis in all strains by assaying for APase activity with the fluorogenic substrate 6,8- Difluoro-4-methylumbelliferyl phosphate (DiFMUP). Hydrolysis of DiFMUP produces the fluorescent product 6,8-Difluoro-7-hydroxy-4-methylcoumarin (DiFMU). The rate of DiFMUP hydrolysis to DiFMU was monitored on a temperature controlled Turner fluorometer by excitation of the fluorophore at 358 nm and monitoring emission at 450 nm. A range of DiFMU standards (0-4 μM) was prepared in sterile 50mM Tris in a 96-well palte and enzymatic activity determined by monitoring the rate of DiFMU production over time. Filters or aliquots of lysate were incubated with 10 μM DiFMUP to determine APase activity. This concentration of substrate was determined to be saturating and as a result enzymatic activities are interpreted as maximum activities.

The fraction of the cellular community expressing APase was determined by enzyme labeled fluorescence (ELF) staining. Cells were dual-stained with ELF97 and a DNA stain, 4',6-diamidino-2-phenylindole (DAPI), and monitored with a DAPI long-pass filter set on an epifluorescence microscope. Dual staining was used for only *Synechococcus* and *E.coli* to understand community expression due to an overlap in emission spectra of the *Procholorococcus* MED4 chlorophyll-a and ELF97 substrates. ELF staining allowed for determination of the fraction of pure culture expressing APase.

Cells were lysed by treatment with egg-white lysozyme at a final concentration of 5mg/ml for 1hr at 37°C in 50mM Tris buffer pH = 8.0. Cells were centrifuged at 8000G and rinsed with 50mM Tris three times prior to lysis to remove residual phosphate from growth medium. Subsequent to lysis, cell lysate incubations were immediately assayed for both soluble reactive phosphorus (SRP) and alkaline phosphatase activity (APase). Measurements of total dissolved phosphorus were aliquoted for and frozen at -20°C until analysis. Effective lysis was

determined by visual inspection using an epifluorescence microscope and through DNA quantification to estimate intracellular released and DNA/cell as a test of DNA yield.

Orthophosphate was measured using the Murphy and Riley (1968) method adapted for this study by matrix matching of standards and samples. Samples and standards contained same final concentration of lysozyme. Samples and standards were analyzed in 50mM Tris and often diluted to remain within the linear portion of the [SRP] (0-15 μM) standard curve.

Total dissolved phosphorus (TDP) was measured using previous published methods, where [TDP] = [SRP] + [DOP] (Monaghan and Ruttenberg, 1999). Samples were acid hydrolyzed and subsequently ashed, prior to final measurement as TDP. Standards and samples were carried through treatment with 1.0M HCl and 50(w/v)% $Mg(NO_3)_2$ in combusted and acid cleaned glassware at 80°C for 24hrs and dried for ≥ 24hrs at 120°C. Following drying, samples were ashed in a muffle furnace at 500°C for 2hrs. Ashed material was dissolved in 0.75M HCl and the pH adjusted prior to final measurement as SRP, as discussed above. To determine yields and method effectiveness spike solutions were prepared in which known amounts of model DOP compounds (glycerophosphate and Na-5'AMP) and potassium phosphate standard solutions were spiked into vials to determine recovery following combustion and acid hydrolysis.

2.2 North Atlantic Field Data Collection

A variety of surface ocean nutrient regeneration experiments were conducted aboard the R/V Atlantic Explorer AE1421 from October 21-28, 2014, in the central North Atlantic near the Bermuda Atlantic Time Series (BATS) and Ocean Flux Program (OFP) sites. Cells from the mixed layer (0-100m) were concentrated on 0.22 μm Sterivex filters by filtration of 6-6.5 L of water from the rosette via gravity filtration. Residual solution from the filtration was expelled

from the Sterivex unit by syringe and replaced with a lysozyme lysis buffer. Filtration units were incubated at 37°C for 1 hour and spiked with mercuric chloride (70 μM final concentration) to prevent continued microbial activity. Immediately following lysis, aliquots were sampled for SRP and TDP. Lysate was spiked with a range of DOP (Final [DOP] = 1mM) including glycerophosphate (GYP), adenosine monophosphate (AMP), ribonucleic acid (RNA), and DL-2-amino-phosphopropionic acid (DL2APA) to represent substrates different DOP classes, phosphoesters and phosphonates, commonly found in oligotrophic regions of the ocean (Dyhrman *et al*, 2006). Samples for TDP were immediately frozen at -20°C, while SRP analyses were performed shipboard. An adapted method from Murphy and Riley (1968) and Karl and Tien (1992) was used for SRP analyses to limit interference of lysozyme in solution. To limit dilution of sample and remove slight lysozyme interference in SRP measurements, 500 μl of sample was carried through a magneisium-induced coprecipitation (MAGIC) to remove lysozyme interference and allow for a 2-fold final sample dilution factor.

Alkaline phosphatase activity was measured by incubation of filtered cells with DiFMUP and the fraction of the community expressing APase was determined by incubation of cells with ELF-97 and subsequent epifluorescence visualization. Typically, 50 ml of water from a specified depth was filtered through a 0.2 μm Supor filter at vacuum <10psi. The volume of water was varied at times to determine scaling of measured rates of APase to volume filtered. Supor filters were immediately frozen at -20°C and stored for analysis within 2 weeks of sampling. Filters were analyzed as is previously described for DiFMUP (Ruttenberg and Dyhrman, 2005). Samples for ELF97 were collected by filtration of 20 ml of seawater through a 0.2 μm black polycarbonate filter. First, filters were stained with ELF97 at a final concentration of 1ug/ml for 30 min. Filters were then placed cell side up on an acetate pad soaked with 1mM PBS and 1%

paraformaldehyde (PFA) for 15 min prior to a final DAPI staining with 1ug/ml DAPI for 15 min Filters were mounted on a microscope slide and stored at -20°C until analysis via epifluorescence microscopy (Duhamel, personal communication).

3. Results and Discussion

3.1 Tracking and quantifying phosphorus regeneration subsequent to cell lysis

Intracellular reservoirs of DOP and SRP are released from bacterial cells immediately following lysis. The magnitude of this nutrient flux and its character positively correlate with strain and nutrient status of the cell prior to lysis. Figure 2.1 shows the time course of SRP concentrations in the 2 ml of lysate immediately following the lysozyme treatment for pure culture experiments. The same pattern of SRP release is apparent for all strains. An initial pulse of SRP is released during the lysozyme treatment that is followed by a slower sustained release rate. In the right panels in Figure 2.1, the measured [SRP] in lysate is normalized to SRP release per cell to facilitate more direct comparisons among strains.

Phosphate-replete and phosphate-deplete *E.coli* MG1655 exhibit different releases of phosphate upon lysis, but follow similar rates of regeneration in the lysate. The initial phosphate pulse after lysis in phosphate-replete cells is 20.8 μM, while phosphate-deplete cells contribute to lysate phosphate of 14.6 μM (Figure 2.1). This initial release of phosphate represents only a fraction of the total amount of orthophosphate regenerated from lysed cells. Phosphate concentrations increase exponentially following the initial release reaching a maximum of 68.4 and 60.8 μM in phosphate replete and deplete cells, respectively. Therefore, the initial pulse of phosphate comprises only 24% of the phosphate regenerated in phosphate deplete cells and 30% of the phosphate regenerated in phosphate replete cells. Although nutrient repelete *E.coli* releases

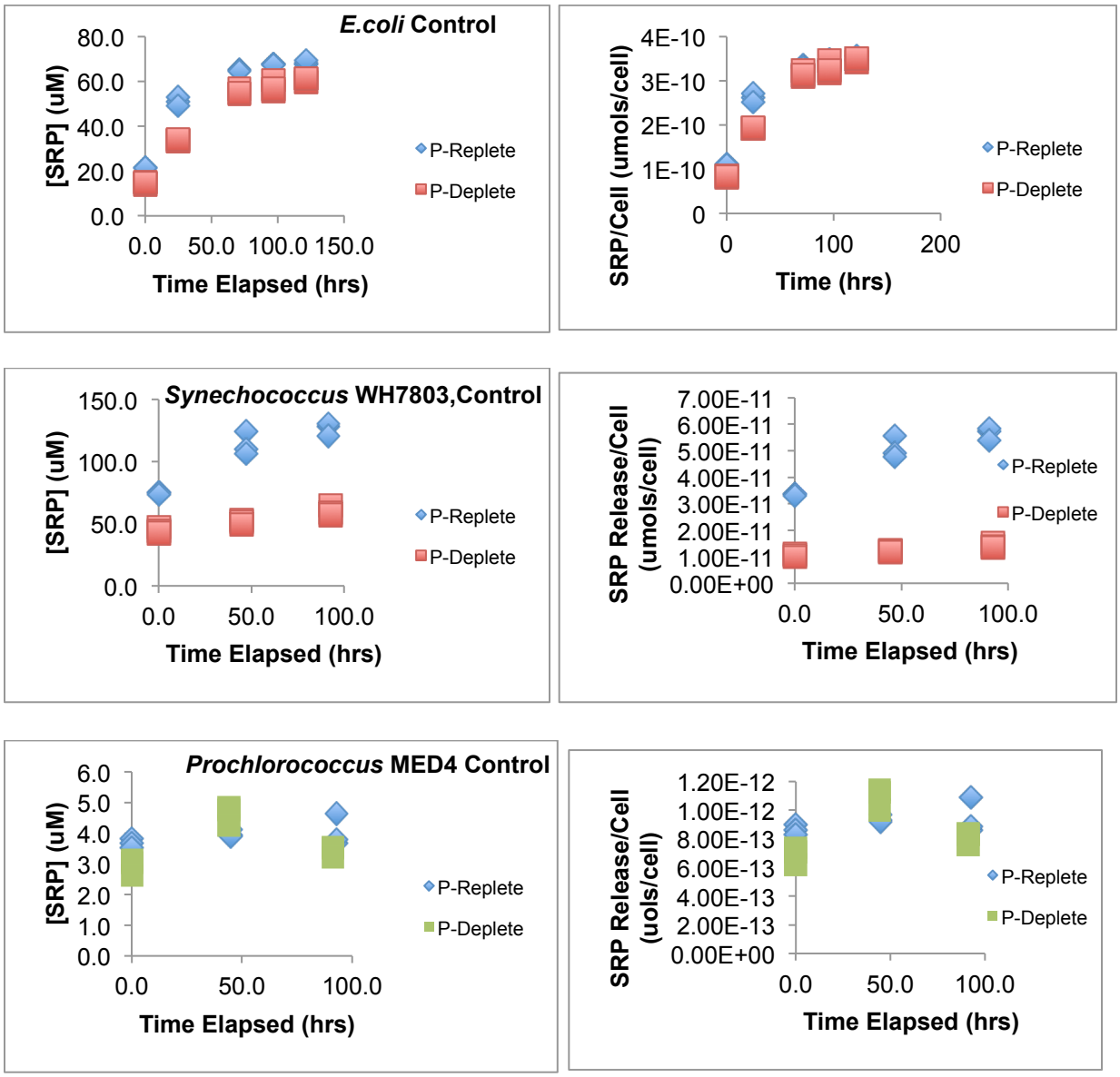

Figure 2.1 [SRP] Changes in Time
Initial pulses of phosphate are followed by sustained remineralization leading to increasing SRP over time. Panels on the left represent [SRP] changes over time, while right panels are SRP release normalized to the number of cells.

more phosphate initially, the amount of orthophosphate remineralized from DOM breakdown is greater in phosphate-starved cells.

Synechococcus WH7803 cells are similar in that the initial phosphate release is greatest in phosphate-replete cells, and lower in phosphate deplete cells. However, the control of nutrient status on the regeneration trajectory is different. The lysis pulse of phosphate from p-replete cells is 74.6 μM and the release from analogous p-deplete cells is 44.6 μM. As a fraction of the amount of phosphate remineralized in the lysate, this initial release represents 59% of total phosphate remineralized from phosphate replete cells and 74% of the remineralized phosphate from deplete cells. This presents a different mode of regeneration than was observed in *E.coli* experiments. In *Synechococcus* experiments, the regenerative flux of phosphate is greater from phosphate-replete cells than from phosphate deplete cells. This finding indicates important ties between the release following lysis and the intracellular reservoirs of phosphate prior to lysis. Moreover, this mode of remineralization supports phosphatases other than APase as being significant in the nutrient regeneration.

Finally, *Prochlorococcus* MED4 releases a pulse of orthophosphate during lysis that comprises a significant fraction of the total amount of dissolved phosphate released. Phosphate-replete *Prochlorococcus* cells release 3.7 μM phosphate compared to slightly lower releases in deplete cells, 2.9 μM. The change in phosphate over time in these incubations is small, ~0.5 μM. The phosphate release at t0 in these incubations accounts for 91% of phosphate-replete phosphate and 86% of phosphate deplete orthophosphate remineralized by the end of the lysate incubation. Lower nutrient releases after lysis and smaller regenerative fluxes in MED4 further highlight the role of nutrient status in controlling the nutrient flux.

Nutrient status is tightly coupled to the initial pulse of phosphate following lysis. All lysate incubations showed higher SRP initially in phosphate-replete cells versus phosphate deplete cells. Differences in the magnitude of the initial pulse of phosphate and in the final concentration of phosphate could arise from several mechanisms. First, phosphate-replete cells exhibiting auxillary storage of phosphate in reservoirs such as polyP would support observations in *Synechococcus* WH7803 experiments. In this scenario, lysis releases intracellular stores of polyP that are subsequently degraded in the lysate, leading to higher observed phosphate remineralized in phosphate replete cells. Second, intracellular partitioning of orthophosphate is strain-specific. Shifts in phosphate storage from intracellular dissolved reservoirs to DOP or refractory cellular compartments might limit the magnitude of the nutrient release upon lysis. Third, the immediate pulse of SRP might also be affected by rapid degradation of labile DOP. In this case the SRP measured following lysis actually represents an orthophosphate release and the immediate degradation of extremely labile DOP. Each of these scenarios can explain differences in the flux following lysis, however the relative contributions are complex. Nonetheless, there exists a tight coupling between phosphate availability prior to lysis and phosphate release.

To further elucidate the link between nutrient status and orthophosphate release, determination of phosphate release per cell provides useful insight towards intracellular phosphate releases. Phosphate release from *E.coli* MG1655, *Synechococcus* WH7803, and *Prochlorococcus* MED4 might be related to cytosolic volume and phosphate status of the cells prior to lysis. *Prochlorococcus* MED4 releases only 0.7-1.0 amol SRP/cell while larger cyanobacteria *Synechococcous* WH7803 release between 10.5-33.4 amol SRP/cell, both of which are minor compared to 80.5 - 99.3 amol SRP/cell released from *E.coli* (Figure 2.2). The lower end of each of those ranges represents the phosphate-deplete condition and the upper end

in the phosphate-replete condition. The dynamic range of phosphate release following lysis is a product of the nutrient status prior to lysis. For example, cells grown under phosphate-replete conditions exhibit larger initial pulses of phosphate following lysis. *Synechococcus* exhibits a 3-fold decline in phosphate released when comparing nutrient replete conditions to phosphate deplete counterparts, suggesting cytosolic shifts in phosphate concentration. Surface ocean lysate samples follow a narrower range of phosphate releases, 6.5-28.7 amol SRP/cell, which highlights the fact that these samples are mixtures of heterotrophs and photoautorophs each with individual cytosolic reservoirs of DOP and SRP that are released during whole community lysis. Therefore the lysed flux is a complex mixture of organic and inorganic phosphate derived from cytosolic and potentially labile particulate reservoirs. Fluctuations in the magnitude of the lysed flux of orthophosphate support hypotheses that allocation of phosphate within the cell has controls on the phosphate released.

Back of the envelope calculations that consider the cell volume and cytosolic P_i concentration cannot alone explain the variability in this flux. Estimates of intracellular phosphate concentration are estimated at approximately 10 mM. Assuming an intracellular SRP concentration of 10mM and cell volumes of 0.2, 0.38, and 1 μm^3 for *Prochlorococcus* MED4, *Synechococcus* WH7803, and *E.coli* MG1655, respectively, one can calculate expected releases of SRP following lysis. These calculations suggest an orthophosphate release of 2, 3.8, and 10 amol P/cell for *Prochlorococcus* MED4, *Synechococcus* WH7803, and *E.coli* MG1655, respectively. Except for measured *Prochlorococcus* MED4 phosphate release, these estimates are well below observed releases for *Synechococcus* WH7803 and *E.coli* MG1655. This suggests either the cytosol concentrations of P_i can vary a great deal, or there is a labile form of P_i that is much more abundant in some strains and during certain nutrient stress conditions. Moreover,

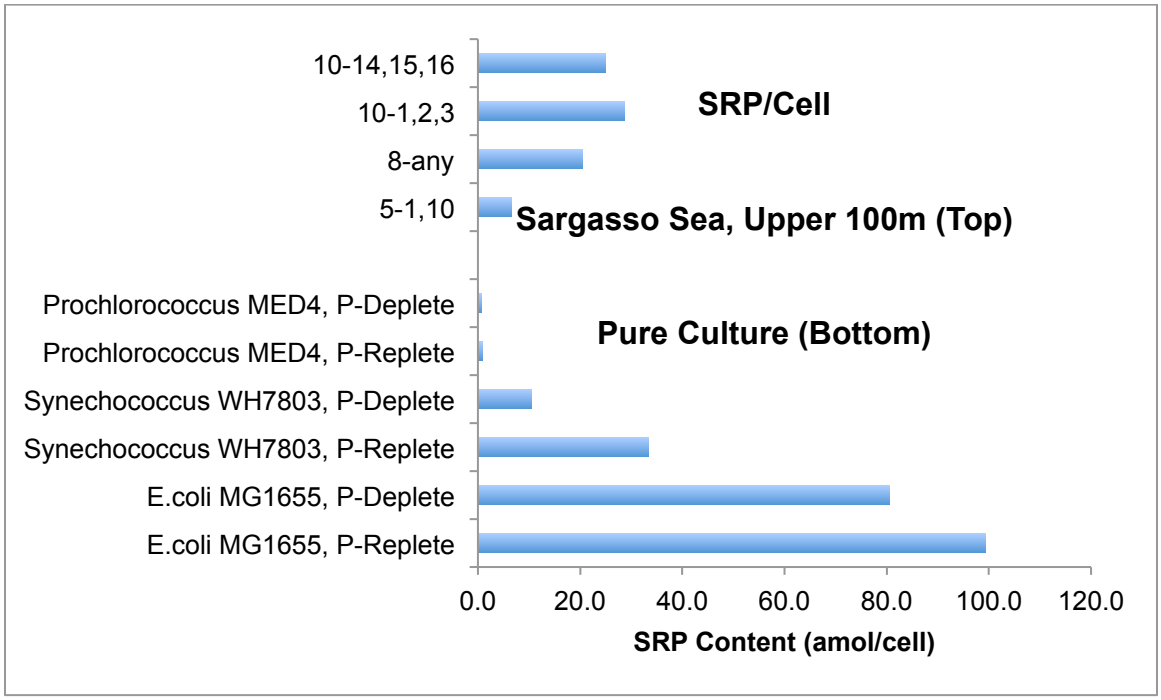

Figure 2.2 Phosphate Release Upon Lysis
Compared to cultured data phosphate release in oligotrophic surface ocean microbes is within the range observed for cultured cyanobacteria.

observed variation in the amount of phosphate released does not appear to be related to differential effects of lyzosyme treatment on different strains either. Fluorescence microscopy reveals similar visualizations of chromosomal DNA leaking from cells from all three strains (Figure A4).

Phosphate-starved medium appears to shift phosphate partitioning within the cell, where intracellular pools decline and/or phosphate is stored in more refractory DOP. Moreover, P-replete cells exhibit an opposite effect, where phosphate is present at higher concentrations intracellularly or is partitioned into auxillary reservoirs such as polyP. The wide range in phosphate release per cell suggests a dynamic intracellular system, where complexities of cellular metabolism, nutrient status, and intracellular volume are significant in the lysis release. These results suggest nutrient status prior to lysis is linked to the orthophosphate flux following lysis as a result of modulation of the intracellular reservoir of phosphorus during growth. Allocation of nutrient resources within the cell to reservoirs with unknown lability and uncharacterized stability outside the cell highlights the requirement for further investigation of the specifics of remineralization.

Measurements of TDP provide useful information about the relative contributions of organic and inorganic phosphate reservoirs to the phosphorus reservoir in the lysate. TDP lysate measurements of *Synechococcus* WH7803 and *Prochlorococcus* MED 4 indicate higher [TDP] in phosphate deplete cell lysates (Figure 2.3). Concentrations of TDP in *Synechcoccus* WH7803 phosphate deplete lysates are 169 μM as compared to phosphate-replete lysates where [TDP] = 151 μM following lysis. The same trend is observed in *Prochlorococcus* MED4 lysates, phosphate-replete lysates are 3.4 μM versus phosphate deplete counterparts that are more concentrated in TDP at 4.2 μM. TDP measurements indicate findings similar to SRP analyses

linking nutrient status of the cells to the character of the lysed phosphate pool. However, TDP values provide evidence that the fraction of phosphate released as DOP is greater in phosphate deplete lysates, than in phosphate replete lysates. Following lysis, 39% of phosphate is released as DOP in *Prochlorococcus* MED4 lysates, and 74% of phosphate is DOP in *Synechococcus* phosphate deplete lysates. Alternatively, 0% of phosphate is released as DOP in phosphate replete *Prochlorococcus* MED4 experiments and 50% of phosphate is DOP in phosphate replete *Synechcococcus* WH7083 lysates. Investigations of surface ocean Sargasso Sea samples reveal significant pulses of DOP in the lysate. The TDP release from lysis of surface ocean populations spans a wide range from 6.7 μM on 20m cast 5 to 21.5 μM on 20m cast 10 and 100m cast 8. The fraction of this TDP pool is 58% in 20m cast 5 samples and varies between 33% and 54% for cast 10 at 20m and cast 8 at 100m respectively. Surface ocean contributions of DOP to the phosphate pool are similar to those observed in pure cultures lysates mentioned above.

Moreover, surface ocean samples represent a more complex community of mixed populations where the lysed pool is a mixture of DOP and SRP from mixed community of heterotrophs, photoautotrophs, and picoeukaryotes Fluctuations in the magnitude of DOP and SRP provide further evidence to support links between nutrient status and the nutrient pool in the lysate.

Lysed cells release particulate reservoirs of nutrient in addition to important DOP and SRP components. Dissolved reservoirs of phosphate are well characterized by DOP, SRP, and TDP; however cellular debris, and fractions of the cell that remain as particulate phosphorus are significant to determining regeneration as well. The stability of particulate material is important

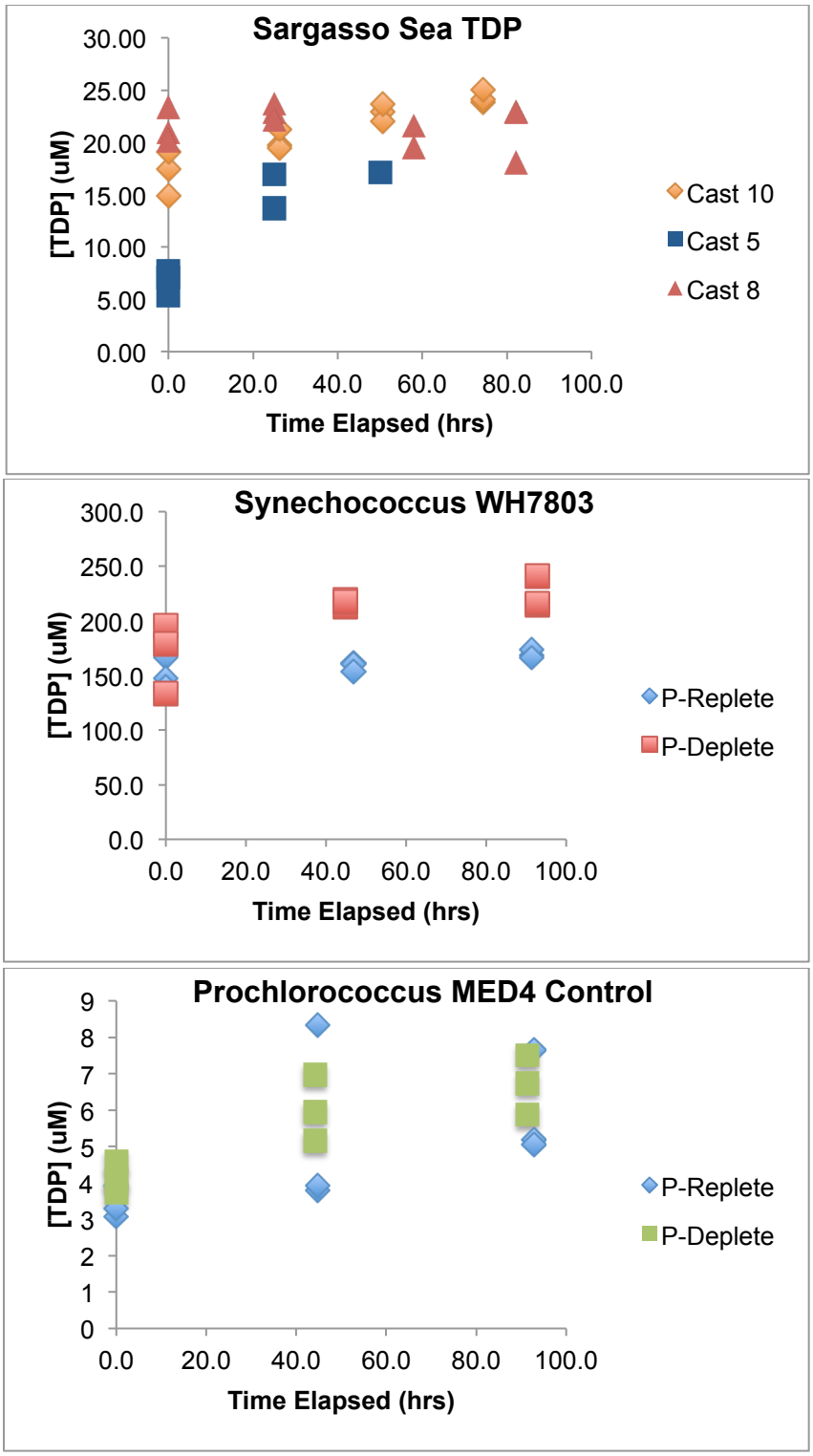

Figure 2.3 [TDP] of Cell Lysates.
Cell lysis releases a pulse of DOP. [TDP] in ocean lysates and culture lysates shows relatively constant or slightly changing [TDP]. Increases in [TDP] may be due to contributions from particulate phosphorus to the dissolved pool. Cast 5, 8, and 10 all are from 20m depth.

to quantifying contributions of particulate phosphate, via dissolution to DOP, to changes in the amount of DOP in the lysate. The total dissolved phosphate reservoir in cultured lysates and environmental samples increases slightly in several of the lysates incubations (Figure 2.3). The rate of TDP increase in phosphate-replete *Synechococcus* WH7803 lysates (0.58 μmol $L^{-1}hr^{-1}$) is more than double the observed rate in the phosphate-deplete analog (0.20 μmol $L^{-1}hr^{-1}$). Moreover TDP increases in *Synechcococcus* WH7803 are at least one order of magnitude greater than observed increases in surface ocean and cultured lysate TDP. Changes in TDP concentration in the lysate signify the potential for particulate stores of phosphate to contribute to remineralization fluxes of phosphate. The stability of particulate phosphate following lysis may be product of the mode of lysis and the storage of phosphate in particulate resevoirs prior to lysis. Enhanced fragmentation of cellular debris and particulate material could enhance surface area further promoting degradation. Increased surface area is also important in the accessibility of substrate to membrane and particulate-bound enzymes.

The regeneration of the DOP pool is a function of enzymes present, where phosphorus starvation enzymes such as APase could have a direct effect on the magnitude of the regenerative flux. In this work, nutrient status and strain are important in the release of phosphate during lysis. Measuring APase activity is a means to understand how a well-identified nutrient-starved phosphatase would affect regeneration rates when activity is either absent and present. Assays of APase activity in cellular lysates indicate that enzymatic function is maintained for a period of days following initial lysis (Figure 2.4). This evidence is further corroborated by previous figures showing increasing orthophosphate after cell lysis. Pure culture p-starved strains all exhibit orders of magnitude higher APase activity in the lysate compared against analogous incubations with cells grown in phosphate-rich medium. P-starved *Prochloroccous* MED4 APase activity is

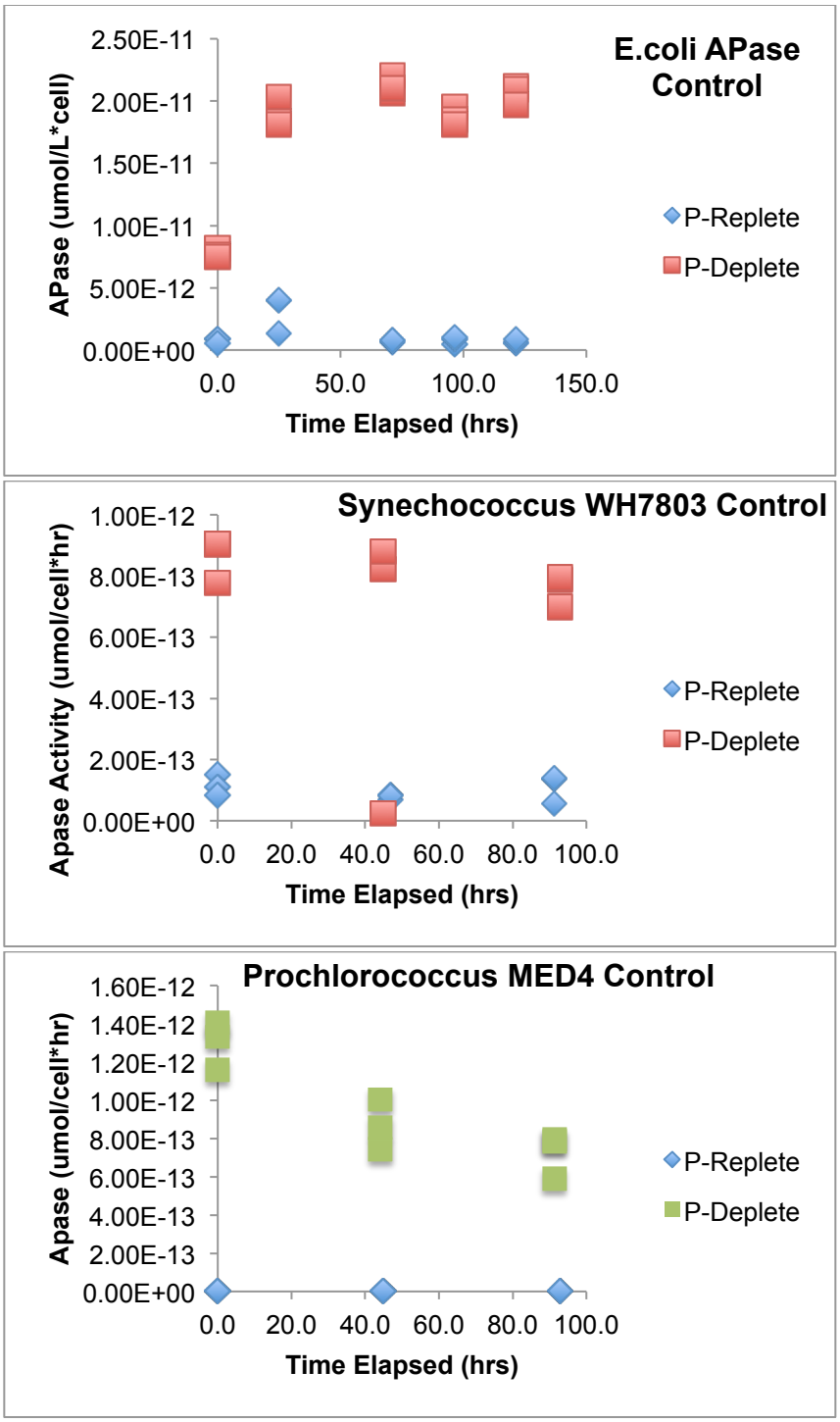

Figure 2.4 APase Activity Over Time.
"Control" refers to the lack of a DOP spike. Subsequent to lysis APase activity declines in cyanobacterial lysates. High [DOP] in *E.coli* lysates leads to competitive inhibition of DiFMUP and DOP, causing apparent spikes in APase activity at 24hrs.

approximately 1.3 x 10^{-12} μmol $cell^{-1}hr^{-1}$1following lysis, while p-starved Synechcococcus WH7803 is lower, 8.5 x 10^{-12} μmol $cell^{-1}hr^{-1}$. However, phosphate-replete cells hovered close to the detection limit for APase activity after cell lysis. Declining APase activity is observed in cyanobacterial lysates over time as enzymes lose function and the ability to hydrolyze. APase activity in *E.coli* lysates is higher 8.5 x10^{-11} μmol $cell^{-1}hr^{-1}$. In addition, *E.coli* eventually stabilizes at an APase activity higher than the initial time point due to competitive inhibition between ambient DOP and DiFMUP substrate. Characterization of enzymatic activity in the lysate underscores the importance of phosphatases, especially APase, in the hydrolysis of DOP in the lysate. The ability of enzymes to continue to hydrolyze following lysis is an important mechanism for local nutrient relief.

Continued SRP production without APase activity in the lysate suggests other phosphatases present in the lysate are as important in nutrient regeneration and are unquantifiable by the DiFMUP assay. Moreover, other phosphatases released during lysis may have higher affinity for DOP substrate than APase. Varied substrate affinity and a diversity of phosphatases in the lysate highlight the complexity of nutrient regeneration and its tie to cellular metabolism and phosphate availability. Nonetheless the phosphatases released following lysis maintain function for days and continue to hydrolyze. This work presents a new mechanism for nutrient regeneration where cell lysis and the continued enzymatic functioning facilitates the breakdown of associated cellular organics and also ambient DOP. Continued processing of DOP in the surface ocean has important controls phosphorus regeneration and in the fraction of DOP and POP that is exported from the euphotic zone.

Comparing APase in this study derived from lysates to previously determined rates is useful for determining how lysis might shift phosphatase activity. Table 2.1 compares measured

ID	Nutrient Status/Location	APase Activity amol cell^{-1} hr^{-1}
Synechococcus 7803	Phosphate-replete	0.11
Synechococcus 7803	Phosphate-deplete	0.86
Prochlorococcus MED4	Phosphate-replete	b.d
Prochlorococcus MED4	Phosphate-deplete	1.30
Moore *et al*, 2005	Pro MED4 P-Starved	1.0 - 5.0
Moore *et al*, 2005	Syn WH7803 P-Starved	0.05 - 0.2
5-1,10	OFP, Sargasso Sea	3.31
8-any	OFP, Sargasso Sea	3.00
10-1,2,3	OFP, Sargasso Sea	0.69
10-14,15,16	OFP, Sargasso Sea	0.13

Table 2.1 Compilation of APase Activity.
Rates of APase activity normalized to cell density provides a useful comparison between pure cultures and environments. A wide range of APase activities is observed in culture and in the upper 100m of the Sargasso Sea.

APase activities in this study with others in the laboratory. Only rates of per cell APase activity are compared here, due to difficulties in interpreting data presented as a rate per volume where the volume is often not clearly defined. APase rates in cyanobacterial lysates in this study 1.3 amol P $cell^{-1}hr^{-1}$ fall within observed ranges of 1-5 amol P $cell^{-1}hr^{-1}$ in cultured *Prochlorococcus* MED4 laboratory grown cells. However, APase activity of experimental lysate *Synechococcus* WH7803 is more than an order of magnitude greater than previous laboratory rates of APase activity. The capacity of other phosphatases in the lysate to hydrolyze the APase fluorophore might explain observed offsets in for *Synechococcus* rates. Evidence of phosphatases other than APase is apparent in SRP regeneration in p-replete *Synechococcus*, APase activity is below detection limits, but large increases in phosphate are observed.

Understanding allocation of phosphate in labile and refractory reservoirs is significant for determining export of phosphorus from the euphotic zone and in the ultimate regenerative flux following lysis. The ability of phosphatases to hydrolyze phosphate-rich reservoirs, such as polyP, has important implications for export and nutrient regeneration fluxes. Regeneration of polyP is dependent on phosphatase specificity for phosphoryl groups within the polyphosphate chain, and the stability of the chain polyP extracellularly. *Synechcococcus* WH7803 phosphate-replete conditions suggest the amount of phosphate generated is greater from cells grown with excess phosphate in the medium, highlighting the potential for polyP as the reservoir from which phosphate is regenerated. This model suggests polyP is stable upon release from the cell is subsequently degraded in the lysate by phosphatases other than APase, given low measureable APase activity. However, the stability of polyphosphate relies on charge balancing ions that are in abundance intracellularly. Therefore, present polyP hydrolysis may be a combination of phosphatase hydrolysis when released in a lower ion content lysate. Cellular modulation of the

phosphate reservoir appears to dictate the initial release of phosphate and the regeneration of phosphate from organic forms.

Cellular P quota estimates of previous pure culture cyanobacteria provide valuable constraints for the "regenerative potential" from a given cyanobacterium. Estimates of total phosphate allow one to decipher the relative contribution of the phosphate from intracellular and labile organic reservoirs upon lysis as well as the presence/absence of polyphosphate. Total phosphorus quotas for *Synechococcus* WH7803 vary from 1.3-7.9 fg P/cell. Approximately 33.4 amol of orthophosphate is released upon lysis of p-replete *Synechococcus* WH7803 cells. If cellular volume of *Synechoccocus* is 1.0 um^3, this suggests intracellular [SRP] is approximately 33mM, which above the 1-20mM reported in the literature. Moreover, this requires that ~1fg of P is released upon lysis as orthophosphate, which is a large component of cellular P quota depending on growth condition. This estimate suggests that polyP may be an important reservoir within the cell, especially under p-replete conditions. This calculation might also indicate rapid transition of DOP to SRP as a result of instability in extracellular medium. Therefore in understanding the regenerative flux, considerations of intracellular phosphate are important, but the release upon lysis may be a mixture of unstable LMW DOP compounds, polyP, and orthophosphate.

3.2 Cell Lysis and the Hydrolysis of DOP

Initially, tests were carried out using *E.coli* as a model organism to test the regeneration of phosphate from a range of DOP compounds in the lysate. Nutrient status was varied and the addition of a range of DOP compounds assessed the capacity of cells grown under different nutrient statuses to hydrolyze representative DOP compounds. These experiments emphasize the

role of the intracellular enzyme pool in the regeneration flux. Phosphate-replete and deplete *E.coli* both exhibit the ability to hydrolyze the range of DOP compound tested (Figure 2.5). However, the affinity for DOP compound has strong controls on the fraction of the DOP ultimately hydrolyzed (Figure 2.5). For instance, nearly 95% of 5'AMP is hydrolyzed in both p-deplete and p-replete lysates after 96hrs of incubation time. DOP incubations of other DOP compounds follow different regeneration paths. Phosphate deplete lysates hydrolyze 100% of glycerophospahte (GYP) after 96hrs, while phosphate-replete cells break down only 50% of the added GYP. Regeneration of RNA follows a similar non-linear path in phosphate replete and deplete cells, except that only 10-15% of spiked DOP is hydrolyzed over a 96hr incubation. Variations in the fraction of DOP hydrolyzed in *E.coli* lysates indicate that the phosphatases present in the lysate derive from different nutrient conditions and are coupled to the fraction of DOP hydrolyzed in the lysate. These results informed future studies in cyanobacteria and surface ocean samples aimed at testing how relative affinity in the lysate for DOP substrate is coupled to the amount of phosphate hydrolyzed.

Cultured cyanobacterial cell lysates were incubated in the presence of GYP, a component of glycerophospholipids, because of its prevalence in cell membranes and for phosphate storage in the cell. Phosphorus starved *Prochlorococcus* MED4 exhibits rapid hydrolysis of GYP leading to 100 μM increases in [SRP] in less than 48hrs (Figure 2.6). Phosphorus-starved *E.coli* lysate shows similarly rapid increases in [SRP] as GYP is hydrolyzed, approaching phosphate concentrations of 1mM where inhibition of APase is documented. However, *Synechococcus* WH7803 exhibits most rapid GYP hydrolysis in P-replete lysate. Rates of DOP hydrolysis observed in phosphate replete *Synechococcus* WH7803 cells are 0.3 amol P $cell^{-1}hr^{-1}$, while phosphate-deplete cells hydrolyze DOP at 0.04 amol P $cell^{-1}hr^{-1}$, highlighting importance of

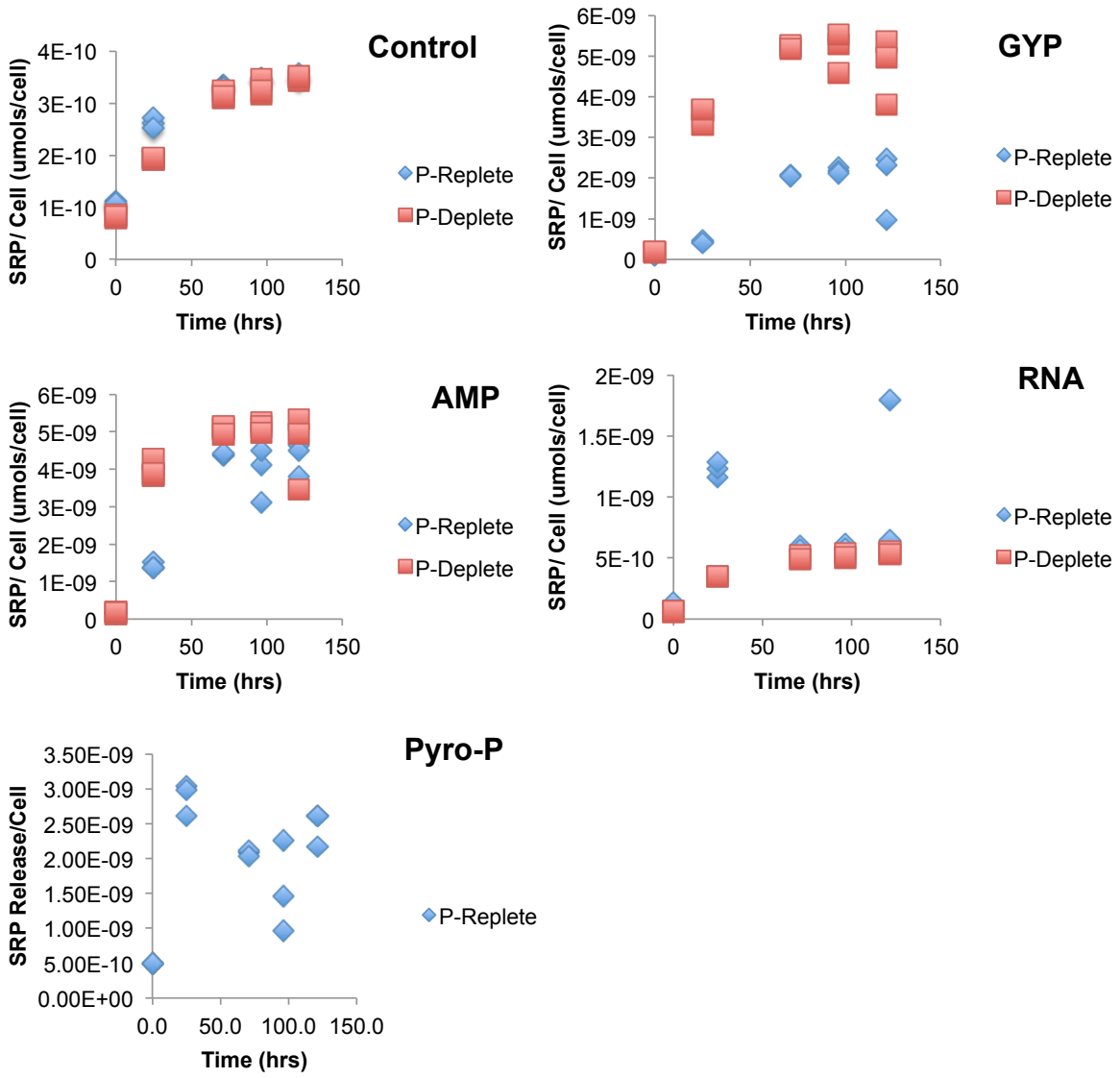

Figure 2.5 DOP Compounds in E.coli Lysates.
E.coli MG1655 P-Deplete and P-Replete lysates incubated with a range of DOP compounds added to lysate monitored over time.

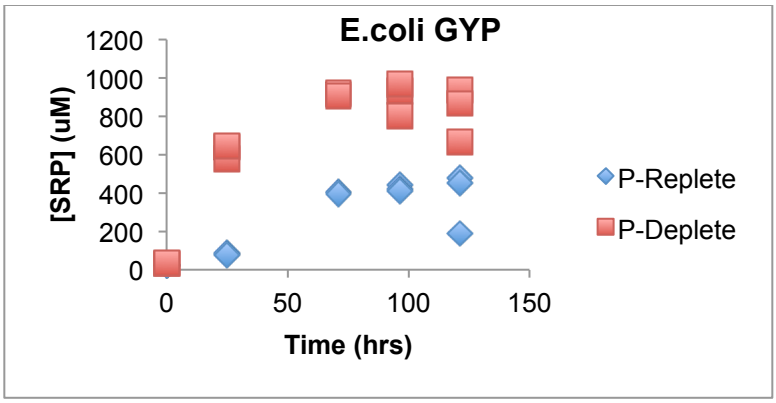

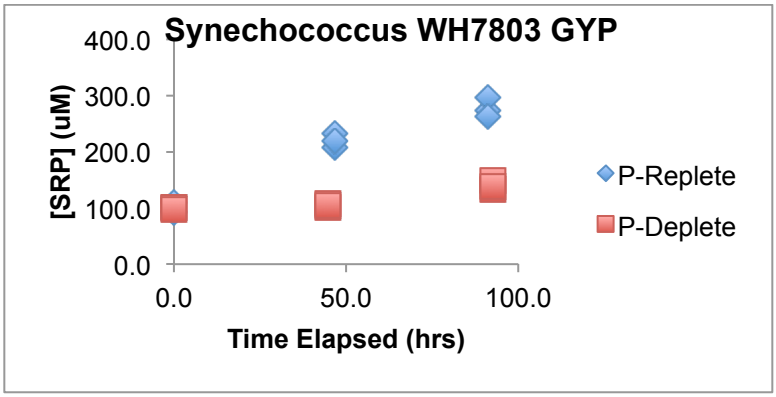

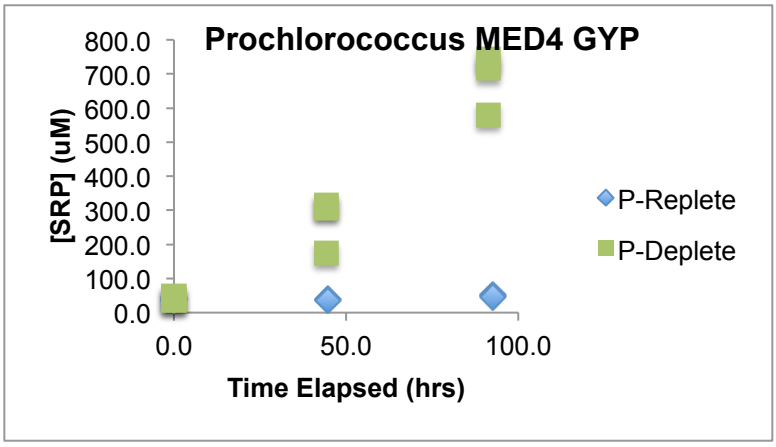

Figure 2.6 GYP Incubations.
Figures represent pure culture lysates where a 1mM glycerophosphate spike was added to the lysate and monitored for 96hrs.

phosphatase specificity in DOP hydrolysis. However, *Prochlorococcus* MED4 shows similar rates of DOP hydrolysis in phosphate replete and deplete lysates (0.001 amol P $cell^{-1}hr^{-1}$) when model DOP compounds such as GYP are absent. Rapid hydrolysis of GYP (80% hydrolyzed) in *Prochlorococcus* MED4 lysates is observed only during phosphate-deplete lysis when APase activity is high. This suggests that the initial lysis release of phosphatases is dynamic and strain specific with substrate specificity for concomitant DOP driving the regeneration of SRP. Measured rates of DOP hydrolysis in the lysate point towards the DOP released and phosphatases present as strong determinants of the regenerative flux following lysis.

To explore how phosphatase substrate affinity leads to variation in regeneration of phosphate additional tests with a range of DOP compounds were completed with oligotrophic cell lysates. Oligotrophic lysate incubations spiked with DOP compounds indicate varying affinity for DOP substrate is linked to the magnitude of the regenerative flux for respective compounds. Rates of DOP hydrolysis vary from 0.2 to 20 μM hr^{-1} over the range of DOP compounds tested (Figure 2.7 and 2.8). Abundant intracellular compounds, 5'adenosine monophosphate (AMP) and pyrophosphate (PP_i) are rapidly hydrolyzed following cell lysis, where > 50% of spiked DOP is hydrolyzed after a 72hr period. GYP is regenerated at ca. 1.2 μM hr^{-1}, but with a maximum of 15% of the DOP spike hydrolyzed after a 72 hr lysate incubation at the DCM. Phosphonates and RNA show low rates of hydrolysis indistinguishable from control incubations with no DOP spike, ca. 0.4 μM hr^{-1}. Phosphonates are a refractory DOP compound class requiring a C-P lysase for complete breakdown. Not all microbes contain genes and subsequent enzymes necessary for utilization of phosphonates, which might place phosphonate regeneration rates lower than other compound classes tested. Our results suggest that lysis releases a range of phosphatases at different concentrations and with varied activity and

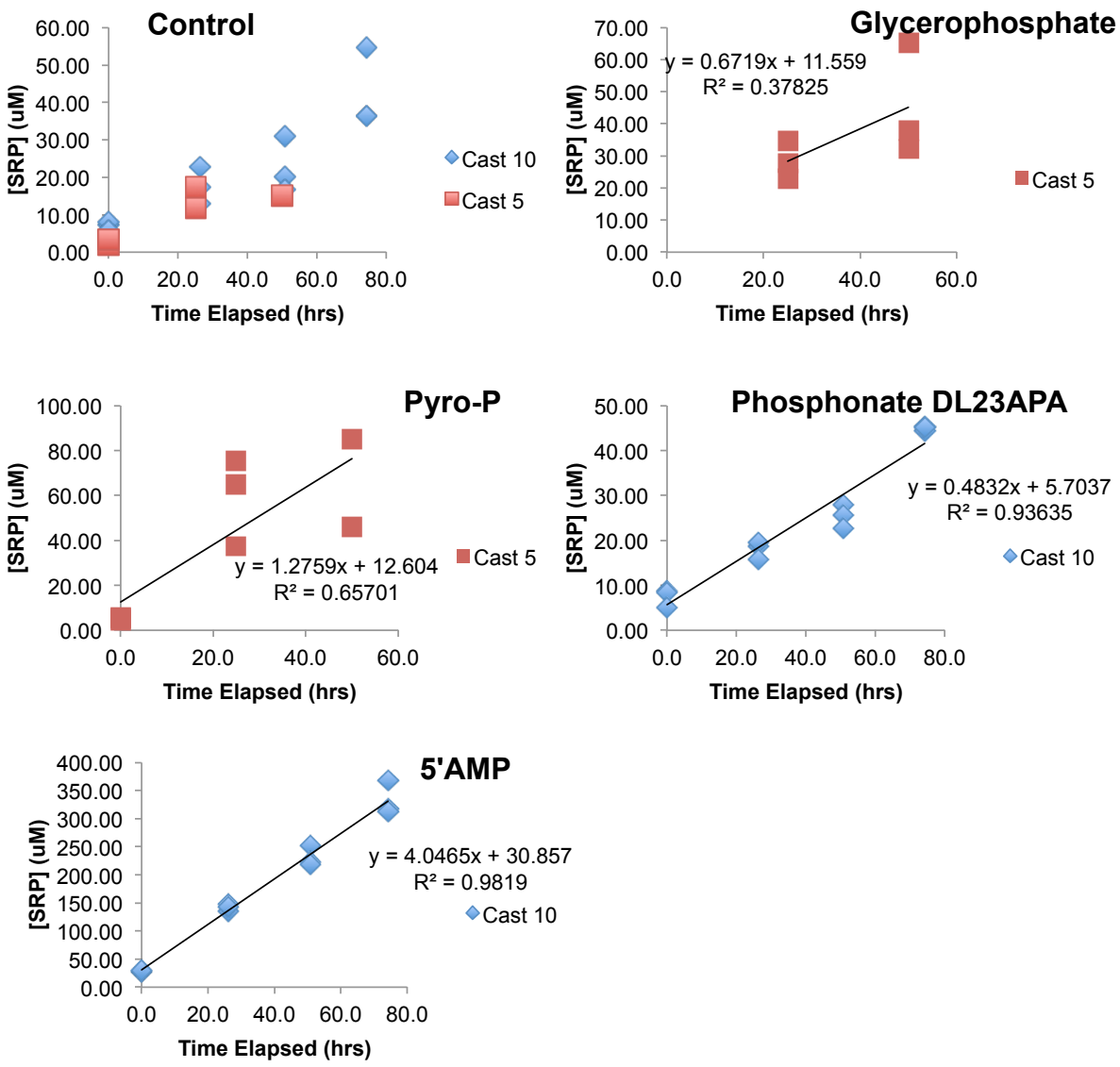

Figure 2.7 20m Bermuda Lysate Incubations.
Lysis of surface ocean microbes causes a pulse of SRP followed by DOP hydrolysis leading to increasing phosphate in the lysate. Enzymatic activity in the lysate continues to hydrolyze DOP compounds in controls and incubations where DOP was added (Cast 5 = 20m, Cast 10 = 20m).

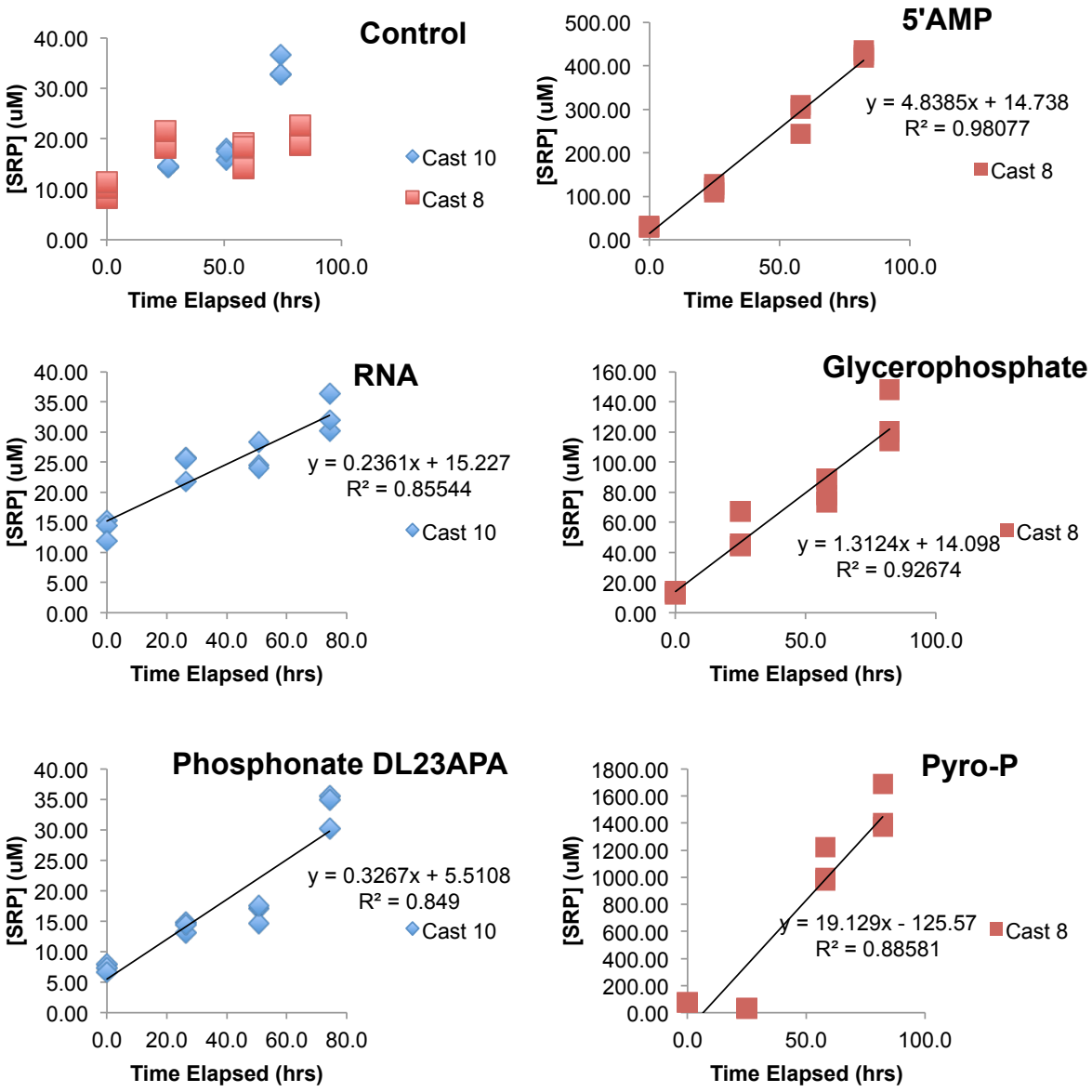

Figure 2.8 Deep chlorophyll Maximum (DCM) Lysate Incubations.
Surface ocean populations exhibit large micromolar pulses of orthophosphate followed by increasing [SRP] due to DOP hydrolysis. Lysate incubations with DOP spikes show marked increases in [SRP] at differential rates, suggesting enzymatic substrate specificity is important in DOP hydrolysis and phosphate regeneration in the surface ocean. (Cast 8 = 85m, Cast 10 = 100m).

specificity for substrates. Rapidly cycled intracellular components, AMP and pyrophosphate, show most rapid hydrolysis perhaps as a result of their abundance intracellularly prior to lysis. Oligotrophic lysate experiments suggest that substrate affinity and intracellular pool dynamics are important predictors of initial release following lysis and have significant control on the regenerative phosphorus flux. Surface ocean experiments offer useful insights towards regeneration in a more complex mixed surface ocean community. Moreover, pure culture and oligotrophic lysates underscore the importance of the strain, nutrient status, and the phosphatases present in the regeneration of phosphorus.

3.3 Comparing Regeneration Rates and Reservoirs

To assess the relative significance of cell lysis as a mode of nutrient relief in the surface ocean, rates of SRP regeneration in Sargasso Sea lysate experiments must be viewed alongside measured rates of DOP and SRP uptake in oligotrophic regions. Rates of regeneration from the Sargasso Sea experiments are compiled in Table 2.2 to compare against ambient rates of uptake of DOP and SRP in other oligotrophic regions. The per cell release of SRP and DOP measured in these experiments is then used to estimates the release of nutrients assuming a steady state surface ocean microbial population. SRP release from cell lysis contributes 0.04 – 0.15 nmol SRP/hr, which is similar to the observed range of orthophosphate demand by surface ocean communities from both HOT and BATS. Moreover, higher DOP release rates 0.05-0.19 nmol DOP/hr are above ATP uptake rates in upper 100m at HOT and near the mid point of the observed ATP uptake rate at BATS. Cell lysis nutrient release rates measured in this study invoke viral lysis as an important means of supplementing nutrients in the surface ocean when compared to determined rates of nutrient uptake in the ocean. More complex models considering

A.

Source	Location	Community SRP Uptake (nmol/(L*hr))	Community ATP Uptake (nmol/(L*hr))
Casey *et al,* 2009	BATS	0.5-1.5	0.01-1.4
Bjorkman *et al*, 2012; Bjorkman *et al,* 2003	HOT	0.06 -0.38	0.00058-0.00288

B.

Sargasso Sea ID/Strain	Depth, Experiment	SRP Flux (nmol/(L*hr)	Residence Time (days)	DOP Flux (nmol/(L*hr))	Residence Time (days)
5-1,10	20m, Control	0.04	11.0	0.05	7.9
8-any	20m, Control	0.13	3.3	0.15	2.8
10-1,2,3	20m, Control	0.09	4.5	0.19	2.2
10-14,15,16	DCM, Control	0.15	2.9	0.13	3.3

Table 2.2 Phosphorus Utilization and Regeneration Rates.
(A) Measured rates for whole community uptake in oligtrophic time series, HOT and BATS. (B) Rates of SRP and DOP released to the surface ocean and calculated residence times.

the dynamic range of SRP and DOP released as a function of the nutrient status and strain type would provide an even more detailed understanding of how lysed cells contribute to nutrient pools and modulate nutrient reservoirs.

Turnover times of phosphate in the oligotrophic surface ocean are relatively short. Estimates of turnover rates of SRP at Station ALOHA (3-21 days) are long compared to turnover times at BATS (<12 hr). Moreover, using the SRP and DOP flux estimates one can derive the turnover rate for this lysed nutrient pool only and compare against surface ocean SRP turnover. Turnover time estimates for lysed SRP contributions span 2.2-7.9 days, longer than those observed at BATS, but within the range measured at HOT. Given the assumptions in these calculations, the release rate of SRP from lysed cells is an important supplement to surface ocean phosphate reservoirs. Nutrient releases via cell lysis can potentially support observed turnover rates at HOT, however rapid orthophosphate turnover times at BATS indicate relative importance of DOP in sustaining growth.

This work presents the significance of delayed enzyme-mediated regeneration by lysed cells and associated phosphatases in the microbial loop. The lysate and associated enyzmes to maintain hydrolyzing capacity following lysis allows for continued processing of DOP and potentially local nutrient relief. Nutrient regeneration is a complex, dynamic process controlled by a range of important factors including nutrient status, strain, enzymatic functioning, and lability of DOP. These factors all contribute to the magnitude of the regenerative flux and the availability of nutrients as a result. This study underscores the importance of nutrient regeneration pathways on biogeochemical dynamics in marine ecosystems and ultimately the amount of carbon exported to the deep ocean.

4. Conclusions

Cell lysis is invoked as a primary mechanism for nutrient release of organic and inorganic nutrients from microbes, although quantification of this process is limited. This work identifies significant processes of the microbial loop by quantifying nutrient regeneration as a result of cell lysis. We used pure culture cyanobacterial strains and environmental surface ocean populations to study the role of an array important factors, cell strain, nutrient status, and cellular enzymes, in the process of regeneration and the magnitude of the remineralization flux. The phosphate pool and associated enzymes monitored during lysis and for a period following lysis characterize the nutrient flux and processing of lysed nutrients following cell death. The primary findings of this study suggest lysis of laboratory and surface ocean microbes is a dynamic process where nutrient release is a function of cellular content, nutrient status, and enzymes present. Moreover, enzymes that act on organic moieties following lysis supplement the immediate release of phosphate by hydrolytic breakdown of organic phosphate. The combined flux of organic and inorganic nutrient forms and enzymes allows for rapid degradation of DOP and local nutrient relief. These findings accentuate the role of lysis in nutrient regeneration and relief of nutrient stress in oligotrophic regions of the ocean.

Quantification of the SRP pulse suggests that oligotrophic communities release amounts of phosphate similar to cultured cyanobacteria following lysis, where pulses of phosphate range from 0.5-33 amol/cell. Larger heterotrophs, such as *E.coli*, exhibit markedly higher phosphate release following lysis (80-99 amol/cell). The survey of pure culture and surface ocean cell lysates provides a broad view of the nutrient flux following lysis. This flux is best characterized as a mix of SRP and DOP, where the relative abundance of either inorganic or organic phosphate is driven by the nutrient status prior to lysis. Initial orthophosphate releases are greater in cells

grown with ample medium phosphate and lower in cells grown in phosphate-starved medium. The initial pulse of DOP is also tied to nutrient status, however p-starved conditions lead to increased DOP concentrations in the lysate.

The relative contributions of DOP and SRP vary in the lysed flux of phosphate are essential in determining transformations of phosphate during regeneration. Variability in the relative DOP and SRP flux is also related to nutrient status prior to lysis. Manipulation of phosphate content in lipids and storage of phosphate as polyP are well-documented examples of reallocation of nutrients within the cell. Limiting the amount of phosphate partitioned to DOP prior to lysis is important in extracelullar reactivity of DOP and the DOP flux. Phosphate storage under p-replete conditions in reservoirs such as polyP might enhance the regenerative flux of phosphate from hydrolytic breakdown of polyP in the lysate as is hypothesized for phosphate-replete *Synechococcus* WH7803. However, further work is needed to constrain the stability and potential for hydrolysis of polyP outside the cell and to determine its role in regeneration. Alternatively, storage of phosphate in more refractory DOP reservoirs with limited hydrolytic reactivity would limit the regeneration of phosphate from DOP. The remineralization flux of DOP is tightly coupled to nutrient status and the fraction of phosphate released as DOP has significant controls on the ultimate regenerative flux of phosphate. Moreover, releases of equal and greater amounts of phosphate as DOP relative to SRP points toward the significance of enzyme-mediated reactions following lysis in the process of nutrient regeneration.

Lysed cells release particulate reservoirs of nutrient in addition to important DOP and SRP components. Changes in TDP concentration in the lysate signify the potential for particulate stores of phosphate to contribute to remineralization fluxes of phosphate. The stability of particulate phosphate following lysis may be product of the mode of lysis and the storage of

phosphate in particulate resevoirs prior to lysis. Enhanced fragmentation of cellular debris and particulate material could enhance surface area further promoting degradation. Increased surface area is also important in the accessibility of substrate to membrane and particulate-bound enzymes.

Following the initial pulse of SRP, regeneration of phosphate from DOP hydrolysis continues for a period of days subsequent to lysis. Continued enzymatic activity was measured by assays of significant phosphatases, such as APase, and inferred from the hydrolytic release of phosphate from DOP. Losses of activity in APase of approximately 50% after 96hrs of lysate incubation suggest enzymes maintain function without cellular upkeep. Moreover, cultured lysates contain >80% of observed enzymatic activity is in the unfiltered fraction. Therefore particulate and debris-associated enzymes maintaining function following lysis is a significant mechanism to regenerate phosphate.

Our results indicate that lysis releases a mixture of phosphatases with varied activity and specificity for substrates. The nutrient status of the cell prior to lysis is tied to the diversity of phosphatases released from the cell and in the regeneration flux. Pure culture cyanobacterial lysates of *Synechococcus* WH7803 and *E.coli* MG1655 release phosphatases capable of hydrolyzing DOP under both phosphate replete and deplete conditions. In contrast Prochlorococcus MED4, which does not hydrolyze DOP added to lysate under p-replete conditions. The contrast in regeneration rates and enzymatic specificities in culture lysates is evidence that the phosphatase present are a function of internal cell cycling of enzymes prior to lysis. The specificity of lysed phosphatases for the concomitant DOP released has controls the remineralization flux of SRP that extends to interpretation of surface ocean lysates.

All surface ocean lysate incubations where model DOP compounds (5'AMP, GYP, and Pyro-P) were added to lysates exhibited rapid hydrolytic activity. Phosphonates and RNA showed low rates of hydrolysis indistinguishable from control incubations with no DOP spike, ca. 0.4 μM hr^{-1}. Phosphonates are a refractory DOP compound class requiring a C-P lysase for complete breakdown. Not all microbes contain genes and subsequent enzymes necessary for utilization of phosphonates, which places phosphonate regeneration rates lower than other compound classes tested. Oliogotrophic lysate experiments underscore the role of substrate affinity and enzyme specificity in determining phosphate regenerative flux from the DOP released during lysis. Continued hydrolytic activity of APase and other relevant phosphatases supports consideration of phosphatases in particulate and dissolved forms in nutrient regeneration.

Activity of membrane bound enzymes in particulate matter is important in understanding the role of cell lysis in the observed decoupling of carbon and phosphorus cycles in the surface ocean. Particulate-associated enzyme activity is a means to limit the export of phosphate from via the enhancement phosphate regeneration from DOP and POP in the euphotic zone. Our results suggest membrane bound enzymes such as APase maintain activity for a period of days following lysis and continue to breakdown ambient DOP. This has broader significance in understanding oligotrophic export fluxes of phosphate.

This work identifies cell lysis as a critical component of nutrient remineralization. Quantification of the release of phosphate in organic and inorganic forms suggests strain, cellular nutrient storage, and nutrient status are all determinants of the initial phosphate release. Relative amounts of DOP and SRP in the lysed flux are linked to partitioning of phosphate within the cell in labile and refractory nutrient reservoirs. The subsequent regeneration of nutrients following

lysis is a function of the relative amounts of DOP and SRP as well as the enzymes present and their associated substrate specificity. Continued enzymatic activity following lysis results in the production of phosphate via hydrolytic breakdown of DOP. Persistent enzymatic activity following lysis has important controls on regeneration of phosphate, phosphate availability, and particulate export of phosphate from the euphotic zone. Moreover, this work highlights the importance of microbe-scale nutrient cycling and regeneration in understanding larger, global scale nutrient cycling and biogeochemistry.

Chapter 3 – Virally-Mediated Nutrient Regeneration in Cyanobacterium *Synechococcus* WH7803

Abstract

Viruses exhibit important control over nutrient cycling throughout the oceans via infection and subsequent lysis, releasing dissolved organic matter (DOM). Nutrient status of the host has been shown to be an important driver of phage particle production following infection and in characterization of the pool of DOM released. Moreover, viral infection has the potential to shift metabolic functioning of the host cell to increase phage particle production such that the phage-host interaction is the ultimate determinant of the pool of DOM released. This study examines the affect of phosphorus nutrient status on the phosphorus release and the processing phosphorus following infection and lysis.

Phosphate availability plays a pivotal role in limiting primary production in large regions of the oceans. In order to meet their metabolic needs, microbes use a variety of strategies to overcome phosphate stress. Expression of enzymes such as alkaline phosphatase (APase) allows cells to hydrolyze and use certain ambient dissolved organic phosphorus (DOP) compounds to meet their P demand. Cell lysis releases a range of nutrient forms and enzymes into the ambient environment and is an essential component of the microbial loop. Yet very few studies have attempted to characterize both the immediate and sustained nutrient remineralization linked to the milieu of organophosphorus compounds and enzymatic activity in lysate.

Here I conducted experiments using *Synechococcus* WH7803 grown under nutrient replete and starved conditions to quantify the release of phosphate during viral lysis. Dissolved inorganic and organic phosphorus concentrations and APase activity were monitored over time

following lysis. A significant initial release of orthophosphate accompanies lysis. Following lysis, phosphate concentrations continue to rise for a period of hours to days as organophosphorus compounds continue to hydrolyze. Our observations suggest this is due to a combination of direct hydrolysis of DOP released during lysis, solubilization of POP followed by hydrolysis, and possibly polyphosphate decomposition.

Furthermore, size fractionated enzymatic assays suggest cellular debris associated enzymes and dissolved fractions are both important in DOP hydrolysis in the viral lysate, whereas particle associated APase activity dominates in the lysozyme treatments. Moreover, nutrient status prior to lysis has important controls on the initial nutrient release and subsequent regenerative flux. These findings underscore the significance of lysis and subsequent enzyme-mediated hydrolysis in nutrient regeneration and biogeochemical dynamics in marine ecosystems.

1. Introduction and Background

Nutrient concentrations in the ocean are inextricably tied to rates of primary production in the ocean. Primary limiting nutrients nitrogen and phosphorus are low in large, gyre regions of the ocean where there is limited allochthonous nutrient supply. Low nutrient concentrations in gyre regions have selected for organisms with metabolisms that demand elemental thrift (Karl, 2003). Marine microbes have evolved a variety of strategies for meeting their metabolic needs and overcoming nutrient stress. Orthophosphate, P_i, is the preferred phosphorus substrate for cells and can be readily used for metabolic activities and in structural cell components. Concentrations of P_i in oligotrophic regions of the ocean are low enough such that cells have evolved mechanisms for accessing larger organophosphorus compounds to increase accessibility

to phosphorus (Bjorkman & Karl 2003; Dyhrman et al. 2007). Understanding the coupling of phosphate availability and primary production has important controls on local and global biogeochemical cycling of carbon, nitrogen and phosphorus.

Marine photoautotrophs are responsible for almost 50% of global primary production (Field 1998). Photoautotrophs, including *Prochlorococcus* and *Synechococcus* comprise a significant fraction of the community population in oligotrophic gyre regions of the ocean where allochthonous nutrient supply is low. *Prochlorococcus* alone contributes significant quantities of dissolved organic carbon to the water column supporting up to 40% of total bacterial production in the ocean (Casey et al. 2007). *Synechococcus* and *Prochlorococcus* have evolved streamlined genomes and unique mechanisms for nutrient acquisition to reside in nutrient-starved regions of the ocean. Quantifying nutrient cycling by ubiquitous and abundant photoautotrophs, is a critical component to determining controls on biogeochemical dynamics and the fate of carbon in marine environments.

In oligotrophic regions where photoautrophs are abundant, nutrient regeneration of photoautrophic biomass remains to be quantified. The remineralization of cyanobacterial biomass to into dissolved and particulate organic and inorganic nutrient reservoirs is essential to understanding drivers of bacterial and photoautotrophic production in the oceans. The release of cell material to the surface ocean is facilitated by a range of processes including heterotrophic feeding and exudation, viral lysis and auto-lysis. Quantifying the relative contribution cell lysis processes and the magnitude of the associated nutrient flux is critical to understanding the microbial loop.

Within the microbial loop, viruses are a principal mechanism for nutrient release and play a major role in regulating nutrient cycles in the oceans. Viral infection and subsequent lysis

results in the release of DOM that can act as a nutrient source for other ambient microbes fueling bacterial production (Shelford et al. 2012; Middelboe et al. 2003; Middelboe & Lyck 2002). Moreover, viral lysis shifts photosynthetically fixed organic carbon from secondary consumers, heterotrophs and zooplankton, back to primary producers effectively bypassing propagation of reduced carbon up the food chain (Wilhelm & Suttle 1999). In addition, Viruses shift cellular metabolism to increase nutrient access and overcome nutrient limitation (Zeng & Chisholm 2012). Viral infection is a means to re-partition nutrients within the cell into viral particles and other DOP reservoirs. Therefore, the ability of phage to alter host metabolism and cellular nutrient stoichiometry has significant implications for nutrient release from lysed cells and ultimately nutrient cycling.

To determine the flux of nutrients following viral lysis, previous models have estimated and inferred the nutrient flux given cellular nutrient quotas and rates of viral infection and lysis in the surface ocean. Field and laboratory studies estimated rates of release and regeneration through experiments in which viruses are added or removed from natural assemblages and the resultant nutrient flux monitored following infection and lysis. Model estimates of nutrient release of nitrogen and phosphorus release via viral lysis range from 0.2-1.2 μmol N $L^{-1}hr^{-1}$ and 0.04-0.23 μmol P $L^{-1}hr^{-1}$ respectively (Wilhelm & Suttle 1999) while measured rates of nutrient regeneration of ammonium following viral lysis are 0.024 μmol N $L^{-1}hr^{-1}$(Shelford et al. 2012). Comparison of these rates suggests the initial pulse of nutrients following lysis and the subsequent process of remineralization are both important in characterizing nutrient fluxes following viral lysis. The lysed nutrient flux is a complex reservoir with relative contributions by organic and inorganic nutrient forms varying in time and space. The nutrient forms released exist on a spectrum of labile to recalcitrant nutrient forms. More recent, model characterizations of

this flux, estimate that only a minor fraction of the cellular nutrients are bound in phage particles and the fraction of carbon and nitrogen released in particulate and dissolved forms following lysis is nearly equivalent to the amounts found in whole cells (Weitz & Wilhelm 2012). However, phosphate follows a trajectory dependent on the nutrient status of the host. The relative amount of phosphate necessary for phage particle genes is fixed and unchanging, whereas the lysed particulate and dissolved flux of phosphate shifts as phosphate availability of the host fluctuates (Jover et al. 2014). Therefore, viral lysis is responsible for a nutrient release immediately following lysis where nutrient availability of the host must be considered in the nutrient flux with considerations for the relative contributions of inorganic and organic forms and the lability of the organic pool.

Nutrient status of the host is also critical for phage particle replication and quantifying nutrient fluxes post viral lysis. Previous studies aimed at characterizing the link between nutrient availability and viral infection determined that phosphate limitation had no effect on ability of phage to infect *Synechococcus* WH7803 (Wilson et al. 1996). However, relative to phosphate-replete experiments, phosphate limitation led to an 18-hour increase in the lytic cycle, decrease in cell burst size, and decline in the fraction of cells lysed (Wilson et al. 1996). Therefore phosphate limitation extends to phage, leading to in lengthened timescales for phage replication and infection. This is observed in decreased release of progeny and smaller burst sizes. This work underscores the importance of environmental nutrient availability and mechanisms for nutrient release via viral infection. More recent work highlights the coupling of nutrient availability and infection in another cyanobacterium, *Prochlorococcus* MED4. Phage P-SSM2 is able to manipulate the host, *Prochlorococcus* MED4, two component regulatory system for phosphate uptake during conditions of host phosphate limitation (Zeng & Chisholm 2012). Viral

up-regulation of host phosphate uptake genes provides new insight into the complexity of virus host interactions in the ocean and the necessity of including coupled virus host genetic regulation pathways.

Internal reservoirs of phosphate, such as polyphosphate, are important to consider in understanding virus-host interactions relative to nutrient limitation. Stores of phosphate intracellularly as polyphosphate reflect surplus phosphate storage, however viral access to this reservoir is unknown. Viral access to nutrient-rich reservoirs would provide several advantages to phage replication and release and in turn alter the nutrient release following lysis. In addition, direct release, of polyphosphate provides ambient organisms with access to phosphate rich material to relieve nutrient stress. Recent estimates of polyphosphate in the Sargasso Sea indicate polyphosphate is a significant reservoir, at phosphate concentrations previously assumed to restrict polyphosphate storage (Martin & Van Mooy 2013). Alternatively, reducing cellular p quota to limit phosphate demand by mechanisms such as sulfur replacement in lipids also has consequences for the relative lysed phosphate pool of organic and inorganic phospahte as well as in the lability of this release for remineralization. Moreover, previous work characterizing lysis fluxes following lysozyme treatment of photoauotrophs showed declines in phosphate release in phosphate-starved cells suggesting that intracellular orthophosphate and organic reservoirs shift, highlighting the coupling of the lysed nutrient flux and nutrient availability (Chapter 2).

The quantification of nutrient releases from ubiquitous photoautotrophs is fundamental to understanding the recycling of nutrients in the surface ocean. Viral lysis remains a primary mechanism for the liberation of dissolved and particulate nutrient forms from surface ocean microbes, but quantification of lysed nutrient fluxes is limited. The role of nutrient availability in determining the flux of nutrients following lysis will help to characterize the significance cell

lysis within the framework of microbial loop nutrient cycling. Here we determine the nutrient release during viral infection of *Synechococcus* WH7803 with phage Syn9 to understand the nutrient release induced by viral lysis. To determine the role of phage in determining nutrient release, this study characterizes the enzymes and phosphate flux during viral infection and subsequent to lysis. Phosphate medium status was varied between replete and deplete conditions to monitor changes in nutrient release and nutrient regeneration. Dissolved organic and inorganic reservoirs of phosphate were monitored alongside enzymatic assays for APase to resolve the immediate release of nutrients and the sustained regeneration by phosphatases during infection and lysis. This work has important implications for biogeochemical nutrient cycling given that viral lysis is a dominant mechanism for cell lysis in the surface ocean. In oligotrophic regions, virally released nutrients may be a major nutrient flux to provide local nutrient relief. In addition this represents a significant, previously, un-quantified pathway for release and remineralization of lysed cell DOM.

2. Materials and Methods

Synechococcus WH7803 was isolated from the Sargasso Sea and grown in artificial seawater (ASW), specified in Supplemental Table A2. Cultures were grown at 21°C under white light intensities of 33-40 μE m^{-2} s^{-1} and continuously stirred. All cultures were confirmed to be axenic by inoculation of marine purity broth to check for contaminant growth in the dark.

Cultures considered phosphorus replete were grown in medium with orthophosphate as the sole phosphorus source while P-starved cultures indicate cultures in which cells were grown in P-replete medium, pelleted, and resuspended in phosphorus free medium for 48hrs. Phosphorus-starved cells were prepared by pelleting of phosphorus replete *Synechococcus*

WH7803 at 8000G. Cells were gently rinsed once with phosphate free ASW and resuspended in phosphate-free ASW. To confirm phosphate limitation, APase activity in the phosphate-free medium was monitored for a period of 48hrs using the DiFMUP assay below.

Synechcoccus WH7803 bacteriophage Syn9 was concentrated following infection and clearing of approximately 1L of culture. Cultures were 0.2 μm filtered to remove cellular debris and stored at 4°C prior to concentration. Concentration of phage was completed by centrifugation (5000G) with Amicon Ultra 15 30K centrifugal filter units, washing twice with phosphorus-free ASW and resuspension in the same medium. Phage density was determined by microscopy following SYBR Gold staining of phage and counting on a 0.1 μm Anodisc filter. Phage infection was carried out with a multiplicity of infection of 3 for both p-replete and p-deplete cultures. Phosphorus-replete and phosphorus-deplete cultures were grown to similar cell densities prior to infection with Syn9, confirmed by flow cytometry (Millipore Attune) (Figure A5).

Enzymatic activity of alkaline phosphatase (APase) was assayed by addition of the fluorphore 6,8-Difluoro-4-methylumbelliferyl phosphate (DiFMUP) to un-filtered and 0.2 μm filtered aliquots of control and infected cultures. Hydrolysis of the phosphoryl group releases the fluorescent product difluoro-7-hydroxy-4-methylcoumarin (DiFMU), excitation 358nm and emission 450nm. The rate of DiFMU production was monitored over time in a Turner Monochrome Fluorometer at 21°C on a Turner fluorometer in a 96-well plate at a saturating concentration of substrate (10 μM final concentration). A standard curve of DiFMU (0-4 μM) was prepared in ASW phosphorus free medium to calculate rates of DiFMUP hydrolysis. Blanks were prepared in ASW phosphorus free medium and run alongside samples at saturating

substrate concentration to determine rates of autohydrolysis. No significant autohydrolysis of the substrate was observed.

Soluble reactive phosphorus (SRP) was determined in triplicate by the molybdenum blue reaction (Murphy and Riley, 1962). Briefly, 0.2 μm filtered aliquots of culture were measured in either 1cm or 10cm cuvettes, depending on concentration, and absorbance measured at 883nm. Total dissolved phosphorus (TDP) was measured in triplicate using the method outlined in Monaghan and Ruttenberg, 1999 with acid washed and ashed glassware. Filtered culture aliquots (0.2 μm filtered) were acid hydrolyzed in 0.1M HCl (final concentration) at 80°C until dry and subsequently ashed at 500°C. Following ashing, samples were again acid treated at 80°C with 3ml of 0.75M HCl, cooled, and diluted to 10ml with DI water before final heating to 80°C. Following these steps, total dissolved phosphorus was determined via the molybdenum blue reaction (Murphy and Riley, 1962) in 1cm and 10cm cells for phosphorus replete and phosphorus deplete samples, respectively.

3. Results and Discussion

3.1 Characterization of the phosphate pool following the viral burst

The phosphorus pool following viral lysis is composed primarily of organic phosphorus. Immediately following lysis the release of DOP is also accompanied by a release of orthophosphate, 0.5-14 amol/cell, which is within the range of orthophosphate released for lysozyme lysed *Synechococcus* WH7803 and lysozyme-treated surface ocean populations from the Sargasso Sea. The pulse of DOP and SRP comes 4-6 hours after infection, when SRP concentrations increase to approximately 50nM, double the uninfected controls (Figure 3.1).

A

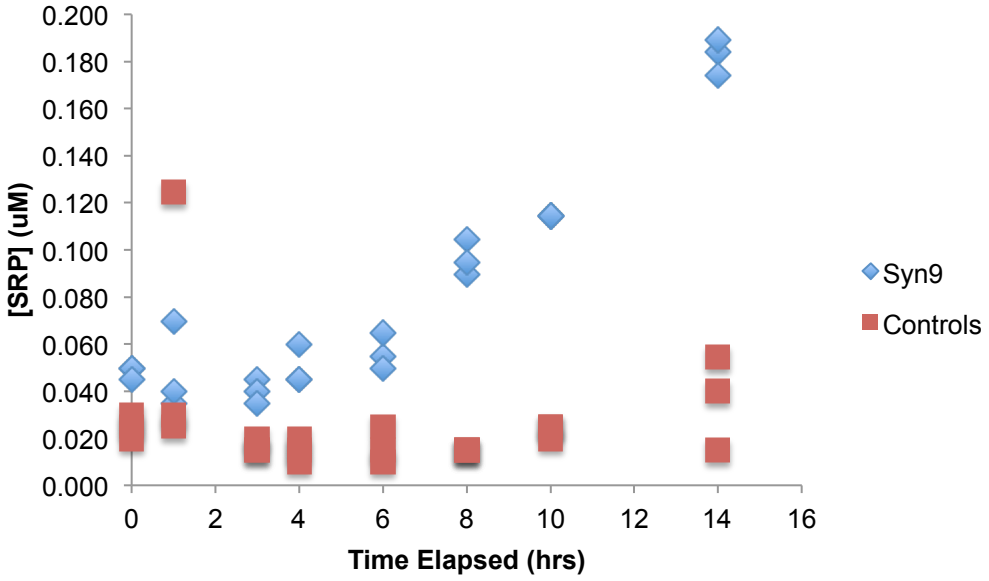

B

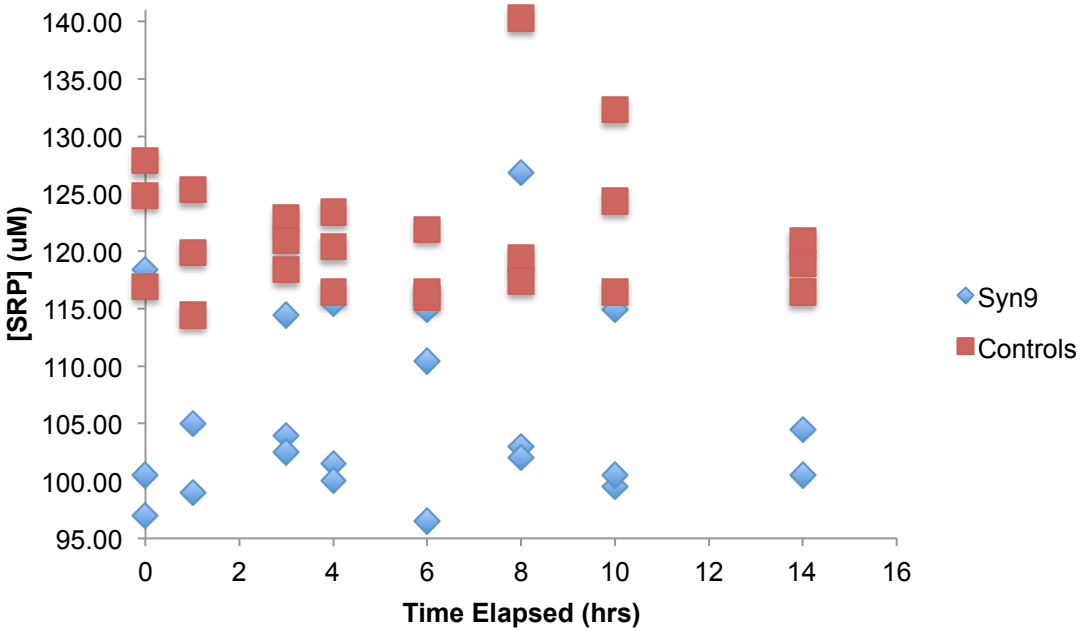

Figure 3.1 [SRP] During Infection and Following Lysis.
Phosphate concentrations in Controls (unifected cells) and Syn9 (phage-infected) cells following infection. (A) SRP changes over time in phosphate-starved *Synechococcus* WH7803 medium. (B) SRP changes in phosphate-replete cells subsequent to infection.

[SRP] continues to rise over the next 6-7 hours reaching a maximum at 14 hours of ~180nM. The release of phosphate following viral lysis is best characterized in the phosphate-deplete experiments as a result of high background phosphate in replete analogs. Dilution of phosphate-replete medium limits detection of the small changes in orthophosphate and DOP necessary for characterization here. Nutrient deplete experiments provide important estimates for flux of both DOP and SRP following lysis. DOP over the same time period as orthophosphate follows a similar pattern increases after the burst at 4-6 hours post-infection. Fourteen hours after infection [DOP] climbs to a maximum [DOP] of 2.25 μM (Figure 3.2). The initial pulse of phosphate is representative of the intracellular release of organic and inorganic phosphate reservoirs. Higher relative contribution by DOP in virally lysed cells versus lysozyme cells points towards viral partitioning of nutrients during infection prior to burst. The role of phage partitioning may also extend to intracellular enzymes present and thus be important in the magnitude of the regenerative flux.

Observed increases in phosphate reflect a balance in DOP hydrolysis and phosphate uptake by intact cells. Ambient, unlysed cells are capable of accessing lysed phosphate in both organic and inorganic reservoirs. Therefore, to estimate the actual phosphate released during lysis and rates of regeneration following lysis, the relative uptake by intact cells must be considered. Published estimates of orthophosphate uptake for *Synechcococcus* range widely from 0.01-2.42 amol $cell^{-1}hr^{-1}$. Uptake of phosphate by intact, unlysed cells is difficult to quantify in this study, however estimates of the regenerative flux that include phosphate uptake only increase the magnitude of the regenerative flux. Measured rates of SRP production, 1.32 amol $cell^{-1}$ hr^{-1} represent a lower bound for rates of phosphate regeneration (Figure 3.3). Correcting the data for uptake by intact cells using p-deplete uptake rates suggests uptake is a minor component

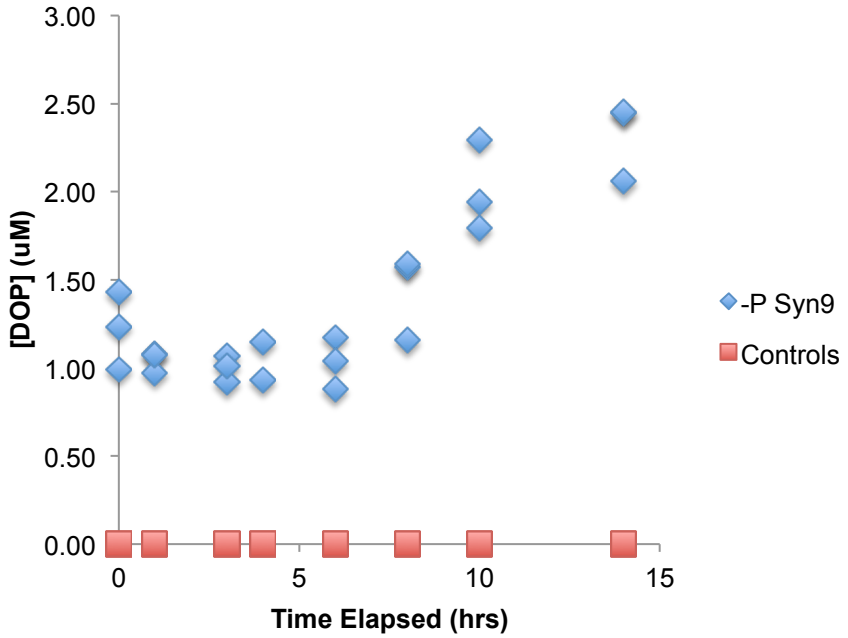

Figure 3.2 [DOP] in P-Starved Cells.
Phosphate-starved *Synechococcus* WH7803 infected with Syn9 shows changes in [DOP] following infection only after the cells have lysed between 4-6hrs. Control experiments show background [DOP] near detection limits.

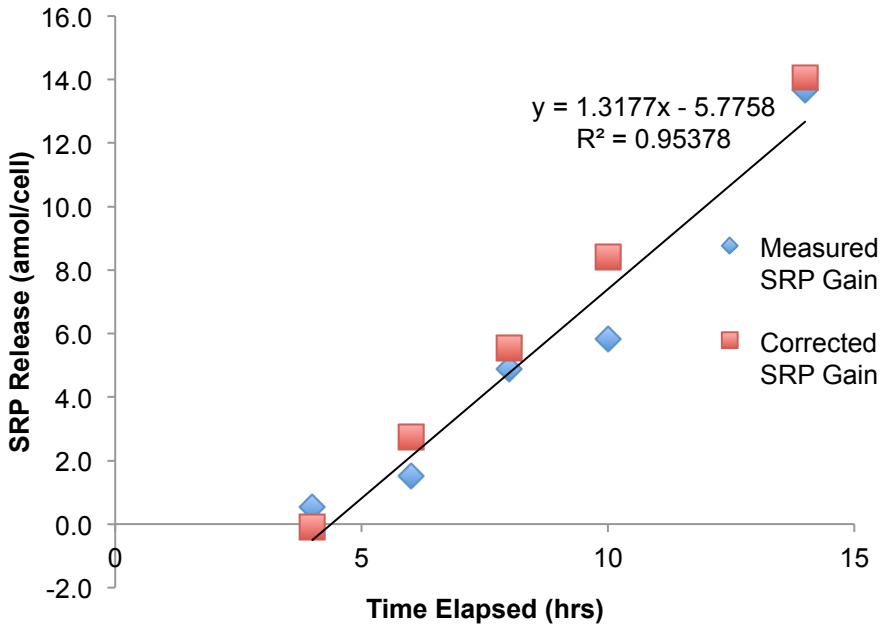

Figure 3.3 Accounting for Phosphate Uptake.
Blue points are the measured SRP released/lysed cell following the viral burst. To determine the fraction of the phosphate released that might be consumed by live, intact cells a correction to the data was applied to monitor the significance of uptake by live cells. The red points are the corrected data where published estimates for phosphate uptake rate/cell were added to measured SRP releases/cell.

in characterizing phosphate cycling post-lysis. Moreover, the flux of orthophosphate following lysis is primarily an initial pulse released from lysed cells followed by hydrolysis of DOP via enzymatic hydrolysis. This model is relevant for the surface where the microbial community is a mixture of infected and uninfected host populations. Uninfected populations have potential to directly uptake freshly lysed material and contribute to alteration of the lysed nutrient pool. Measured rates of regeneration in this study provide useful estimates for understanding environmental viral lysis processes in the surface ocean.

In addition to orthophosphate increasing, DOP increases following the viral burst, indicating particulate phosphorus is relevant to characterizing the DOP reservoir alongside enzymatic activity. Therefore, in understanding processing of the DOP reservoir by lysate enzymatic activity one must also consider a supplementary flux from labile particulate fractions.

3.2 Enzymatic Activity in the Lysate and SRP Regeneration

The effects of enzymatic activity are measured by orthophosphate increases over the infection period. Increasing SRP in the lysate is a result of phosphatase activity in the lysate, where hydrolytic activity facilitates the release of orthophosphate from DOP. Enzymatic assays of APase reveal significantly higher APase activity in cells infected with phage versus those without. APase activity increases exponentially from ~2 amol/cell immediately following adsorption to over 200 amol/cell 14 hours after infection, Figure 3.4. These rates are relative to controls, where APase activity increases, linearly to a maximum of 25 amol/cell after 14 hours. APase activity was near the detection limit in phosphate-replete experiments (Figure 3.4). Two potential mechanisms can explain these findings: either APase activity post-lysis is a result of phage-altered phosphatase expression or newly available DOP induces exponential increases in

A

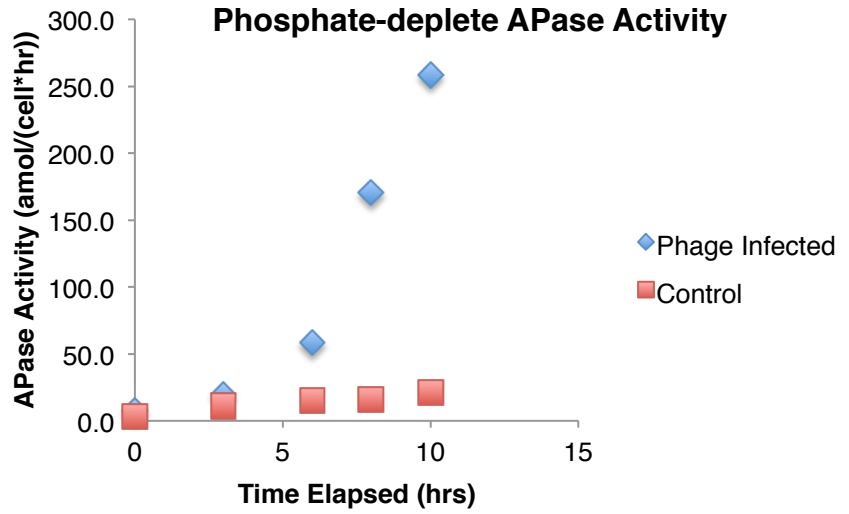

B

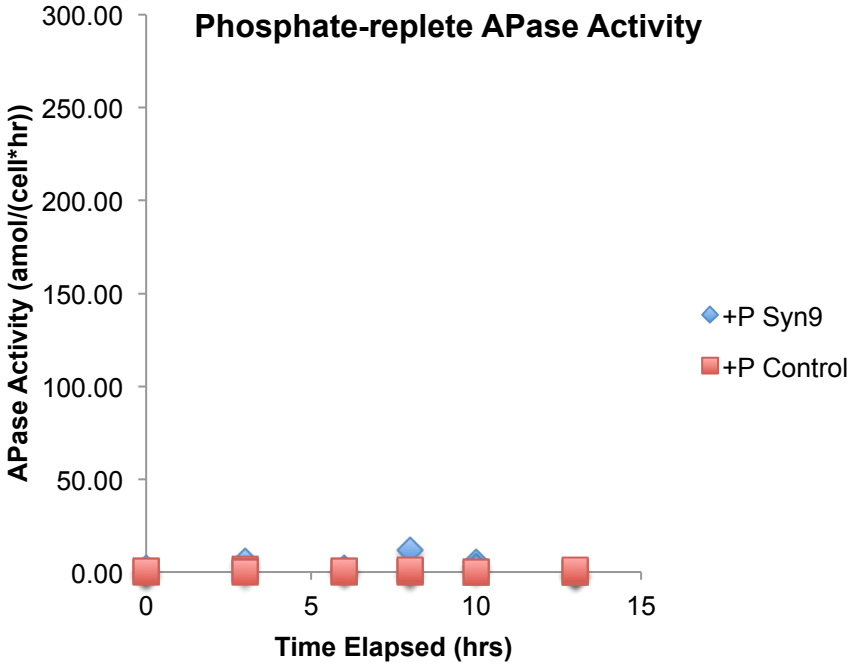

Figure 3.4 Alkaline Phosphatase Activity in Controls and Infected Cells.
Exponential increases in APase activity are observed in A only in the Syn9 infected cells, while controls increase linearly over the course of the infection. Contrast these results with B, where APase activity in p-replete cells was near detection limits throughout the experiment.

APase activity of intact cells. Previous attempts to characterize DOP induced APase expression discounted this hypothesis, however those studies were completed with well-characterized DOP compounds. In this experiment the flux of DOP following lysis is complex and the lability and character of this pool is largely unknown. The reactivity of virally lysed DOP could induce expression in unlysed cells, leading to observed exponential increases. Alternatively, the measured activity of APase might actually represent enzymatic activity a range of phosphatases with broad specificity. In this case, phage encoding of phosphatase activity would lead to up-regulation of a vast pool of non-specific phosphatases that rapidly hydrolyze DiFMUP in an attempt to relieve nutrient stress. This up-regulated enzyme pool would subsequently be released along with phage particles during lysis.

Size fractionated APase activity underscores the importance of intact cells and cellular debris in the processing of DOP following lysis. APase activity in unfiltered fractions is ten times the 0.2μm filtered fraction (Figure A6). However, APase activity in the 0.2μm fraction is nearly equivalent to measured APase activity in the controls. Nominally dissolved APase (<0.2 μm) and particulate bound APase comprise the two dominant reservoirs of enzymes following lysis. Debris-bound, or membrane-associate APase activity contributes more to the regeneration of SRP from DOP hydrolysis. APase activity in the unfiltered, particulate fraction indicates a mechanism of regeneration where intact cells and cell fragments participate in the breakdown of lysate DOM. In this model, particulate and membrane-bound enzymes supplement DOM decomposition by intact cells that hydrolyze DOM for orthophosphate uptake. Observations of particulate-bound APase activity are not unique to this work; particle-bound APase expression is observed in lysozyme treated *Synechococcus* WH7803 experiments as well. In lysozyme treated cells, unfiltered lysate comprises the most important reservoir of enzymatic activity (>80%).

Results from cells lysed via viral infection and lysozyme indicate a spectrum of enzymes in different size fractions, ranging from nominally dissolved (< 0.2μm) to particulate bound that all contribute to nutrient remineralization. This finding provides useful insight towards the relative importance of particulate fractions in the process of remineralization.

3.3 Regeneration Rates in Viral Lysates: Relevance for Surface Ocean Nutrient Cycling

The rate of DOP hydrolysis following lysis is a function of the enzymes present, the affinity of enzymes for substrate, and the substrate concentration. Comparing rates of SRP production and measured APase activities post-lysis provides an estimate of the rate of phosphate regeneration via two independent methods. This comparison is useful in understanding the character and lability of the pool of DOP released, where offsets in the two estimates highlight the importance of substrate affinity and concentration in how much DOP is broken down. SRP is produced as a consequence of phosphatase activity that is indirectly measured by phosphate concentration, while APase activity is directly measured by an incubation with a model DOP compound (DiFMUP) that is also a fluorophore following hydrolysis. Measured rates of DOP hydrolysis, 1.32 amol cell^{-1} hr^{-1}, are almost two orders of magnitude less than APase activities of 103 amol cell^{-1} hr^{-1} (Table 3.1). One explanation is the role of substrate concentrations. Substrate-limited and substrate-replete conditions will lead to different V_{max}. APase determination via DiFMUP involves [DiFMUP] = 10 μM, whereas [DOP] in the lysate is 1-2 μM. Therefore the SRP determined regeneration rate may reflect hydrolysis below V_{max}, during which enzymes are substrate-limited. Another explanation for the offset in these rates is that the mechanism of lysis has controls on the character of the flux of DOM.

	Sample ID	5-1,10	8-any	10-1,2,3	10-14,15,16	*Synechococcus* 7803	*Synechococcus* 7803	*Prochlorococcus* MED4	*Prochlorococcus* MED4
	Location	OFP, 20m	OFP, 20m	OFP, 20m	OFP, DCM				
	P Status					Replete	Deplete	Replete	Deplete
Lysozyme	**DiFMUP Apase Activity (amol cell^{-1} hr^{-1})**		3.004	0.689	0.132	0.114	0.862	b.d	1.296
	DOP Hydrolysis (amol cell^{-1} hr^{-1})	0.664	0.197	1.836	0.842	0.300	0.040	0.001	0.001
	TDP Changes(amol cell^{-1} hr^{-1})	0.543		0.227					
Viral	**DiFMUP Apase Activity (amol cell^{-1} hr^{-1})**						103.000		
	DOP Hydrolysis (amol cell^{-1} hr^{-1})						1.320		
	TDP Changes(amol cell^{-1} hr^{-1})						8.967		

Table 3.1 Comparison of Rates in Lysozyme and Viral Lysis Experiments
Compilation of measured APase activities via the DiFMUP hydrolysis assay outline in Section 2 and DOP hydrolysis rates determined by monitoring increases in SRP. TDP change is the rate of TDP increase measured in lysozyme-treated and virally lysed cells normalized to cell density.

Previous studies have shown phage infection dramatically alters the flux and character of DOM compared to the uninfected lysed controls (Ankrah et al., 2014). In this case the lysozyme DOM, particularly phosphatases and DOP, is different than the phage experiment where phage have altered intracellular reservoirs seeking nutrients for rapid phage particle replication. This offset in measured rates underscores the character of the lysed pool of DOP and lysis mechanism in determining the pool of phosphatases and the rates of phosphate regeneration.

Phosphate regeneration in the lysate is observed in experiments of lysozyme-treated cells and virally-lysed cells. Differences between these modes of lysis might highlight the mechanism for lysis as significant in the nutrient release. How cells are lysed has important controls on the ability of substrate to access the active site of enzymes as well. Substrate access to enzymes of debris-associated enzymes is related to the nature of the cell membrane fragments. Membrane-associated activity is invoked as the mechanism for sustained activity of phosphatases in lysozyme-treated cells, as the membrane provides structural framework for the enzyme to circumvent rapid degradation extracellularly. To contrast how the mechanism of lysis is related to nutrient fluxes and membrane fragmentation, rates of regeneration rates of APase activity and SRP production, lysozyme lysed cells and virally lysed cells were compared (Table 3.1). Rates of phosphate regeneration, or DOP hydrolysis, for these modes of lysis span a broad range, from 0.04-1.84 amol P $cell^{-1}$ hr^{-1}. Virally lysed *Synechococcus* WH7803 regenerates phosphate at a rate of 1.32 amol P $cell^{-1}$ hr^{-1}, with APase rates of 103 amol P $cell^{-1}$ hr^{-1}, in contrast to analogous lysozyme treated cells where the SRP regeneration rate and APase activity are markedly lower, 0.862 amol P $cell^{-1}$ hr^{-1} and 0.04 amol P $cell^{-1}$ hr^{-1}. Phosphate regeneration in virally lysed cells is most similar to rates observed in the Sargasso Sea, where lysozyme treated 20m surface ocean communities regenerated phosphate at 0.3-1.8 amol P $cell^{-1}$ hr^{-1}. The dynamic range in rates of

remineralization is a testament to the complexity of the process of remineralization. Furthermore, fluctuations in the TDP pool suggest contribution from particulate reservoirs is significant in virally lysed cells. TDP reservoir changes were also observed in lysozyme experiments (0.2-0.5 amol P $cell^{-1}$ hr^{-1}) however maximum rates of TDP change were lower than TDP changes in viral lysates (8.9 amol P $cell^{-1}$ hr^{-1}). Different rates of regeneration and APase activity can be explained by several factors where relative significance of one explanation could vary with mode of lysis. These explanations include the following: different accessibility to enzyme active site, destruction of select membrane proteins and enzymes, and finally different lysis modes release forms of DOP with associated, varied lability that contribute different fluxes of POP. The relative influence of these factors is difficult to assess, but warrants consideration in conceptualization of how lysis mode is coupled to the process of remineralization.

Remineralization of organic and particulate nutrient forms to dissolved inorganic nutrients is a fundamental process in determining nutrient availability in the ocean. However, the rates and temporal and spatial variability of these rates are poorly constrained. Estimates for the rates of viral lysis in the ocean provide useful constraints for its relative contribution to nutrient cycling. Model estimates of nutrient release rates use particulate nutrient stoichiometry coupled to viral production rates and burst sizes to estimate a range of carbon, nitrogen, and carbon release fluxes. Nitrogen regeneration rates in model estimates range 0.2-1.2 μmol L^{-1} hr^{-1} and phosphorus rates span 0.04-0.23 μmol L^{-1} hr^{-1} (Wilhelm and Suttle, 1999). However, measured rates of ammonium remineralization from the Mediterranean Sea are markedly lower, 0.02 μmol L^{-1} hr^{-1} (Shelford et al., 2012). Measured rates of phosphate remineralization from this study, 0.014 μmol L^{-1} hr^{-1}, fall below the model estimate range as well. Deviation of model estimates from measured rates derives primarily from assignment of nutrient stoichiometry to a mixed

microbial community. Nutrient stoichiometry for even single strains varies over a dynamic range and relative contributions by individual cell strains to the nutrient pool will vary in time and space. Normalization of regeneration to per cell units estimates provides a more accurate measure of the relative contribution by each community member to nutrient flux. Coupling of measured regeneration rates to previously determined rates of phosphate uptake highlights the biogeochemical implications of this work. Although this work involves infection and lysis of a greater fraction of *Synechococcus* than would occur from a single lysis event in the ocean, per cell rates of regeneration are significant. Rates of phosphate uptake measure at BATS and HOT are 0.24-48 nmol L^{-1} hr^{-1} and 2.3-9.1 nmol L^{-1} hr^{-1} respectively. Therefore volumetric rates of phosphate remineralization presented in this study estimate viral lysis can support 25-100% of phosphate demand in oligotrophic regions. In oligotrophic regions such as Sargasso Sea and North Pacific Subtropical Gyre, photoautotrophs comprise a significant fraction of the microbial population. Understanding the relative efficacy of nutrient cycling by *Synechcococcus* WH7803 is a primary goal to determining the role of lysis in the processing of nutrients through the microbial loop.

4. Conclusions

Viral infection of surface ocean microbes and subsequent viral lysis represents as significant pathway in facilitating the transformation of dissolved and particulate nutrient forms. Quantification of associated viral nutrient fluxes was previously limited. The aim of this work was to quantify nutrient releases from photoautotrophs to understand the recycling of nutrients in the ocean. Here we determined the nutrient release following viral lysis of *Synechococcus* WH7803 with phage Syn9 to understand its relevance to nutrient cycling in the oceans. Our

assessment of the nutrient flux indicates viral lysis contributes significantly to dissolved inorganic and organic reservoirs of phosphate subsequent to lysis. In addition, the processing of lysate is facilitated by phosphatases and other enzymes that breakdown DOP and release orthophosphate. Intracellular reservoirs of enzymes and nutrients have important controls on the enzymes present in the lysis flux and in the regenerated flux. Moreover, phage infection is tightly coupled to enzymatic expression and activity in the lysate.

This work highlights viral lysis as a pathway for release and remineralization of cellular DOM. Viewed alongside previous laboratory and field based lysis experiments, the release of nutrients during cell lysis is a process of the microbial loop warranting further study in understanding nutrient dynamics in the surface ocean. Estimates of phosphate regeneration indicate that viral lysis is a mode of nutrient supply able to support measured rates of phosphate uptake in oligotrophic gyre regions. This work provides quantification of a vastly important flux with implications for broader global-scale nutrient cycling. Cyanobacteria are some of most abundant cells on earth. Determining nutrient release and recycling by these cells constitutes a better understanding of phosphorus dynamics in nutrient-starved, vast region of the ocean.

Dissertation Conclusions

Primary production in oligotrophic gyres is supported through efficient recycling of organic matter in the surface ocean. Low phosphate concentrations in the Sargasso Sea and North Pacific Subtropical gyre limit production, demanding microbial access to organic and inorganic reservoirs of phosphate to meet cellular demand. Rapid turnover of phosphate leads to carbon and phosphorus decoupling in these regions, where phosphorus is preferentially remineralized for direct uptake to support microbial activity. Although uptake of orthophosphate and DOP in the surface ocean is well characterized, the release of these dissolved components back to the environment following cell death has eluded this field. This work quantifies the phosphate release via cell lysis and processing of nutrients subsequent to lysis in order to assess the significance of these mechanisms in meeting ambient microbial phosphate demand. Efficient turnover in oligotrophic regions suggests the release of inorganic nutrients forms is followed by rapid consumption. However, the transformation of lysed cellular debris and ambient DOP by freshly released enzymes is also significant to characterizing nutrient availability. An understanding of the uptake and release fluxes of phosphate is necessary to determining the mechanisms by which recycling supports primary production. Moreover, to predict changes in primary production and model ocean biogeochemistry quantification of mechanisms to controlling nutrient availability is required.

This work has quantified the release of phosphate from lysed cells in laboratory and surface ocean environments to provide constraints of these fluxes in understanding the microbial loop of phosphate. These findings highlight the initial pulse of phosphate as an intracellular release of orthophosphate from the cell. The magnitude of orthophosphate released is a function

of strain and the nutrient status of the cell prior to lysis. Continued enzymatic activity by debris and particulate-bound enzymes transforms particulate and predominantly dissolved organic phosphate to orthophosphate. In addition, these remineralization reactions are linked to the enzymatic expression and activity of the cell prior to lysis. Phosphate-starved cells, expressing alkaline phosphatase, are conditioned to remineralize more phosphate from DOP than phosphate replete cells. However, other phosphatases are significant in the regeneration of orthophosphate from DOP as was observed in both *E.coli* and *Synechococcus*. In nutrient-replete experiments these cells also have the capacity to hydrolyze significant DOP in the lysate via phosphatases other than APase. The significance of our findings of phosphate release and transformation in the lysate are further corroborated by cells lysed via viral infection, a common means of cell lysis in the surface ocean as compared to lysozyme treatment of populations.

Similar to cells lysed via lysozyme treatment, virally infected cells release an initial pulse of DOP and orthophosphate subsequent to lysis. Moreover, virally lysed cells underscore the importance of enzymatic activity in debris and particulate-bound reservoirs in nutrient regeneration. The initial release of phosphate is only 20% of the total orthophosphate produced via breakdown of DOP in the lysate by enzymes. In addition, the flux of DOP from virally lysed cells was greater than cells ruptured via lysozyme treatment suggesting phage altered metabolism could alter lysed nutrient fluxes. Characterization of phosphate release via viral and lysozyme treatment shows that cell lysis is an important mechanism in the release and regeneration of nutrients in the surface ocean.

Estimates of release and regeneration from this study are most significant when viewed alongside previous measured rates of phosphate uptake in oligotrophic regions.

Release of orthophosphate and regeneration from breakdown of DOP constitutes a major flux of available phosphate in the surface ocean to relieve nutrient stress. This work suggests that phosphate regeneration by enzymatic activity after cell death alone can support phosphate demand in oligotrophic regions of the ocean. Clearly, cell lysis of surface ocean bacteria is a means to relieve nutrient stress in both the NPSG and Sargasso Sea.

This work contributed to our understanding of the microbial underpinning of nutrient cycling in the oceans and its effects on ocean biogeochemistry. Through this work I have identified lysis of surface ocean bacteria as an important means to relieve local nutrient stress and facilitate the transformation of organic matter. In addition, the enzymatic processing of organic matter by dead cell-bound enzymes presents a new mechanism for phosphorus remineralization and pathway that helps explain carbon and phosphorus decoupling in the surface ocean. Quantifying the regeneration of phosphate provides new estimates for rates of nutrient cycling and is valuable in larger-scale models aimed at determining and predicting ecosystem change. Moreover, refinement of stable isotope tools allows one to address larger biogeochemical cycling of phosphate and its link to carbon fluxes in the ocean.

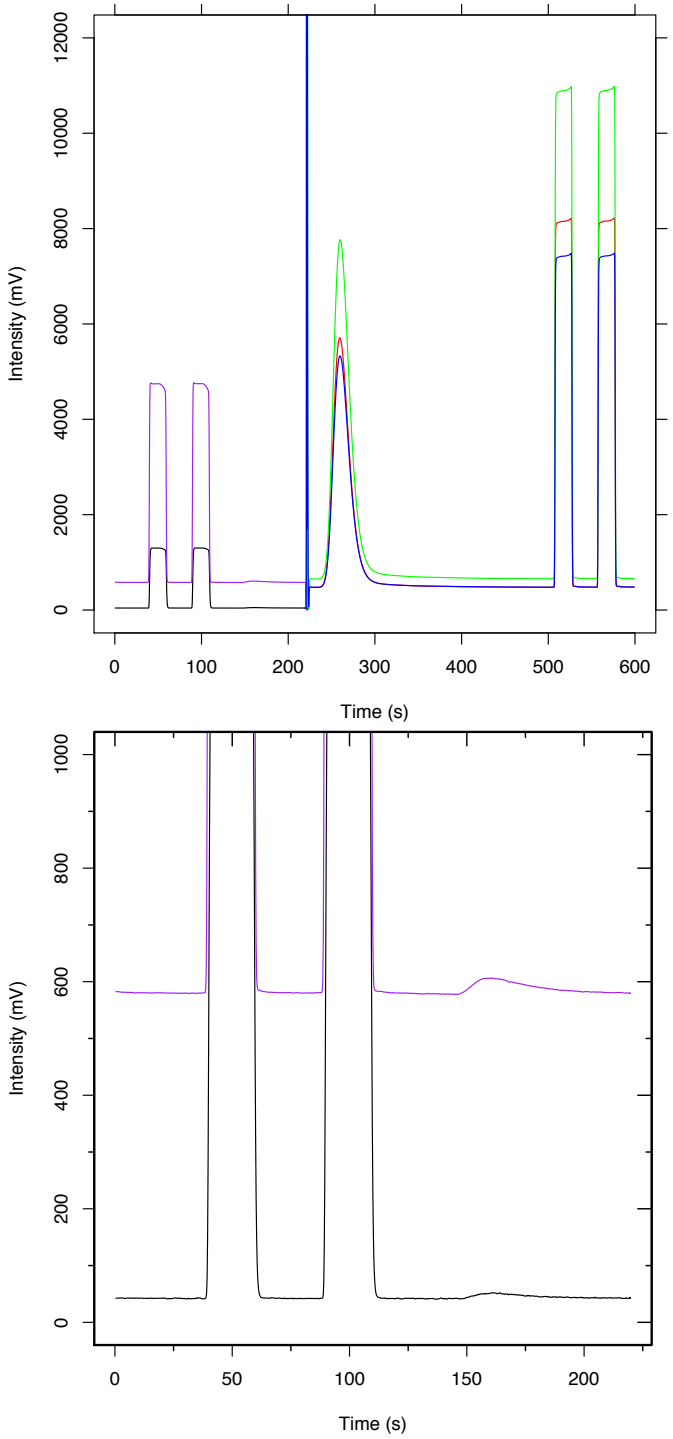

Figure A1 Isotopic Acquisition Trace.
Trace hydrogen in TC/EA analysis of Ag_3PO_4: Shown is an example isotopic acquisition trace, where hydrogen and oxygen were measured in the single sample run. The top is the sample run

Figure A1 continued…excluding the sample CO peak at 260s and reference CO peaks at 550 and 580s. On the bottom is the hydrogen acquisition region expanded to show no detectable hydrogen from water.

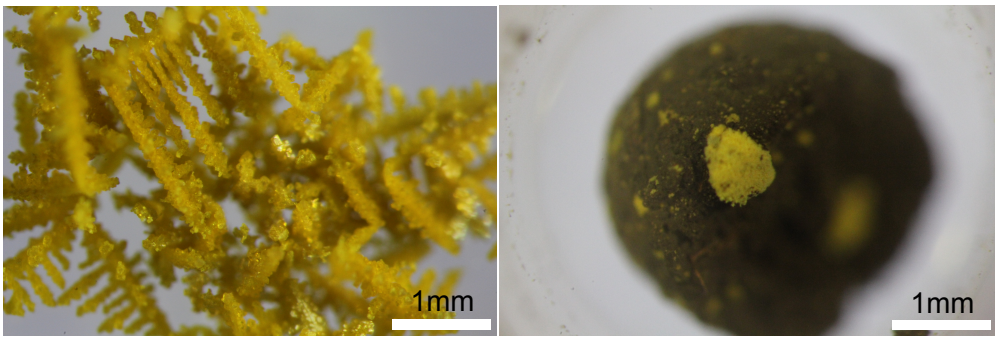

Figure A2 Optical Microscopy Images.
A characterstic slow microprecipitation (left) and Strem treatment (right). Silver phosphate precipitated via slow method exhibits dendritic bright yellow crystals ca. 2mm in length. The original Strem standard material is visible in bright yellow clasts surrounded by silver oxide overgrowth.

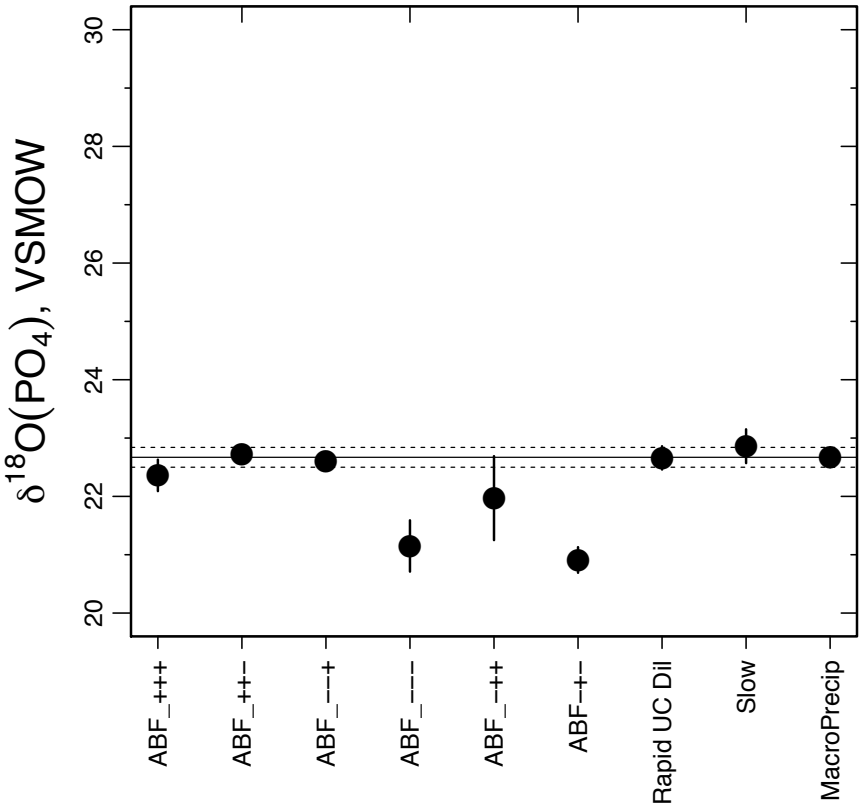

Figure A3 Solution Composition Affects on $\delta^{18}O_p$.
Phosphate oxygen isotope values for different precipitation solution compositions. Initially presence and absence of acid (A), base (B), and (F) in microprecipitation solution was varied to determine how these components might effect $\delta^{18}O_p$ and the fraction of phosphate remaining in solution. Error bars represent the standard deviation for a measurement completed at least in triplicate. Each point represents a precipitation via the set up specified in Table 1 of the same potassium phosphate monobasic solution. Macroprecipitation of this material is used as a baseline with assigned standard deviations (horizontal dotted lines) and mean (solid horizontal line). Certain treatments lacking acid show deviation from expected composition by ca. 1.5 ‰.

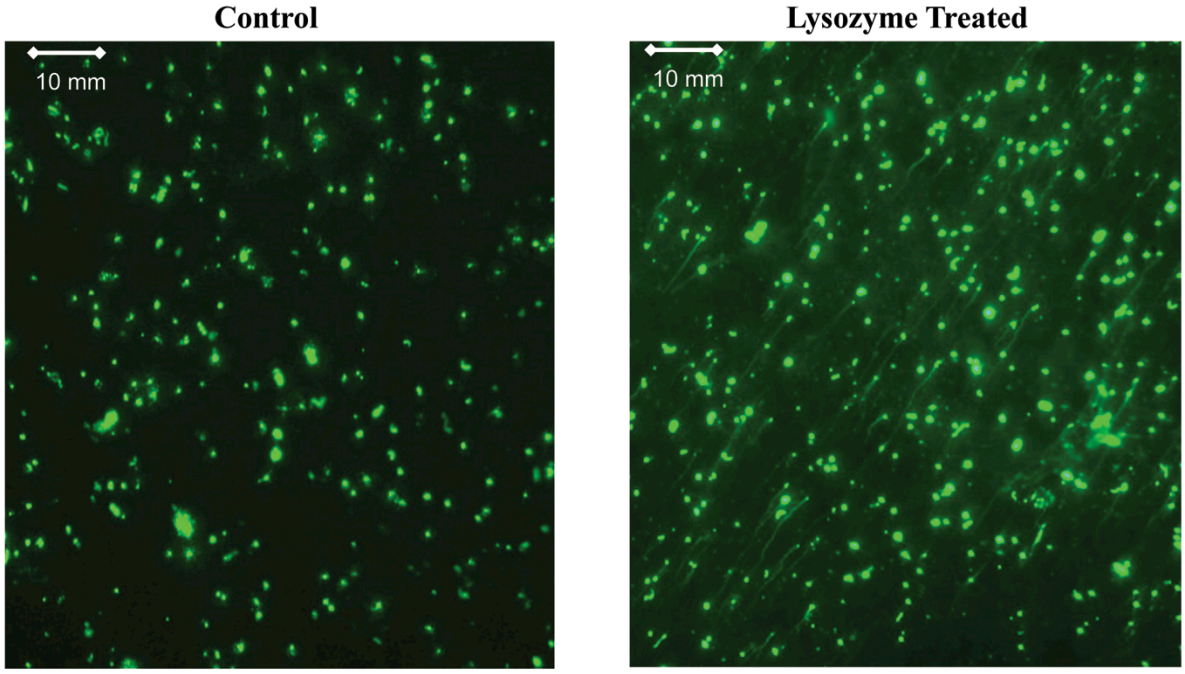

Figure A4 Chromosomal Leakage from Lysed Cells.

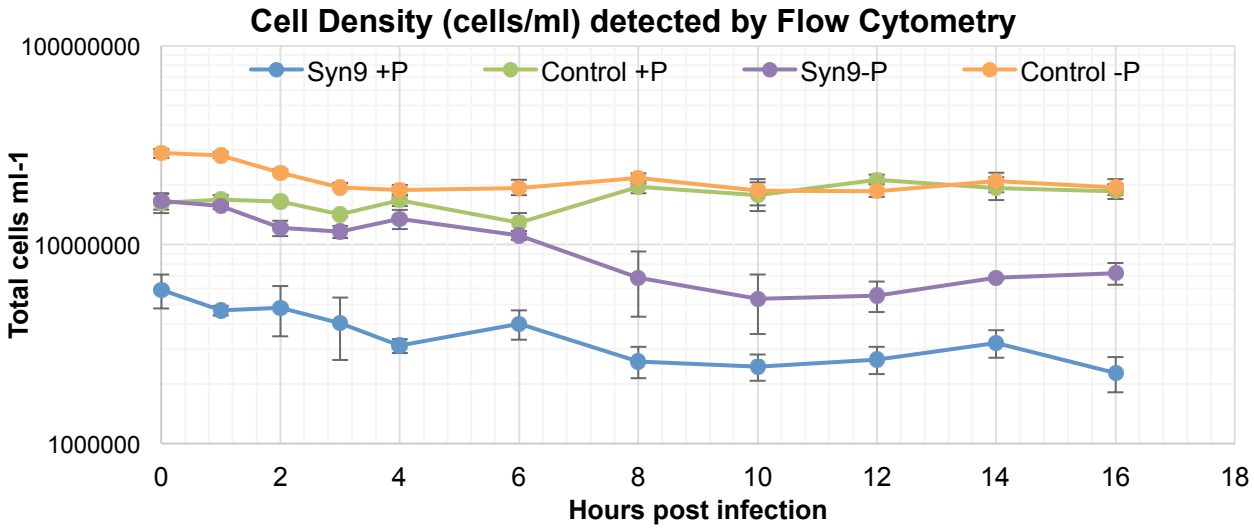

Figure A5 Total Cell Density During Viral Lysis Experiment.
Cell density declines following the viral burst. Control cells show no apparent change over the 16 hour window suggesting there was no cell division during this experiment.

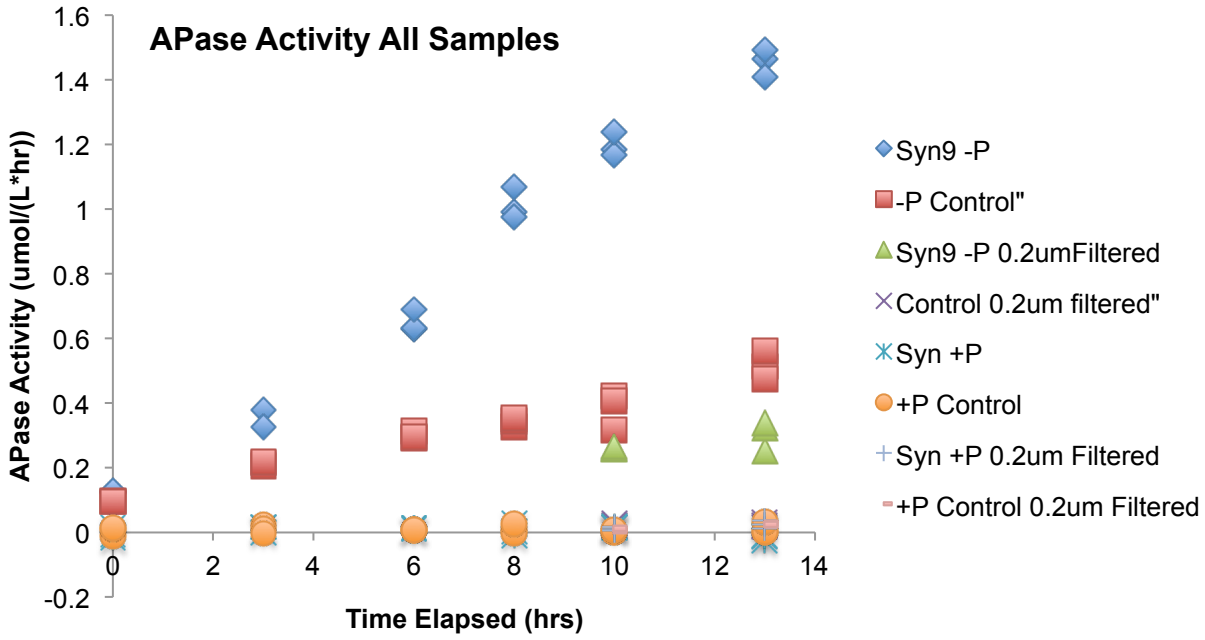

Figure A6 APase Activity Size Fraction.
Blue, red, and green points all represent phosphate-starved cells infected with Syn9. Red symbols are controls, while blue symbols are unfiltered samples, and green symbols are 0.2µm filtered samples. Filtered APase activity is nearly equal to the controls and well above the detection limit and p-replete cells represented along the x-axis near detection limits for the DiFMUP assay.

M9			*P-Replete*		*P-Limited*	
Strain	**Salts**	**[ ] mM**	**Nutrients**	**[ ] mM**	**Nutrients**	**[ ] mM**
E.coli K12 MG1655	NaCl	0.04	Na_2HPO_4	0.24	Na-Glycerophosphate	0.24
	$MgSO_4$	2.00	KH_2PO_4	0.11	-	-
	$CaCl_2$	0.10	Glucose	0.02	Glucose	0.02
			NH_4Cl	0.09	NH_4Cl	0.09

ASW (NO_3^-)			*P-Replete*		*P-Starved*	
Strain	**Salts**	**[ ] mM**	**Nutrients**	**[ ] mM**	**Nutrients**	**[ ] mM**
Synechococcus 7803	NaCl	428	$NaNO_3$	8.8	$NaNO_3$	8.8
	$MgCl_2$	9.8	NaH_2PO_4	0.13	NaH_2PO_4	0
	KCl	6.7	$NaHCO_3$	5.9	$NaHCO_3$	5.9
	$MgSO_4$	14.2				
	$CaCl_2$	3.4				
	Tris	9.1				
	Trace Metal	**[ ] µM**				
	$FeCl_3$	1.1				
	Na_2EDTA	1.3				
	H_3BO_3	46.278				
	$MnCl_2$	9.15				
	$ZnSO_4$	0.772				
	$CuSO_4$	0.032				
	$CoCl_2$	0.025				
	Na_2MoO_4	1.616				

Pro 99			*P-Replete*		*P-Starved*	
Strain	**Salts**	**[ ] mM**	**Nutrients**	**[ ] mM**	**Nutrients**	**[ ] mM**
Prochlorococcus MED4	Sargasso SW, 0.2µm filtered/autoclaved		NaH_2PO_4	0.05	NaH_2PO_4	0
			NH_4Cl	0.8	NH_4Cl	0.8
	Trace Metal	**[ ] µM**				
	$FeCl_3$	1.180				
	Na_2EDTA	1.170				
	$ZnSO_4$	0.008				
	$CoCl_2$	0.005				
	$MnCl_2$	0.090				
	Na_2MoO_4	0.003				
	Na_2SeO_3	0.010				
	$NiCl_2$	0.010				

Table A1 Media Composition.

ASW (NO_3^-)			P-Replete		P-Starved	
Strain	Salts	[ ] mM	Nutrients	[ ] mM	Nutrients	[ ] mM
Synechococcus 7803	NaCl	428	$NaNO_3$	8.8	$NaNO_3$	8.8
	$MgCl_2$	9.8	NaH_2PO_4	0.13	NaH_2PO_4	0
	KCl	6.7	$NaHCO_3$	5.9	$NaHCO_3$	5.9
	$MgSO_4$	14.2				
	$CaCl_2$	3.4				
	Tris	9.1				
	Trace Metal	[ ] µM				
	$FeCl_3$	1.1				
	Na_2EDTA	1.3				
	H_3BO_3	46.278				
	$MnCl_2$	9.15				
	$ZnSO_4$	0.772				
	$CuSO_4$	0.032				
	$CoCl_2$	0.025				
	Na_2MoO_4	1.616				

Table A2 Medium Composition.
Synechcococcus WH7803 was grown in artificial seawater (ASW) medium as specified above. Phosphate-replete conditions contained ample phosphate, while phosphate-starved conditions were achieved by suspension of cells in phosphate-free medium.

References

Azam, F. & Hodson, R.E., 1977. Dissolved ATP in the sea and its utilisation by marine bacteria. *Nature*, 267(5613), pp.696–698.

Bennett, B.D. et al., 2009. Absolute metabolite concentrations and implied enzyme active site occupancy in Escherichia coli. *Nature chemical biology*, 5(8), pp.593–9.

Bertilsson, S. et al., 2003. Elemental composition of marine Prochlorococcus and Synechococcus: Implications for the ecological stoichiometry of the sea. *Limnology and Oceanography*, 48(5), pp.1721–1731.

Bjorkman, K. & Karl, D., 2003. Bioavailability of dissolved organic phosphorus in the euphotic zone at Station ALOHA, North Pacific Subtropical Gyre. *Limnology and Oceanography*, 48(3), pp.1049–1057.

Blake, R.E., O'Neil, J.R., and Garcia, G.A., 1997. Oxygen isotope systematics of biologically mediated reactions of phosphate: I. Microbial degradation of organophosphorus compounds. *Geochimica et Cosmochimica Acta,* 61, pp. 4411-4422.

Blake, R.E., O'Neil, J.R., and Garcia, G.A., 1998. Effects of microbial activity on the $\delta^{18}O$ of dissolved inorganic phosphate and textural features of synthetic apatites. *American Mineralogist,* 83, pp. 1516-1531.

Brum, J., 2005. Concentration, production and turnover of viruses and dissolved DNA pools at Stn ALOHA, North Pacific Subtropical Gyre. *Aquatic Microbial Ecology*, 41, pp.103–113.

Casey, J.R. et al., 2007. Prochlorococcus contributes to new production in the Sargasso Sea deep chlorophyll maximum. *Geophysical Research Letters*, 34(10), p. L10604.

Cavender-Bares, K.K., Karl, D.M. & Chisholm, S.W., 2001. Nutrient gradients in the western North Atlantic Ocean: Relationship to microbial community structure and comparison to patterns in the Pacific Ocean. *Deep Sea Research Part I: Oceanographic Research Papers*, 48(11), pp. 2373–2395.

Coleman, M.L. & Chisholm, S.W., 2007. Code and context: Prochlorococcus as a model for cross-scale biology. *Trends in microbiology*, 15(9), pp. 398–407.

Colman, AS, Blake, RE, Karl, DM, Fogel, MF, & Turekian, KK (2005). Marine phosphate oxygen isotopes and organic matter remineralization in the oceans. *Proc. Nat. Acad. Sci.,* 102, pp.13023-13028.

Colman, A.S. 2002. The oxygen isotope composition of dissolved inorganic phosphate and the marine phosphorus cycle. PhD Dissertation, Yale University.

Crowson, RA and Showers, WJ, 1991. Preparation of Phosphate Samples for Oxygen Isotope Analysis *Analytical Chemistry,* 2397–2400

Dettman, D.L., Kohn, M.J., Quade, J., Ryerson, F.J., Ojha, T.P., and Hamidullah, S., 2001. Seasonal stable isotope evidence for a strong Asian monsoon throughout the past 10.7 m.y. *Geology* 29, pp.31-34.

Dyhrman, S., Ammerman, J. and Mooy, B. Van, 2007. Microbes and the marine phosphorus cycle. *Oceanography*, 20(2), pp.110–116.

Dyhrman, S. and Palenik, B., 2001. A single-cell immunoassay for phosphate stress in the dinoflagellate prorocentrum minimum (dinophyceae). *Journal of Phycology*, 410, pp. 400–410.

Field, C.B., 1998. Primary Production of the Biosphere: Integrating Terrestrial and Oceanic Components. *Science*, 281(5374), pp.237–240.

Firsching, FH 1961. Precipitation of Silver Phosphate from Homogenous Solution, *Analytical Chemistry* 33, pp. 873–874.

Fricke, H, and O'Neil, J.R., 1996. Inter- and intra- tooth variation in the oxygen isotope composition of mammalian tooth enamel phosphate: implications for paleaoclimatological and palaaeobiological research. *Palaeoecology,* 126, pp. 91-99.

Henry, J.T. & Crosson, S., 2013. Chromosome replication and segregation govern the biogenesis and inheritance of inorganic polyphosphate granules. *Molecular biology of the cell*, 24(20), pp.3177–86.

Jover, L.F. et al., 2014. The elemental composition of virus particles: implications for marine biogeochemical cycles. *Nature reviews. Microbiology*, 12(7), pp. 519–28.

Karl, D.M., 2002. Nutrient dynamics in the deep blue sea. *Trends in microbiology*, 10(9), pp. 410–8.

Kettler, G.C. et al., 2007. Patterns and implications of gene gain and loss in the evolution of Prochlorococcus. *PLoS genetics*, 3(12), p. e231.

Knauer, G.A., Martin, J.H., Bruland, K.B., 1978. Fluxes of particulate carbon, nitrogen, and phosphorus in the upper water column of the northeast Pacific. *Deep Sea Research Part A. Oceanographic Research Papers*, 26(8), p.965.

Kolodny, Y., Luz, B., and Navon, O., 1983. Oxygen isotope variations in phosphate of biogenic apatites, I. Fish bone apatite – rechecking the rules of the game. *Earth and Planetary Science Letters,* 64, pp. 398-404.

Kornexl, B., Geher, M., Hofling, R., Werener, R.A., 1999. On-Line $\delta^{18}O$ Measurement of Organic and Inorganic Substances, *Rapid Communications in Mass Spectrometry: RCM* 13, pp. 1685–93.

Lahti, R., 1983. Microbial inorganic pyrophosphatases. *Microbiological reviews*, 47(2), pp.169–78.

Liang, Y., and Blake, R.E., 2006. Oxygen isotope signature of Pi regeneration from organic compounds by phosphomonoesterases and photoxidation. *Geochimica et Cosmochimica Acta* 70, pp. 3957-3969

Loladze, I. & Elser, J.J., 2011. The origins of the Redfield nitrogen-to-phosphorus ratio are in a homoeostatic protein-to-rRNA ratio. *Ecology Letters*, 14(3), pp. 244–250.

Martin, P. & Van Mooy, B. a S., 2013. Fluorometric quantification of polyphosphate in environmental plankton samples: extraction protocols, matrix effects, and nucleic acid interference. *Applied and environmental microbiology*, 79(1), pp.273–81.

Martiny, A.C. et al., 2009. Taxonomic resolution, ecotypes and the biogeography of Prochlorococcus. *Environmental microbiology*, 11(4), pp.823–32.

Middelboe, M., Jørgensen, N.O.G. & Kroer, N., 1996. Effects of viruses on nutrient turnover and growth efficiency of noninfected marine bacterioplankton. *Applied and Environmental Microbiology*, 62(6), pp.1991–1997.

Middelboe, M. & Lyck, P., 2002. Regeneration of dissolved organic matter by viral lysis in marine microbial communities. *Aquatic Microbial Ecology*, 27(1), pp.187–194.

Middelboe, M. et al., 2003. Virus-induced transfer of organic carbon between marine bacteria in a model community. *Aquatic Microbial Ecology*, 33, pp.1–10.

Moore, L. et al., 2005. Ecotypic variation in phosphorus-acquisition mechanisms within marine picocyanobacteria. *Aquatic Microbial Ecology*, 39, pp.257–269.

O'Neil, J.R., Roe, L.J., Reinhard, E., Blake, R.E., 1994. A rapid and precise method of oxygen isotope analysis of biogenic phosphate. *Isr. J. Earth Sci*., 43, pp. 203.

O'Neil, J.R. Vennemann, T.W., and McKenzie, W.F. (2003) Effects of speciation on equilibrium fractionations and rates of oxygen isotope exchange between $(PO_4)_{aq}$ and H_2O. *Geochim. Cosmochim. Acta*, 67, pp. 3135-3144

Partensky, F. & Garczarek, L., 2010. Prochlorococcus : Advantages and Limits of Minimalism. *Annual Review of Marine Science*, 2(1), pp. 305–331.

Perry, M.J., 1972. Alkaline phosphatase activity in subtropical Central North Pacific waters using a sensitive fluorometric method. *Marine Biology*, 15(2), pp.113–119.

Perry, M.J., 1976. Phosphate utilization by an oceanic diatom in phosphorus-limited chemo-stat culture and in the oligotrophic waters of the central North Pacific. *Limnology and Oceanography*, 21, pp.88–107.

Poorvin, L. et al., 2004. Viral release of iron and its bioavailability to marine plankton. *Limnology and Oceanography*, 49(5), pp.1734–1741.

Riemann, B., 1979. The occurrence and ecological importance of dissolved ATP in fresh water. *Freshwater Biology*, 9, pp.481–490.

Riemann, L., Holmfeldt, K. & Titelman, J., 2009. Importance of viral lysis and dissolved dna for bacterioplankton activity in a P-limited estuary, northern baltic sea. *Microbial Ecology*, 57(2), pp.286–294.

Scanlan, D.J., Mann, N.H. & Carr, N.G., 1993. The response of the picoplanktonic marine cyanobacterium Synechococcus species WH7803 to phosphate starvation involves a protein homologous to the periplasmic phosphate-binding protein of Escherichia coli. *Molecular microbiology*, 10(1), pp.181–91.

Shelford, E.J. et al., 2012. Virus-driven nitrogen cycling enhances phytoplankton growth. *Aquatic Microbial Ecology*, 66(1), pp.41–46.

Shemesh, A, Kolodny, Y., and Luz, B., 1983. Oxygen Isotope Variations in Phosphate of Biogenic Apatites, II. Phosphorite Rocks: 64 405–416.

Stephan, E, 2000. Oxygen Isotope Analysis of Animal Bone Phosphate: Method Refinement, Influence of Consolidants, and Reconstruction of Palaeotemperatures for Holocene Sites, *Journal of Archaeological Science*, 27, pp. 523–535.

Tudge, A.P., 1960. A Method of Analysis of Oxygen Isotopes in Orthophosphate—its Use in the Measurement of Paleotemperatures," *Geochimica et Cosmochimica Acta* 18, 81-93

Van Mooy, B. a S. et al., 2006. Sulfolipids dramatically decrease phosphorus demand by picocyanobacteria in oligotrophic marine environments. *Proceedings of the National Academy of Sciences of the United States of America*, 103(23), pp. 8607–12.

Van Mooy, B. a. S. & Devol, A.H., 2008. Assessing nutrient limitation of Prochlorococcus in the North Pacific subtropical gyre by using an RNA capture method. *Limnology and Oceanography*, 53(1), pp. 78–88.

Vennemann, T.W., H.C. Fricke, R.E. Blake, J.R. O'Neil, and A. Colman, 2002. Oxygen isotope analysis of phosphates: a comparison of techniques for analysis of Ag_3PO_4. *Chemical. Geology*, 185, 321-336.

Weitz, J. & Wilhelm, S., 2012. Ocean viruses and their effects on microbial communities and biogeochemical cycles. *F1000 Biology Reports*, 8 (September), pp.2–9.

Wenzel, B., Lecuyer, C., and Joachimski, M.M., 2000. Comparing oxygen isotope records of Silurian calcite and phosphate – δ18O compositions of brachiopods and conodonts. *Geochimica et Cosmochimica Acta,* 64, pp. 1859-1872.

Wiedemann-Bidlack, F.B., A.S. Colman, and M.L. Fogel, 2008. Stable isotope analyses of phosphate oxygen from biological apatite: a new technique for microsampling, microprecipitation of Ag_3PO_4, and removal of organic contamination. *Rapid Commun. Mass Spectrom*., 22, pp. 1807-1816.

Wilhelm, S.W. & Suttle, C. a., 1999. Viruses and Nutrient Cycles in the Sea. *BioScience*, 49(10), p.781.

Wilson, W., Carr, N. & Mann, N., 1996. The effect of phosphate status on the kinetics of cyanophage infection in the oceanic cyanobacterium Synechococcus sp. WH7803. *Journal of Phycology*, 23, pp.506–516.

Wright, E. and Hoering, T.C. 1989. Separation and purification of phosphates for oxygen isotope analysis. *Annual Report of the Director Geophysical Laboratory,* 2150. 137-141.

Zeng, Q. & Chisholm, S.W., 2012. Marine viruses exploit their host's two-component regulatory system in response to resource limitation. *Current biology : CB*, 22(2), pp.124–8.